

HOURLY RADIATION UTILIZABILITY AND ITS
APPLICATION TO PHOTOVOLTAIC SYSTEMS

DANIEL REED CLARK

MASTER OF SCIENCE
(ENGINEERING)

UNIVERSITY OF WISCONSIN-MADISON
1982



HOURLY RADIATION UTILIZABILITY AND ITS
APPLICATION TO PHOTOVOLTAIC SYSTEMS

BY

DANIEL REED CLARK

A thesis submitted in partial fulfillment of the
requirements for the degree of

MASTER OF SCIENCE
(Engineering)

at the

UNIVERSITY OF WISCONSIN-MADISON

1982

ABSTRACT

This thesis first examines the hourly utilizability approach to the analysis of solar energy systems. A simple and highly accurate empirical method is developed for evaluating the hourly utilizability function. This correlation can be used for surfaces of any orientation to predict the usable fraction of incident solar energy, and is applicable to many types of solar energy systems.

The hourly utilizability approach is then applied to the analysis of photovoltaic systems. An existing design method is extended, using hourly utilizability, to predict the performance of photovoltaic systems without electrical storage for any electrical demand profile. Finally, a correlation is proposed for estimating the effect of storage batteries on the performance of photovoltaic systems, again for any load profile.

ACKNOWLEDGMENTS

I would like to thank my advisors for their support and guidance: Professor Sanford A. Klein, for answering difficult questions, and Professor William A. Beckman, for asking difficult questions. I also thank Professor V.V.Satyamurti for many valuable discussions.

The assistance and interest of the Solar Energy Laboratory students and staff, particularly Warren Buckles and Jim Braun, is greatly appreciated. Special thanks go to my wife, Valerie, for her help in preparing the figures and for all of her support, patience, and love.

Financial support through a grant from the Department of Energy is gratefully acknowledged.

TABLE OF CONTENTS

List of Figures	vi
List of Tables	vii
Nomenclature	ix
INTRODUCTION	1
CHAPTER 1 Development of the Utilizability Concept	
1.1 Origin of the Utilizability Concept	5
1.2 Utilizability and the Statistical Distribution of Solar Radiation	8
1.3 Basic Equations	15
1.4 Review of Generalized Utilizability: Graphical Methods	19
1.5 Analytical Methods	26
CHAPTER 2 Curve-Fitting the Utilizability Function	
2.1 Introduction: Generation of a Data Base	32
2.2 Derivation of Form for Correlation	35
2.3 Empirical Correlation Procedure	39
2.4 Correlation Results and Comparisons	57
2.5 Recommendations for Further Work	67
CHAPTER 3 Photovoltaic Design Methods	
3.1 Introduction	71
3.2 Photovoltaic Systems	72
3.3 Computer Simulation Models	76

3.4	Previous Design Methods for Photovoltaic Systems	79
3.5	Estimation of the Effect of Electrical Storage	86
3.6	Analysis of Design Method Results	101
3.7	Sample Calculation	111
3.8	Recommendations for Further Work	119
	APPENDIX	122
	BIBLIOGRAPHY	135

LIST OF FIGURES

<u>Figure</u>	<u>Page</u>
1.1-1 Definition of the Utilizability Function	7
1.2-1 Derivation of the Utilizability Function	9
1.2-2 Effect of Insolation Distribution Width on the Utilizability Function	13
1.2-3 Effect of Insolation Distribution Skew on the Utilizability Function	14
1.4-1 Cumulative Frequency Distributions of the Daily Clearness Index from Odegard (21); adapted from Liu and Jordan (18)	20
1.4-2 Generalized ϕ -Curves from Duffie and Beckman (6); adapted from Liu and Jordan (19)	22
1.4-3 Generalized Hourly ϕ -Curves from Odegard (21)	25
1.5-1 Gamma (from Eq. 1.5-2) vs. the Hourly Clearness Index	29
2.2-1 Form of Correlation for ϕ	36
2.4-1 Comparison of Correlations with Long-term Weather Data Results	59
2.5-1 Alternative Form for Correlation of ϕ	69
3.2-1 Schematic of Photovoltaic System Configuration	73
3.5-1 Form of Correlation for Δf_g	89
3.5-2 Load Distributions Used in First Set of Hourly Simulations	92
3.6-1 Simulated vs. Estimated Monthly Load Fractions Identified by Location	106
3.6-2 Simulated vs. Estimated Monthly Load Fractions Identified by Storage Capacity	107

LIST OF TABLES

<u>Table</u>		<u>Page</u>
1.5-1	Gamma (from Eq. 1.5-2) vs. the Hourly Clearness Index	28
2.1-1	Hours considered in developing the correlation for ϕ	34
2.3-1	Unavoidable error from the use of Eq. 2.2-13: Hourly results	41
2.3-2	Unavoidable error from the use of Eq. 2.2-13: Annual results	43
2.3-3	Example of Correlation Procedure	44
2.3-4	Linear estimation of X_m (optimum s)	45
2.3-5	Estimation of X_m and ϕ	47
2.3-6	Linear estimation of X_m ($s = 1$) excluding Seattle data	48
2.3-7	Linear estimation of X_m ($s = 1$)	49
2.3-8	Estimation of ϕ	50
2.3-9	Effects of Location and Azimuth Angle	52
2.3-10	Modifications to Model for X_m	54
2.3-11	Correlation Coefficients with Error in X_m	55
2.3-12	Final Correlation Data and Results	56
2.4-1	Comparison of correlation results and long-term weather results	63
2.4-2	rms error of present correlation for a vertical south-facing surface in Albuquerque	65
2.4-3	Energy-weighted comparisons of correlations for ϕ	66
3.3-1	Comparison of simulation models	78

<u>Table</u>	<u>Page</u>
3.4-1 Optimum slope (S_m) of south-facing arrays for use in Eq. 3.4-3	89
3.4-2 Comparison between design method of Evans (9) and hourly simulation	82
3.4-3 Comparison between design methods (9, 24) and hourly simulation	85
3.5-1 Parameter values for first set of hourly simulations: 56 years (672 months)	91
3.5-2 Parameter values for second set of hourly simulations: 9 years (108 months)	94
3.5-3 Parameter values for third set of hourly simulations: 8 years (96 months)	96
3.5-4 Attempted correlations for the parameter A in Eq. 3.5-8: 56 years of data	98
3.5-5 Attempted correlations for the parameter A in Eq. 3.5-8: 73 years of data	99
3.5-6 Correlation coefficients with error in Δf_s	100
3.6-1 Accuracy of design method relative to first set of hourly simulations	103
3.6-2 Accuracy of design method relative to second set of hourly simulations	105
3.6-3 Results of factorial analysis of variance	109
3.7-1 Photovoltaic system characteristics for sample calculation	112
3.7-2 Results from sample calculation for January	117
3.7-3 Results from design method and from hourly simulation using TRNSYS (16)	120

Nomenclature

This list contains the major parameters used in this study.

Others are defined locally.

a	Utilizability correlation parameter (Eq. 2.2-9)
A	Electrical storage correlation parameter (Eq. 3.5-8)
A_c	Total photovoltaic cell area
B_c	Battery storage capacity
D	Energy dissipated
D_a	Energy dissipated from system with storage
E	Electrical energy generated
E_L	Electrical energy sent directly to load (not via storage)
f	(1) Cumulative frequency of occurrence (2) Monthly fraction of the load met by solar energy
F	Annual fraction of the load met by solar energy
G	Instantaneous insolation
G_{sc}	Solar constant
H	Total daily insolation on a horizontal surface
H_d	Daily diffuse insolation on a horizontal surface
H_T	Total daily insolation on a tilted surface
H_o	Daily extraterrestrial radiation on a horizontal surface
I	Total hourly insolation on a horizontal surface
I_c	Critical hourly insolation level
I_d	Hourly diffuse radiation on a horizontal surface
I_T	Total hourly insolation on a tilted surface

I_o	Hourly extraterrestrial radiation on a horizontal surface
k	Hourly clearness index
K	Daily clearness index
L	(1) Latitude (2) Load
$P()$	Probability of () occurring
r	Correlation coefficient
R	Ratio of total hourly insolation on a tilted surface to that on a horizontal surface
\overline{R}	Ratio of monthly-average daily insolation on a tilted surface to that on a horizontal surface
\tilde{R}	Ratio of monthly-average hourly insolation on a tilted surface to that on a horizontal surface
R_b	Ratio of hourly beam radiation on a tilted surface to that on a horizontal surface
s	Utilizability correlation parameter (Eq. 2.2-8)
T_a	Ambient temperature
T_c	Photovoltaic cell temperature
T_r	Reference temperature corresponding to η_r
U_L	Collector thermal loss coefficient
V_{bd}	Hourly beam-diffuse view factor
\overline{V}_{bd}	Daily beam-diffuse view factor
x	Ratio of effective storage capacity to load (Eq. 3.5-2)
X_c	Critical insolation ratio
X_m	Minimum critical insolation ratio at which $\phi = 0$

α	Photovoltaic cell absorptance
β	(1) Collector slope (2) Photovoltaic cell temperature coefficient
γ	Azimuth angle
δ	Declination
Δf_{\max}	Increase in monthly solar load fraction due to storage at very large storage capacity to load ratios (Eq. 3.5-7)
Δf_s	Increase in monthly solar load fraction due to electrical storage
ΔF_s	Increase in annual solar load fraction due to electrical storage
η_b	Battery storage efficiency
η_e	Photovoltaic electrical conversion efficiency
η_{mp}	Maximum power tracking circuitry efficiency
η_{pc}	Power conditioning equipment efficiency (excluding maximum power tracker)
η_r	Photovoltaic reference efficiency at a reference temperature, T_r
θ_z	Solar zenith angle
ρ	Ground reflectance
τ	Collector cover transmittance
ϕ	Monthly-average hourly utilizability
$\bar{\phi}$	Monthly-average daily utilizability
ω	Hour angle
ω_s	Sunset hour angle

Subscripts

- act "Actual," i.e., calculated from many years of hourly horizontal measurements
- est Estimated from monthly-average weather statistics
- opt Optimum, i.e., minimizing the standard deviation of differences from "actual" values
- o In the absence of electrical storage (except as noted above)
- An overbar $\overline{\quad}$ indicates monthly-average, except as noted above

Introduction

Utilizability is an approach to the analysis of solar energy systems. The utilizability approach is based on a solar radiation statistic, designated ϕ , defined as the fraction of the total incident solar energy which strikes the surface at an intensity exceeding a specified threshold. The threshold intensity is generally called the critical radiation intensity level, or more simply the critical level. Since ϕ is a ratio of solar energy quantities, the time interval over which it is defined must be specified. Generally ϕ is defined on a monthly average basis over a period of an hour-- for example, the hour from 9 AM to 10 AM in January. A monthly-average daily value of ϕ , designated $\bar{\phi}$, can also be defined using a constant critical level throughout the day. Daily utilizability has been treated extensively elsewhere (14, 28, 5, 12) and will not be considered here.

The utilizability concept was first proposed (29) as an approach to analyzing flat-plate solar collector performance. In this context, the critical radiation level is defined as the intensity of incoming solar radiation at which thermal losses from the collector are equal to thermal gains; the net useful energy collection is then zero. When incident radiation falls below the critical level, fluid flow through the collector must be turned off or the working fluid will be cooled rather than heated. Only that portion of the total solar input which exceeds the critical intensity can be used; hence the name utilizability.

In recent years the utilizability approach has been applied to a variety of situations (15, 20, 21, 24). For some applications, including photovoltaic systems, the critical level is defined as an upper limit on useful radiation, rather than a lower limit. In such situations ϕ represents a non-useful energy fraction rather than a useful fraction, and the term unutilizability would be more appropriate. In this sense the term utilizability is a somewhat unfortunate choice of nomenclature. In the present work this distinction is ignored; the term utilizability is applied to ϕ regardless of how the critical level is defined.

The present work began as an investigation into simple methods for predicting the performance of photovoltaic systems, using widely available monthly-average weather statistics rather than detailed hour-by-hour calculations requiring more extensive weather data and access to a mainframe computer. Methods exist (24, 8, 9) for estimating the monthly-average efficiency of a photovoltaic array. For photovoltaic systems without dedicated energy storage, Siegel (24, 25) has applied the daily utilizability function, $\bar{\phi}$, to the calculation of system performance. This method is limited to systems which experience a constant 24-hour load, since the daily utilizability function requires a constant critical level.

Odegard (21) and Huget (12) have developed approximate methods for calculating ϕ on an hourly basis. The necessary equations are algebraically complicated but represent a major improvement over previously available methods. A computer program which evaluates

the equations given by Huget has been written and is listed in Appendix A.

Given the means for evaluating ϕ for any hour, the photovoltaic design method of Siegel can be extended to accommodate loads which vary throughout the day. Thus modified, the method is considerably more flexible but still limited to systems without energy storage. At present, the majority of photovoltaic systems are in remote locations where connection to the utility grid is impractical, and electrical storage is likely to be an important consideration.

In Chapter 3 the effect of electrical storage on the performance of photovoltaic systems is examined, and a correlation is developed for estimating the improvement in system performance due to a given storage capacity. The correlation is suitable for use with any load profile. Combined with the modified method of Siegel, the correlation agrees closely with the results of hour-by-hour simulations.

Mathematically, the equation used in the storage correlation describes a hyperbola. Examination of utilizability curves suggested that a similar equation might be used advantageously to describe the utilizability function. Initial investigations yielded highly promising results, and led ultimately to the development of a new correlation for evaluating ϕ , as described in Chapter 2. This new correlation is much simpler than the procedures of Odegard and Huget. Based on extensive data from a limited number of locations, the present utilizability correlation appears to be at least

as accurate as the method of Huget, and perhaps slightly more accurate. The agreement of the correlation with values obtained from many years of hourly horizontal radiation measurements is excellent.

The aspects of the present work pertaining to utilizability have been emphasized because of the versatility of the hourly utilizability approach. While daily utilizability methods require fewer calculations for each month, they also require knowledge of an effective average daily critical level. Hourly utilizability allows the critical level to be defined independently for each hour of the day, a crucial consideration for some applications (notably photovoltaic systems). In addition, even if a daily average critical level is known, the hourly approach greatly facilitates calculation of utilizability for surfaces that do not face south.

Chapter 1. Development of the Utilizability Concept

1.1 Origin of the Utilizability Concept

The utilizability concept was first proposed by Whillier (29) as a method for predicting the long-term average performance of flat plate collectors.

The hourly rate of useful energy collection per unit area is given by the Hottel-Whillier equation:

$$q_u = F_R [I_T (\tau\alpha) - U_L (T_i - T_a)]^+ \quad (1.1-1)$$

where F_R is the collector heat removal factor, I_T is the total hourly solar radiation incident on the tilted surface of the collector, $(\tau\alpha)$ is the collector transmittance-absorptance product, U_L is the thermal loss coefficient, T_i is the inlet fluid temperature, T_a is the ambient temperature, and the superscript + indicates that only positive values are considered. Further information on the derivation and use of this equation can be found in reference (6).

Whillier defined a critical radiation level, I_c , as the radiation intensity at which q_u , the useful energy collection rate, is zero:

$$I_c = \frac{U_L (T_i - T_a)}{(\tau\alpha)} \quad (1.1-2)$$

Equation (1.1-1) can be rewritten in terms of I_c :

$$q_u = F_R(\tau\alpha) (I_T - I_c)^+ \quad (1.1-3)$$

For a given hour of the day throughout a month, a monthly-average hourly rate of useful energy gain can be defined:

$$\bar{q}_u = \frac{1}{n} \sum_{i=1}^n F_R(\tau\alpha) (I_{T_i} - I_c)^+ = F_R(\tau\alpha) \frac{1}{n} \sum_{i=1}^n (I_{T_i} - I_c)^+ \quad (1.1-4)$$

where n is the number of values being averaged, generally equal to the number of years of data available times thirty hours for a thirty-day month, or sixty hours if hour pairs symmetric about noon are averaged together. Whillier (29) recommends using at least ten years of data to obtain a reliable long-term average.

The utilizability function is defined as the long-term average fraction of the average hourly radiation that exceeds the critical intensity:

$$\phi = \frac{\frac{1}{n} \sum_{i=1}^n (I_{T_i} - I_c)^+}{\frac{1}{n} \sum_{i=1}^n (I_{T_i})} = \frac{\frac{1}{n} \sum_{i=1}^n (I_{T_i} - I_c)^+}{\bar{I}_T} \quad (1.1-5)$$

The relationship between ϕ and hourly average useful gain is obtained by substituting eq. 1.1-5 into eq. 1.1-4:

$$\bar{q}_u = F_R(\tau\alpha) \bar{I}_T \phi \quad (1.1-6)$$

Figure 1.1-1 provides a graphical representation of equation 1.1-5 for $n = 3$. The rectangles represent insolation during an hour in the afternoon on three days. ϕ is given by the ratio of the total shaded area to the total area of the rectangles. Two sequences of

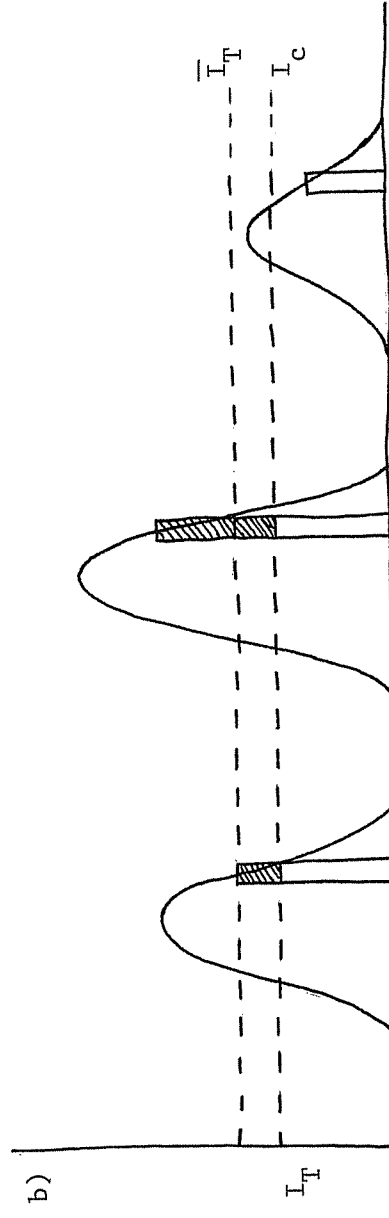
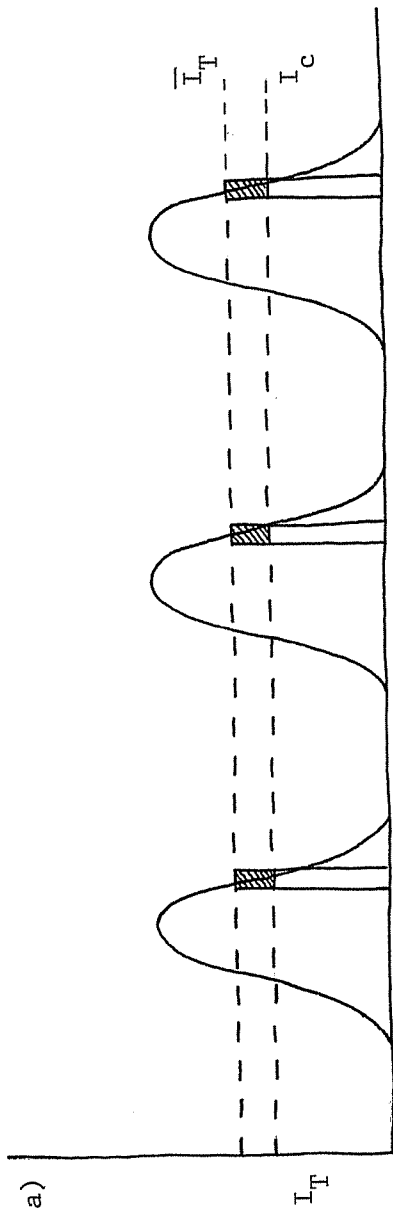


Figure 1.1-1 Definition of the Utilizability Function

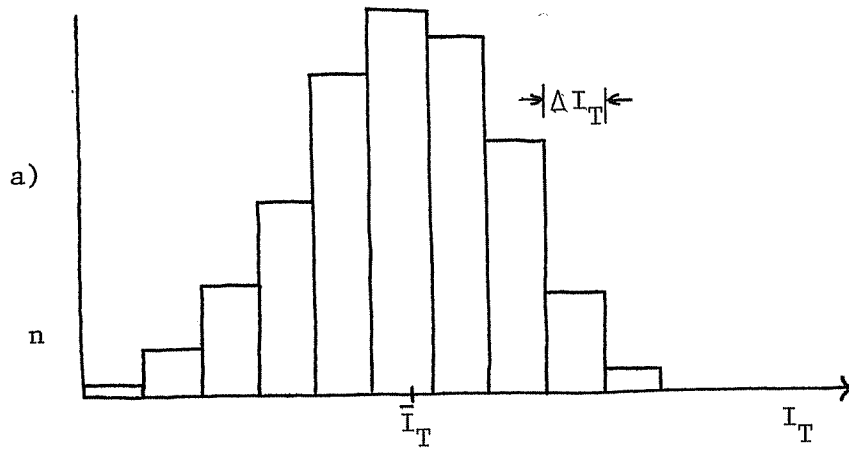
three days are shown; both sequences have the same average radiation, \bar{I}_T , and the same critical level, I_c , but the total shaded area (and hence ϕ) is smaller for the sequence of identical days than for the sequence of variable days. In the next section, the relationship between ϕ and the distribution of insolation is examined in more detail.

1.2 Utilizability and the Statistical Distribution of Solar Radiation

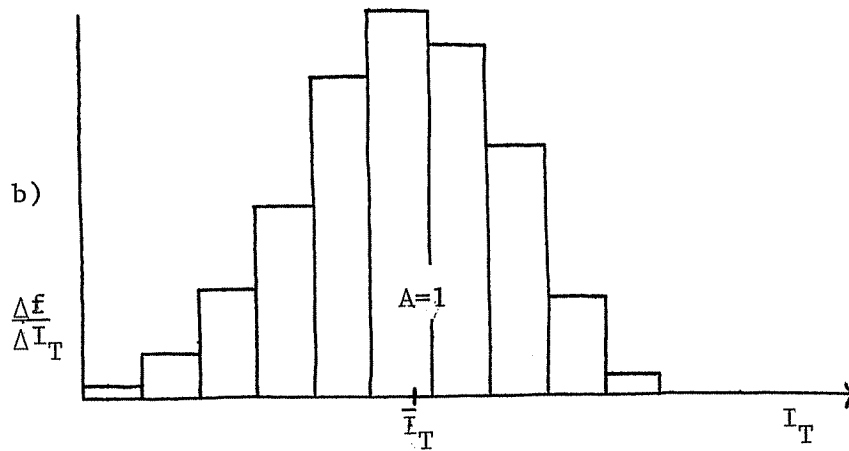
Figure 1.2-1a is a histogram of hourly radiation intensities for a particular hour (e.g., 9-10 A.M.) for a month. Ranges of radiation intensity are marked along the abscissa; the ordinate gives the number of observations in each range. The fraction of observations that fall within the i^{th} intensity range ΔI_{T_i} is given by

$$\Delta f_i = \frac{n_i}{N} \quad (1.2-1)$$

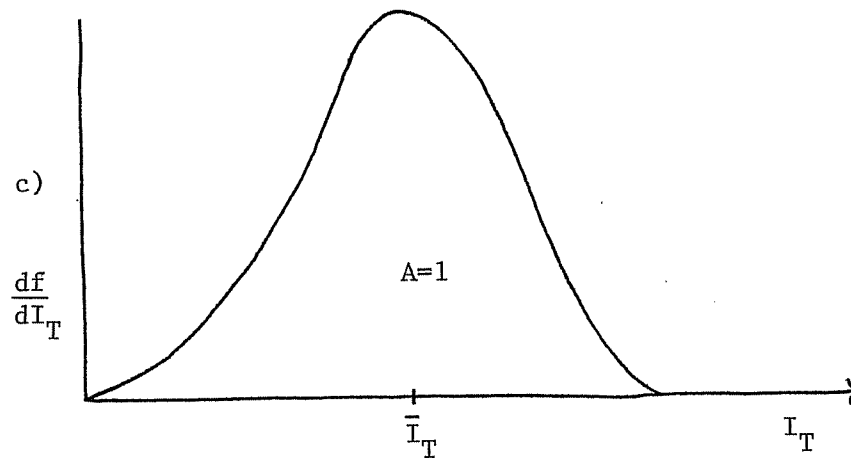
where n_i is the number of observations in the specified range and N is the total number of observations. The ratio $\Delta f_i / \Delta I_{T_i}$, which is independent of the increment size ΔI_{T_i} , is referred to as the probability density. A probability density distribution is obtained from the radiation intensity histogram by simply rescaling the vertical axis, as shown in Figure 1.2-1b. The total area of the rectangles is now unity. In the limit as ΔI_{T_i} approaches zero, the histogram approaches a continuous distribution, as in Figure 1.2-1c.



Discrete distribution histogram



Normalized discrete distribution



Continuous distribution

Figure 1.2-1 Derivation of the Utilizability Function

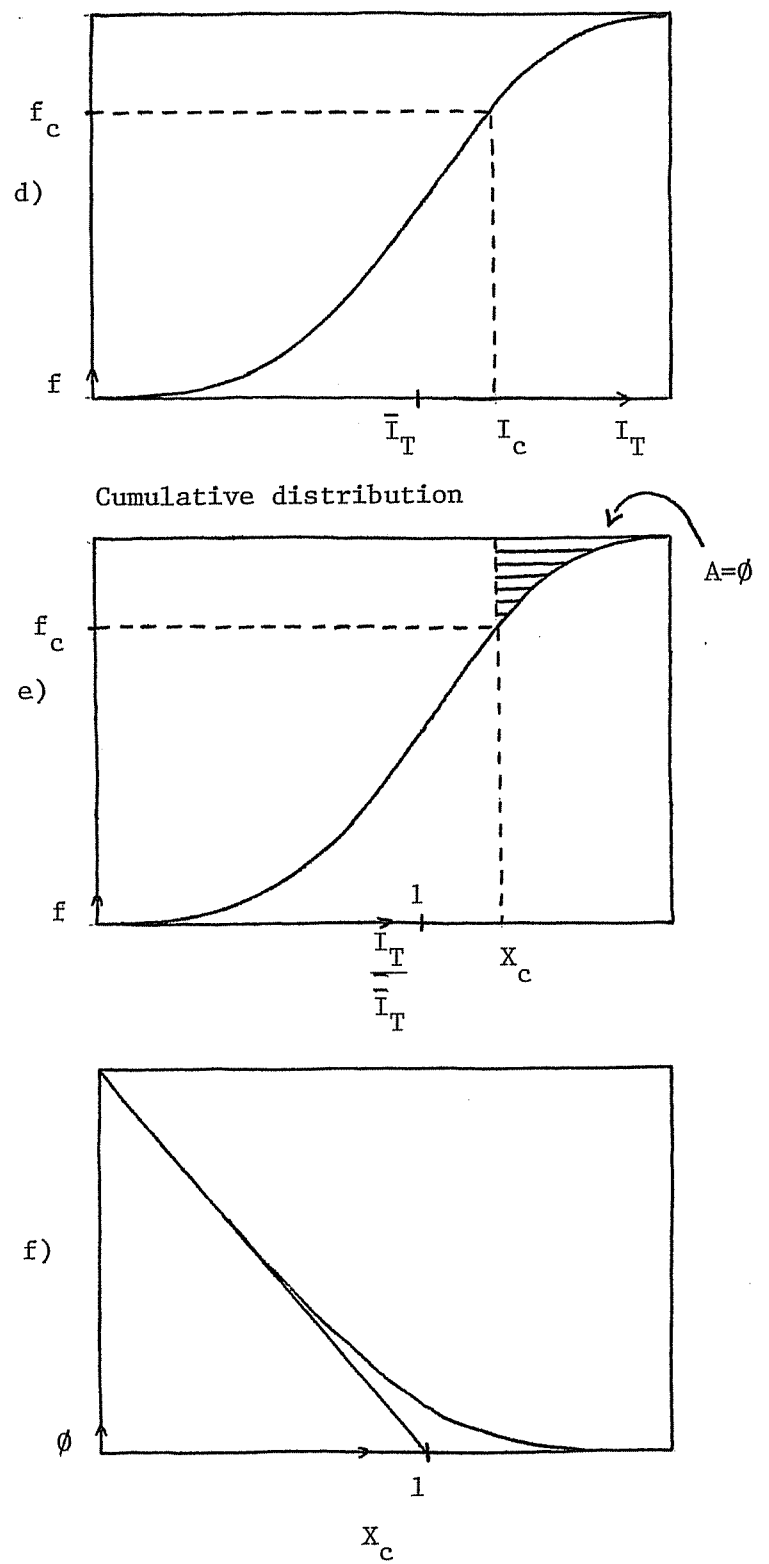


Figure 1.2-1 (continued)

The probability density distribution can be integrated to yield a cumulative frequency distribution as in Figure 1.2-1d. From this curve one can find the frequency (f_c) of occasions when the observed radiation intensity is less than a specified intensity I_c -- in other words, the probability that the observed intensity will be less than I_c . The probability that hourly radiation will be greater than I_c during the hour under consideration is given by $(1 - f_c)$.

The definition of ϕ given by Equation 1.1-5 can be re-written in continuous form in terms of the cumulative frequency distribution:

$$\phi = \frac{\int_{f_c}^1 (I_T - I_c) df}{\bar{I}_T} = \int_{f_c}^1 \left(\frac{I_T}{\bar{I}_T} - \frac{I_c}{\bar{I}_T} \right) df \quad (1.2-2)$$

The ratio I_c/\bar{I}_T is commonly referred to as the critical ratio and is given the symbol X_c :

$$X_c = \frac{I_c}{\bar{I}_T} \quad (1.2-3)$$

Figure 1.2-1e is a repetition of 1.2-1d with the scale changed on the abscissa. As indicated on this figure, the value of ϕ corresponding to a given critical ratio X_c can be found by integration over the cumulative frequency curve. Figure 1.2-1f shows the result of performing this integration for many values of X_c and plotting the integral vs. X_c .

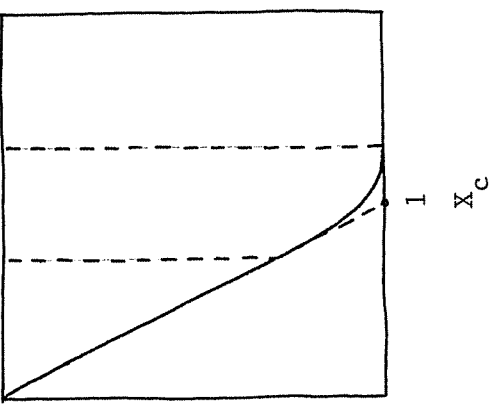
Equation 1.2-2 can be written in terms of the probability density distribution rather than the cumulative distribution with the use of the following substitution:

$$df = \frac{df}{dI_T} dI_T \quad (1.2-4)$$

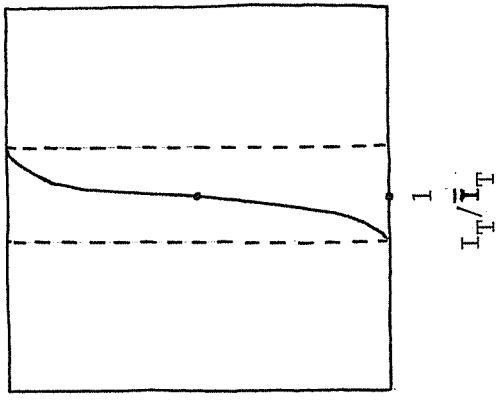
The methods for estimating ϕ reviewed in Section 1.5 rely on probability density distributions, not cumulative distributions.

It is worthwhile to examine the relationship between the shape of the frequency distribution and the shape of the ϕ -curve. Figure 1.2-2 shows two hypothetical frequency distributions, corresponding cumulative frequency distributions, and the resulting ϕ -curves. In Fig. 1.2-2a the distribution is narrow, with most observations quite close to the mean. For the limiting case of identical days, all observations would be exactly equal to the mean and the resulting ϕ -curve would be a straight line with a slope of -1. As the distribution gets broader, as in 1.2-2d, the ϕ curves fan upward, yielding a higher value of ϕ for a given X_c .

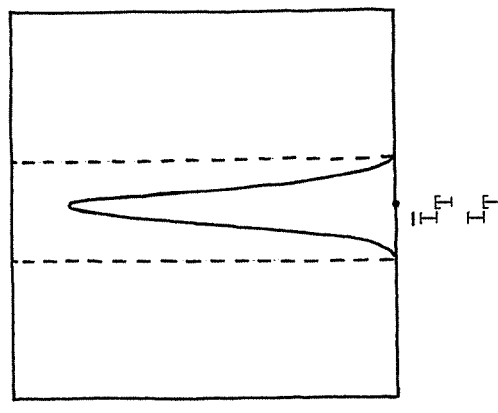
The effect of skewing the distribution is shown in Figure 1.2-3. Skewing the distribution toward high values of I_T effectively decreases the value of X_c at which $\phi = 0$. Skewing the distribution toward low values of I_T has qualitatively the same effect as broadening the distribution: it increases the value of ϕ corresponding to a given value of X_c .



c) \emptyset



b) f

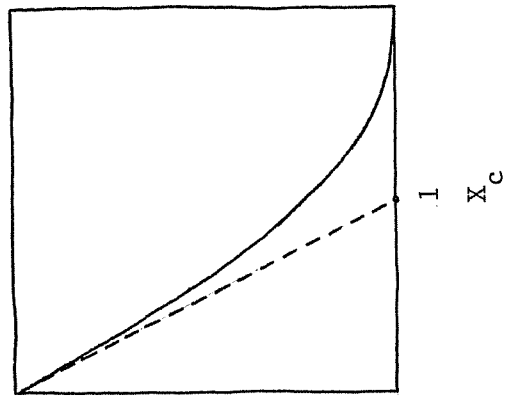


a) $\frac{df}{dI_T}$

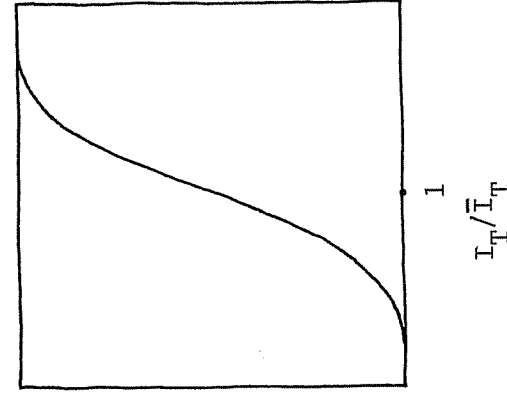
Utilizability function

Cumulative frequency distribution

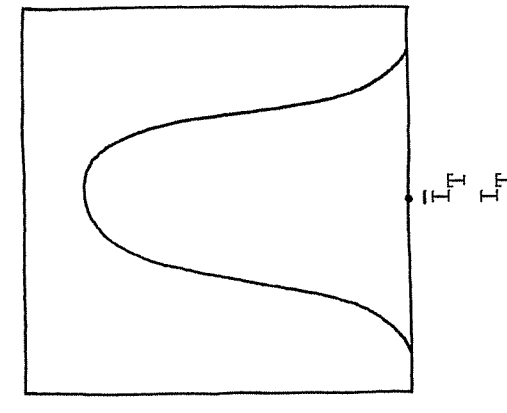
Frequency distribution



f) \emptyset



e) f



d) $\frac{df}{dI_T}$

Utilizability function

Cumulative frequency distribution

Frequency distribution

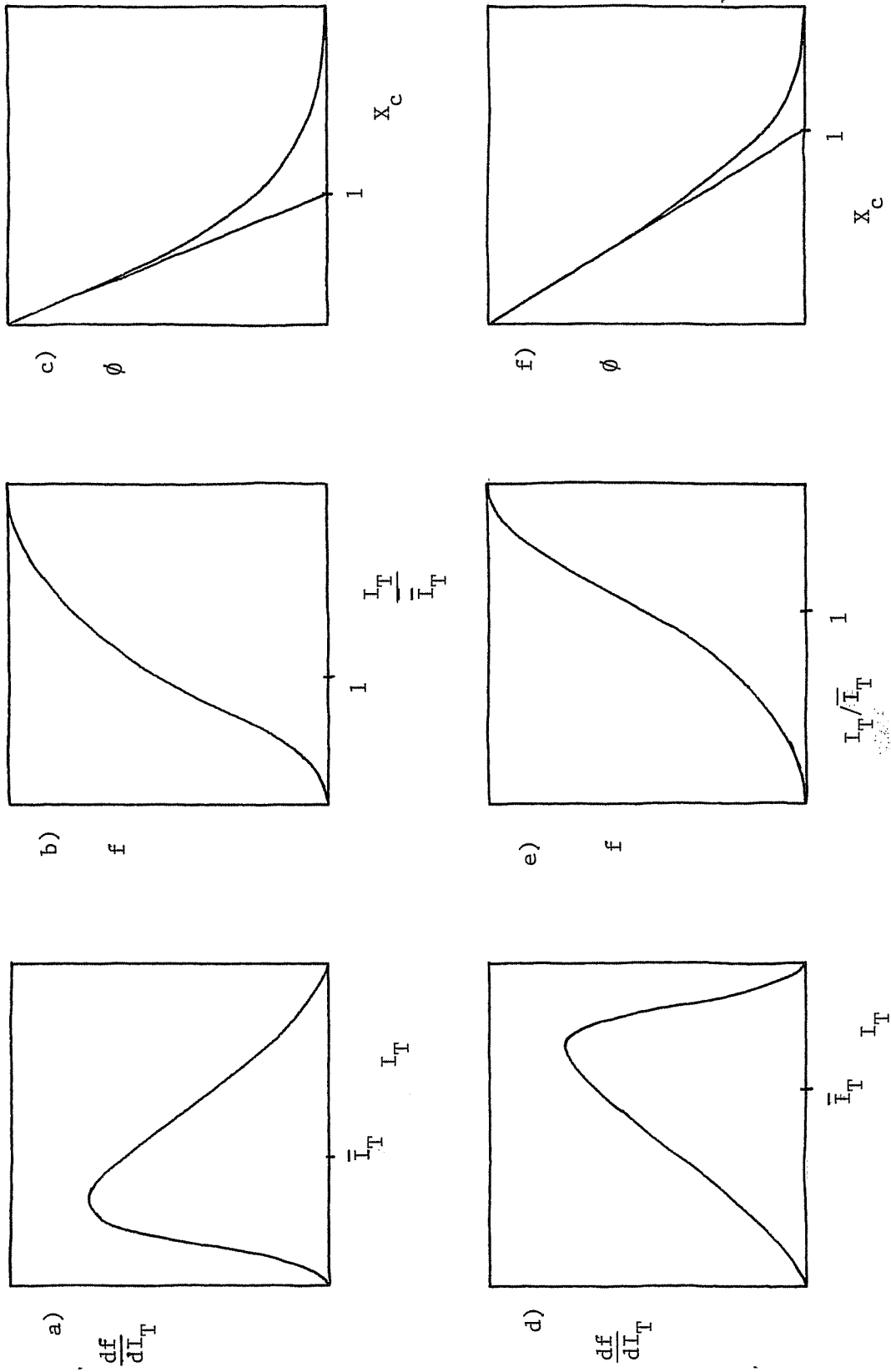


Figure 1.2-3 Effect of Insolation Distribution Skew on the Utilization Function

1.3 Basic Equations

In the preceding sections, utilizability has been defined in terms of radiation incident on a surface of arbitrary orientation. For the most part, however, solar radiation data are available only on horizontal surfaces. In this section conversion factors are given for estimating tilted surface intensities from horizontal data. Some other necessary quantities must first be defined. All of the equations in this section can be found in reference (6). The original sources will not be referenced here.

The daily clearness index, K , is defined by:

$$K = H/H_o \quad (1.3-1)$$

where: H = Daily total horizontal surface insolation

H_o = Daily extraterrestrial insolation on a
horizontal surface

The monthly-average daily clearness index is similarly defined, using average rather than daily insolation:

$$\bar{K} = \bar{H}/\bar{H}_o \quad (1.3-2)$$

Daily extraterrestrial radiation is given by:

$$H_o = \frac{G_{sc}}{\pi} \left[1 + 0.033 \cos \left(\frac{360n}{365} \right) \right] \left[\cos L \cos \delta \sin \omega_s + \frac{2\pi\omega_s}{360} \sin L \sin \delta \right] \quad (1.3-3)$$

where:

G_{sc} = solar constant (1353 W/m^2)

n = day of the year

L = latitude

δ = declination (Eq. 1.3-4)

ω_s = sunset hour angle (Eq. 1.3-5)

Equation 1.3-3 can also be used to determine \bar{H}_o by using the values of n listed on page 12 of Duffie and Beckman (6). The declination is given by:

$$\delta = 23.45 \sin \left[\frac{360}{365} (284 + n) \right] \quad (1.3-4)$$

and the sunset hour angle is defined by:

$$\omega_s = \arccos (-\tan L \tan \delta) \quad (1.3-5)$$

Clearness indices can also be defined on an hourly basis. The hourly clearness index is given the symbol k :

$$k = I/I_o \quad (1.3-6)$$

Similarly, the monthly-average hourly clearness index is

$$\bar{k} = \bar{I}/\bar{I}_o \quad (1.3-7)$$

Hourly extraterrestrial radiation is given by:

$$I_o = G_{sc} \cos \theta_z \left[1 + 0.033 \cos \left(\frac{360n}{365} \right) \right] \quad (1.3-8)$$

where θ_z is the solar zenith angle:

$$\cos \theta_z = \sin L \sin \delta + \cos L \cos \delta \cos \omega \quad (1.3-9)$$

where ω is the hour angle: zero at noon, 15° per hour after noon. Again, equation 1.3-8 can be used to find \bar{I}_0 by using the values of n given by Duffie and Beckman (6); these are the days on which the extraterrestrial radiation is closest to the monthly average value.

The ratio of instantaneous beam radiation on a tilted surface to beam radiation on a horizontal surface is a strictly geometric term, given by the following equation:

$$\begin{aligned} \frac{I_{b,T}}{I_{b,h}} = R_b = (\cos \theta_z)^{-1} & (\sin \delta \sin L \cos \beta - \sin \delta \cos L \sin \beta \cos \gamma \\ & + \cos \delta \cos L \cos \beta \cos \omega \\ & + \cos \delta \sin L \sin \beta \cos \gamma \cos \omega \\ & + \cos \delta \sin \beta \sin \gamma \sin \omega) \end{aligned} \quad (1.3-10)$$

where β = slope of surface

γ = surface azimuth angle (west positive)

and all other terms are defined above.

The total radiation on a tilted surface can be thought of as consisting of three components: beam radiation, diffuse sky radiation, and ground-reflected radiation:

$$I_T = I_{b,T} + I_{d,T} + I_{r,T} \quad (1.3-11)$$

Assuming that diffuse radiation is uniform over the entire sky, the ratio of total hourly radiation on a tilted surface to that on a horizontal surface is estimated by:

$$\frac{I_T}{I} = R = \left(1 - \frac{I_d}{I}\right) R_b + \frac{I_d}{I} \left(\frac{1 + \cos\beta}{2}\right) + \rho \left(\frac{1 - \cos\beta}{2}\right) \quad (1.3-12)$$

where ρ is the reflectance of the ground. R_b varies continuously throughout the day, but can be considered constant over an hour. Similar equations can be written for the monthly-average hourly ratio, \bar{I}_T/\bar{I} , in terms of a monthly-average diffuse ratio, \bar{I}_d/\bar{I} , and for the daily and monthly-average daily ratios, H_T/H and \bar{H}_T/\bar{H} , in terms of H_d/H and \bar{H}_d/\bar{H} . Daily calculations require the use of \bar{R}_b , an effective average value of R_b , which can be calculated from an equation developed by Klein and Theilacker (17). The symbol \bar{R} is generally used to represent H_T/H ; the symbol \bar{R} will be used here to represent \bar{I}_T/\bar{I} .

Numerous correlations have been proposed for I_d/I and \bar{I}_d/\bar{I} as functions of \bar{k} , and for H_d/H and \bar{H}_d/\bar{H} as functions of \bar{K} . Appropriate correlations will be given later as the need arises.

The relationships between tilted-surface and horizontal radiation can now be expressed simply:

$$I_T = IR = I_o k R \quad (1.3-13)$$

$$H_T = HR = H_o K R \quad (1.3-14)$$

Finally, ϕ can be defined in terms of horizontal radiation:

$$\phi = \frac{\int_{I_c}^{(RI)_{\max}} (RI - I_c) P(I) d(RI)}{\int_0^{(RI)_{\max}} (RI) P(I) d(RI)} \quad (1.3-15)$$

where $P(I)$ represents the long-term average probability of I , also referred to as the probability density function:

$$P(I) = \frac{df}{dI_T} = \frac{df}{d(RI)} \quad (1.3-16)$$

This expression for ϕ is equivalent to the integration described in the previous section.

1.4 Review of Generalized Utilizability: Graphical Methods

A lack of availability of hourly weather data prompted Whillier (29) to suggest that daily insolation values could be used to represent hourly statistical patterns. Liu and Jordan (19) plotted cumulative frequency distributions of hourly and daily tilted-surface insolation ratios, I_T/\bar{I}_T and H_T/\bar{H}_T , and found that they did in fact have very similar shapes. They also found that for measured daily horizontal radiation data, the shape of the cumulative frequency distribution depends primarily on the monthly-average clearness index \bar{K} , and is nearly independent of latitude and declination. Using daily horizontal measurements from several locations, they generated generalized cumulative frequency distributions of K at several values of \bar{K} (Figure 1.4-1). With the relationships given in the

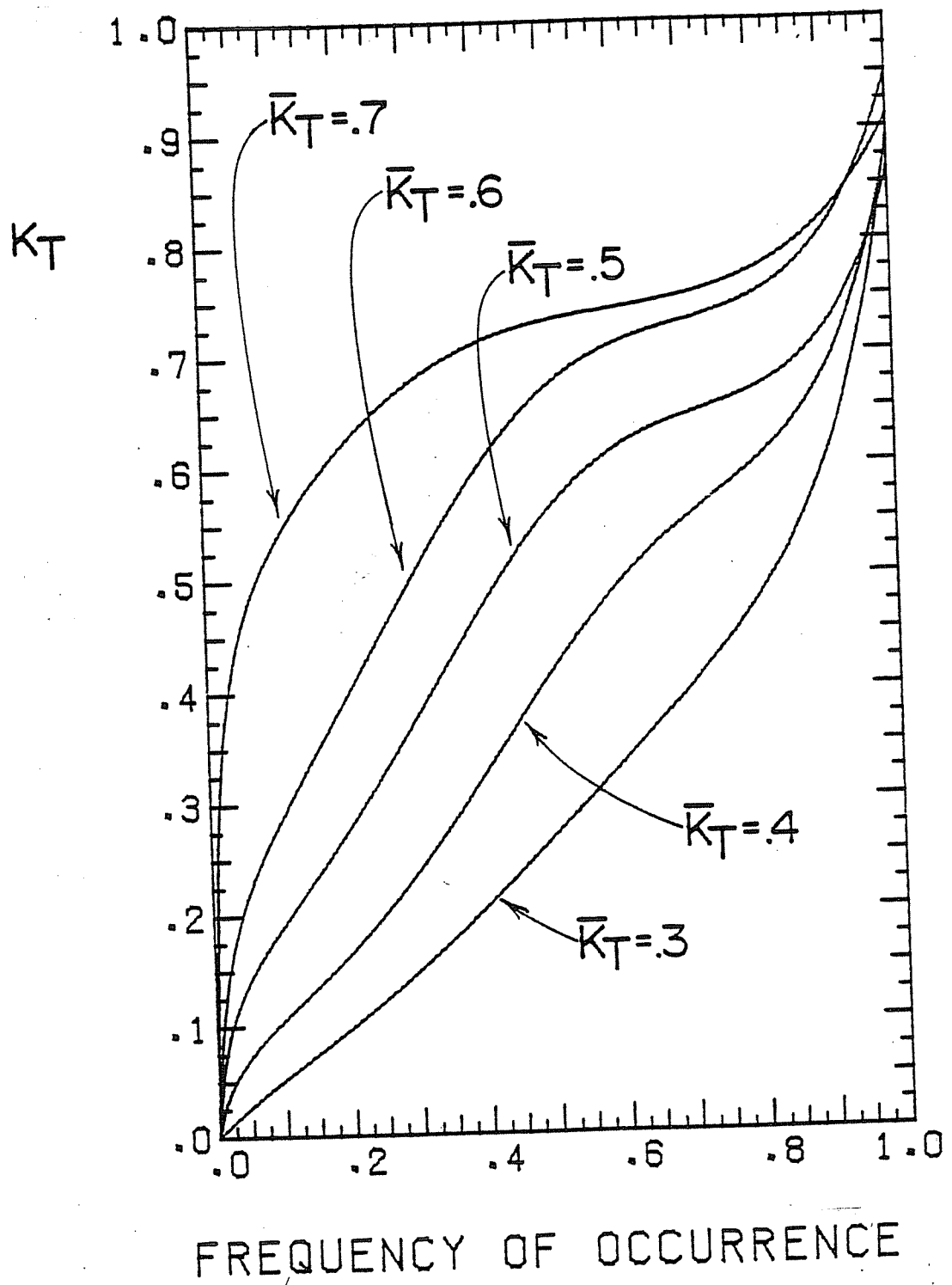


Figure 1.4-1: Cumulative Frequency Distribution of the Daily Clearness Index. From Odegard (21); adapted from Liu and Jordan (18).

previous section these can be converted to cumulative frequency distributions of H_T/\bar{H}_T for any collector slope. These were integrated graphically to obtain the generalized ϕ -curves of Figure 1.4-2. At a given \bar{K} they found the curves to be primarily a function of \bar{R}_b , though the relationship is inexact as indicated by the fact that the curves for a horizontal surface and for $\bar{R}_b = 1$ do not coincide.

Liu and Jordan (18) recommend the following empirical relationship between hourly and daily diffuse radiation:

$$\frac{\bar{I}_d}{\bar{H}_d} = \frac{\bar{I}_o}{\bar{H}_o} \quad (1.4-1)$$

Based on curves presented by Liu and Jordan, Collares-Pereira and Rabl (4) have proposed an equation correlating \bar{k} and \bar{K} :

$$\bar{k} = \bar{K}(a + b \cos \omega) \quad (1.4-2)$$

where: $a = 0.409 + 0.5016 \sin (\omega_s - 60^\circ)$

$$b = 0.6609 - 0.4767 \sin (\omega_s - 60^\circ)$$

and ω_s is the sunset hour angle given by Equation 1.3-5. Using these relationships, hourly diffuse fractions can be estimated from the daily diffuse fraction:

$$\frac{\bar{I}_d}{\bar{I}} = \frac{\bar{H}_d}{\bar{H}} (a + b \cos \omega)^{-1} \quad (1.4-3)$$

Erbs (7) recommends the following correlation for the daily average diffuse fraction:

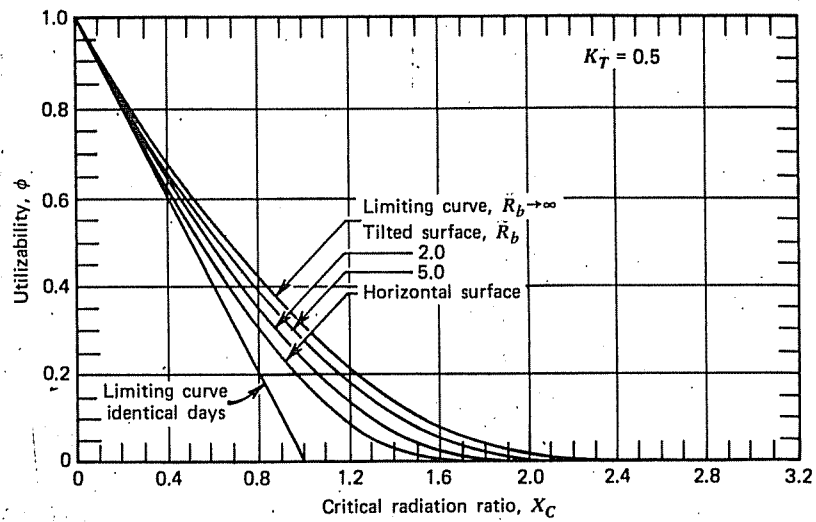
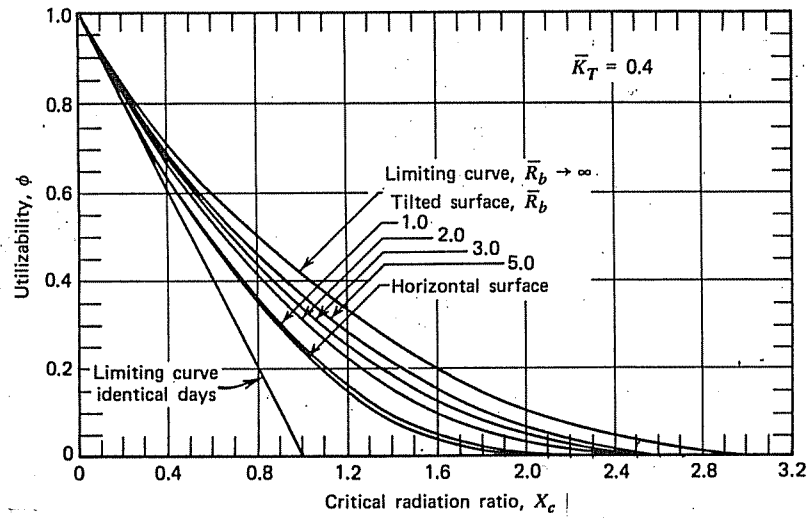


Figure 1.4-2: Generalized ϕ -Curves. From Duffie and Beckman (6); adapted from Liu and Jordan (19).

$$\frac{\overline{H}_d}{\overline{H}} = 1.317 - 3.023 \overline{K} + 3.372 \overline{K}^2 - 1.76 \overline{K}^3 \quad (1.4-4)$$

Thus hourly average radiation incident on a tilted surface can be estimated from the daily average clearness index with the use of Equations 1.4-2 through 1.4-4 and 1.3-8 through 1.3-13.

Odegard (21) has re-examined the effect of collector slope on the generalized utilizability curves. Rewriting equation 1.3-12,

$$R = R_b + (I_d/I) \left(\frac{1 + \cos\beta}{2} - R_b \right) + \rho \left(\frac{1 - \cos\beta}{2} \right) \quad (1.4-5)$$

he notes that R is constant for all I when $R_b = (1 + \cos\beta)/2$. This observation, when applied to Equation 1.3-15, leads to the conclusion that the utilizability function is identical for surfaces of any orientation when R is constant, since a constant R can be cancelled from the numerator and denominator of the equation. On this basis Odegard defines an hourly beam-diffuse view factor

$$V_{bd} = R_b - \frac{1 + \cos\beta}{2} \quad (1.4-6)$$

and its daily counterpart,

$$\overline{V}_{bd} = \overline{R}_b - \frac{1 + \cos\beta}{2} \quad (1.4-7)$$

and shows that relating generalized ϕ -curves to \overline{V}_{bd} rather than \overline{R}_b reduces the uncertainty in ϕ due to the effect of collector slope by about a factor of two.

Using curve fits (3) to the generalized daily clearness index distributions of Liu and Jordan, and a curve fit (13) to the Liu and

Jordan daily diffuse fraction curve, Odegard generated, by numerical integration, a set of generalized ϕ -curves with correlating parameters \bar{k} and V_{bd} . These are reproduced in Figure 1.4-3. Odegard notes that the use of these hourly rather than daily correlating parameters makes it possible to use these curves for other than south-facing surfaces, although their accuracy for off-south orientations has not been examined.

The influence of \bar{k} can be explained qualitatively by Figure 1.2-3. The probability density function df/dI_T is skewed toward low I_T when \bar{k} is low, resulting in long tails on the ϕ -curves. The influence of V_{bd} is slightly less direct but can be explained qualitatively in terms of Figure 1.2-2. If R is constant, the shape of the distribution of I_T/\bar{I}_T remains unaffected by R since I_T and \bar{I}_T are multiplied by the same constant. Rewriting the equation for R :

$$R = R_b + \rho \left(\frac{1 - \cos\beta}{2} \right) - (I_d/I)V_{bd} \quad (1.4-8)$$

Since R_b is essentially constant for a specified hour, the variability of R is due to the variability of the diffuse fraction. When the intensity of horizontal radiation is low, I_d/I is large and (for positive V_{bd}) R is low. Similarly R is large when the horizontal radiation intensity is high. The net effect is a broadening of the distribution of I_T . V_{bd} serves as an indicator of the extent to which the distribution is broadened.

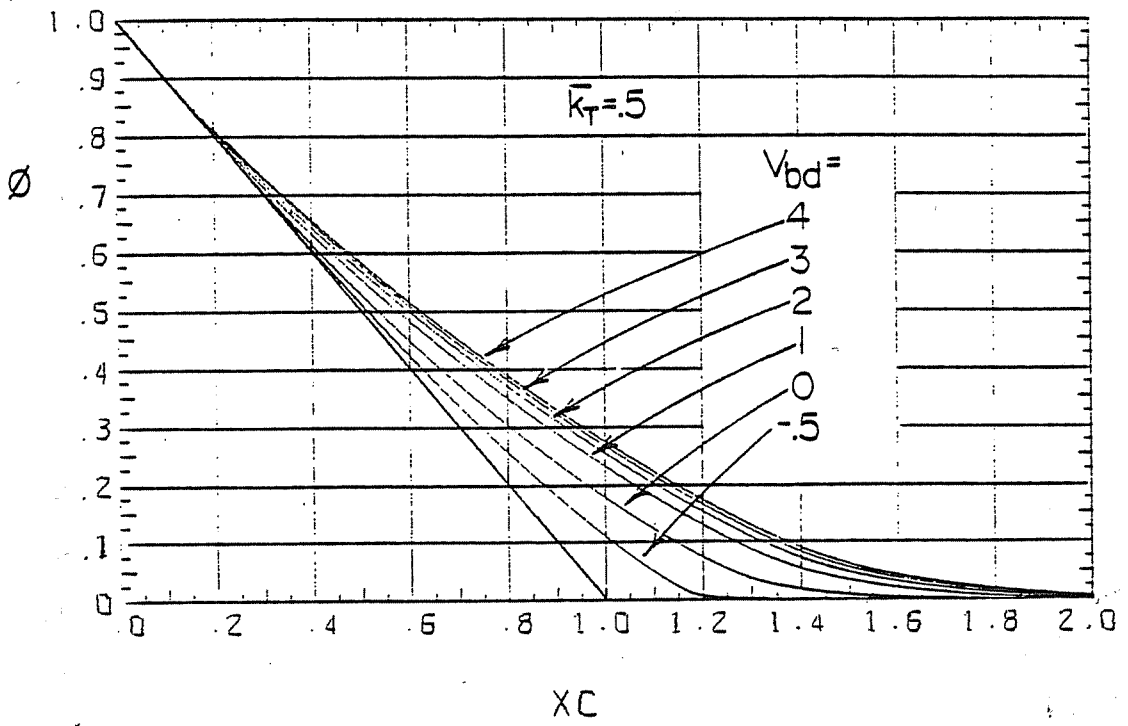
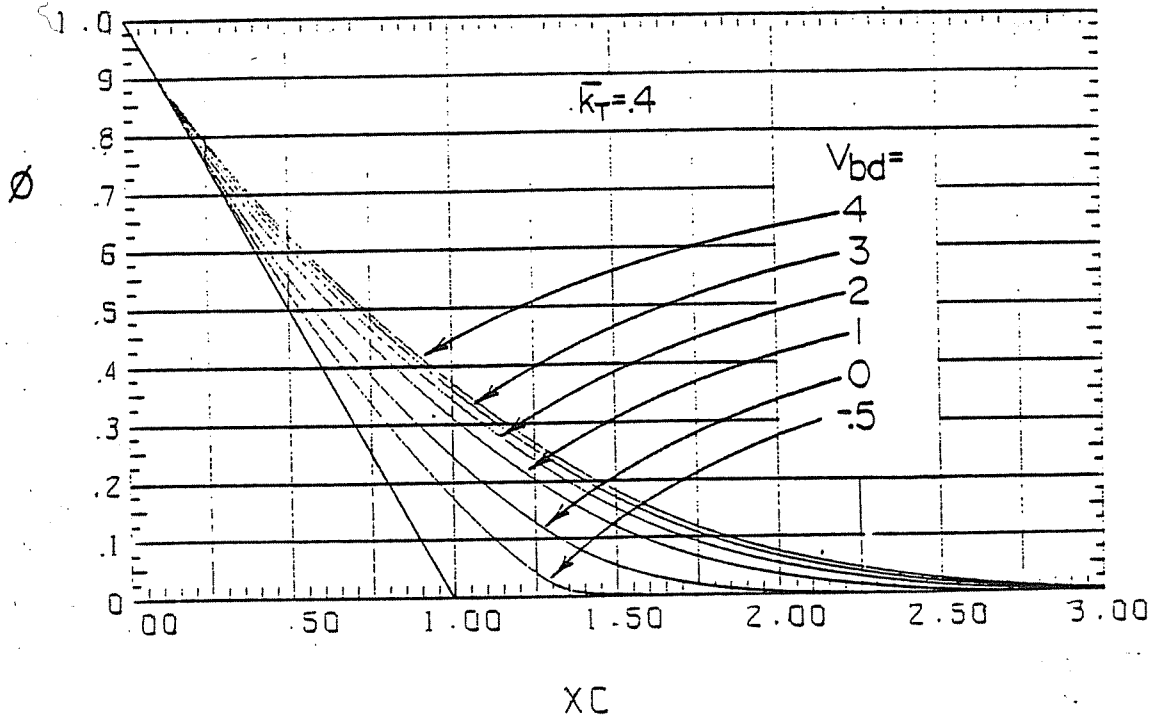


Figure 1.4-3: Generalized Hourly ϕ -Curves. From Odegard (21).

1.5 Analytical Methods

Huget (12) and Odegard (21) have developed equations for calculating hourly utilizability from monthly-average weather statistics. Both methods are based on analytical integration of curve fits to the generalized clearness index distribution curves of Liu and Jordan (Figure 1.4-1). The resulting equations differ in two important respects but have not been compared directly; the method of Huget is given below for reasons to be explained.

An equation for ϕ can be written in terms of the hourly clearness index k , the tilted to horizontal radiation ratio R , and the probability density function $P(k)$:

$$\phi = \frac{\int_{k_c}^{k_{\max}} \left[k \left[R_b + \rho \left(\frac{1 - \cos \beta}{2} \right) \right] + k \left(\frac{I_d}{I} \right) \left(\frac{1 + \cos \beta}{2} - R_b \right) - \frac{I_c}{I_o} \right] P(k) dk}{\int_0^{k_{\max}} \left[k \left[R_b + \rho \left(\frac{1 - \cos \beta}{2} \right) \right] + k \left(\frac{I_d}{I} \right) \left(\frac{1 + \cos \beta}{2} - R_b \right) \right] P(k) dk} \quad (1.5-1)$$

The functional form proposed by Huget for the probability density function $P(k)$ is given by:

$$P(k) = C \left(1 - \frac{k}{k_{\max}} \right) e^{-\gamma k} \quad (1.5-2)$$

where k_{\max} represents the maximum possible value of the hourly clearness index. Approximating k_{\max} as a constant for all locations and hours, Huget's curve fit yields

$$k_{\max} = 0.864 \quad (1.5-3)$$

and γ is a function of \bar{k} only, as given in Table 1.5-1 and Figure 1.5-1.

The diffuse fraction I_d/I used by Huget is the one suggested by Orgill and Hollands (22):

$$\frac{I_d}{I} = P_i - q_i k, \quad i = 1, 3 \quad (1.5-4)$$

$$\begin{aligned} \text{where } P_1 &= 1.0, & q_1 &= 0.249, & k &< 0.35 \\ P_2 &= 1.557, & q_2 &= 1.84, & 0.35 &\leq k \leq 0.75 \\ P_3 &= 0.177, & q_3 &= 0, & k &> 0.75 \end{aligned}$$

The critical clearness index k_c is the value of k at which the integrand in the numerator of equation 1.5-1 is zero. This condition leads to:

$$k_c^2 q_i V_{bd} + k_c \left[R_b + \rho \left(\frac{1 + \cos\beta}{2} \right) - P_i V_{bd} \right] - \frac{I_c}{I_o} = 0 \quad (1.5-5)$$

Equation 1.5-5 has five possible solutions: two at $i = 1$, two at $i = 2$, and one at $i = 3$. Roots which do not lie in the appropriate range of k from Equation 1.5-4 can be rejected; in most cases a single valid solution for k_c remains. However, as Huget demonstrates, in some cases two or even three valid solutions for k_c can occur. This is due to the fact that the ratio of diffuse to extra-terrestrial radiation, I_d/I_o , has a maximum at $k = 0.42$ and a minimum at $k = 0.75$. When two values of k_c are found, the appropriate procedure is to integrate the numerator of Equation 1.5-1 from k_{c1} to k_{c2} rather than from k_c to k_{\max} . When three values occur, the inte-

Table 1.5-1

 γ (from Eq. 1.5-2) vs. Monthly-Average Hourly Clearness Index

\bar{k}	γ	\bar{k}	γ
.288	.0000	.55	5.8206
.29	.0481	.56	6.0911
.30	.2848	.57	6.3724
.31	.5158	.58	6.6660
.32	.7419	.59	6.9735
.33	.9637	.60	7.2968
.34	1.1819	.61	7.6382
.35	1.3971	.62	8.0002
.36	1.6097	.63	8.3860
.37	1.8204	.64	8.7992
.38	2.0296	.65	9.2442
.39	2.2378	.66	9.7262
.40	2.4454	.67	10.2516
.41	2.6529	.68	10.8284
.42	2.8607	.69	11.4661
.43	3.0693	.70	12.1769
.44	3.2790	.71	12.9760
.45	3.4905	.72	13.8827
.46	3.7042	.73	14.9223
.47	3.9205	.74	16.1276
.48	4.1400	.75	17.5433
.49	4.3632	.76	19.2306
.50	4.5909	.77	21.2764
.51	4.8236	.78	23.8093
.52	5.0621	.79	27.0268
.53	5.3071	.80	31.2497
.54	5.5596		

GAMMA VERSUS MONTHLY-AVERAGE HOURLY CLEARNESS INDEX

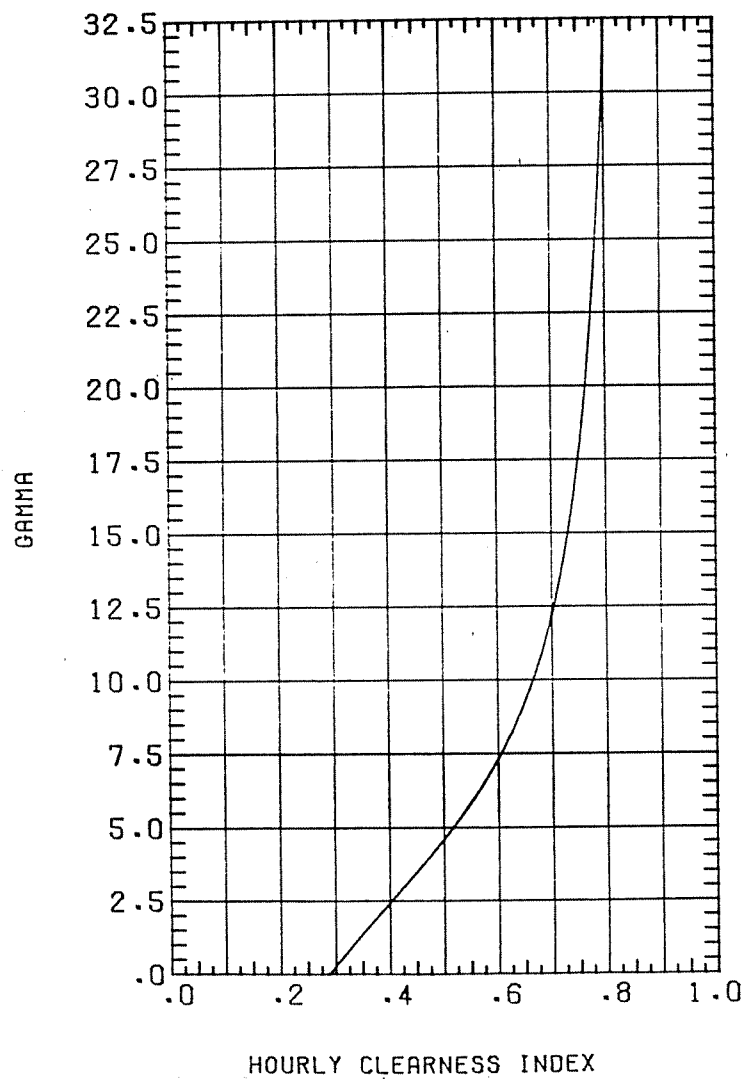


Figure 1.5-1: Gamma (from Eq. 1.5-2) vs. the Hourly Clearness Index

gral is evaluated twice, from k_{c1} to k_{c2} and from k_{c3} to k_{max} .

Huget provides expressions for evaluating the integrals $\int_x^y P(k) dk$, $\int_x^y k P(k) dk$, and $\int_x^y k(I_d/I) P(k) dk$. These expressions can be combined into a single equation:

$$\phi = \frac{\left[A(k) e^{\gamma k} \right]_{k_c}^{k_{max}} - \frac{I_c}{I_o} \left[\left(\epsilon_o - \frac{\epsilon_1(k)}{k_{max}} \right) e^{\gamma k} \right]_{k_c}^{k_{max}}}{\left[A(k) e^{\gamma k} \right]_o^{k_{max}}} \quad (1.5-6)$$

$$\text{where } A = \left[\epsilon_1(k) - \frac{\epsilon_2'(k)}{k_{max}} \right] \left[R_b - p_i \left(R_b - \frac{1+\cos\beta}{2} \right) + \rho \left(\frac{1-\cos\beta}{2} \right) \right] \\ + q_i \left(\epsilon_2(k) - \frac{\epsilon_3(k)}{k_{max}} \right) \left(R_b - \frac{1+\cos\beta}{2} \right)$$

$$\epsilon_o = \frac{1}{\gamma} \text{ [from Table 1.5-1]}$$

$$\epsilon_1(k) = \epsilon_o (k - \epsilon_o)$$

$$\epsilon_2(k) = \epsilon_o (k^2 - 2\epsilon_1(k))$$

$$\epsilon_3(k) = \epsilon_o (k^3 - 3\epsilon_2(k))$$

and p_i and q_i are given in Equation 1.5-4.

Use of this equation requires evaluation of $\epsilon_1(k)$, $\epsilon_2(k)$, $\epsilon_3(k)$, and $A(k)$ at $k = 0$, $k = 0.35^-$, $k = 0.35^+$, $k = 0.75^-$, $k = 0.75^+$, $k = k_{max}$, and $k = k_c$. Additional evaluations are required when more than one value of k_c is obtained from Equation 1.5-5. A computer program which performs these calculations is listed in Appendix A.

The equation for ϕ developed by Odegard differs from the above equation in two important respects. First, Odegard uses for the probability density function a form derived by Bendt et al. (1) from purely statistical considerations on the assumption that the occurrence of k is random, i.e., the value of k for an hour on one day is entirely independent of the value of k for the same hour on the previous day. The form used by Huget more nearly matches the generalized distribution curves of Liu and Jordan.

Second, Odegard uses (on an hourly basis) a curve fit (13) to the Liu and Jordan daily diffuse fraction curve:

$$\frac{I_d}{I} = 1.0045 + 0.04349k - 3.5227k^2 + 2.6313k^3 \quad (1.5-7)$$

An advantage to the use of this diffuse correlation is that Odegard's version of Equation 1.5-6 is evaluated over a single set of limits of integration. A disadvantage is that the critical clearness index k_c must be found using an iterative numerical method, and the occasional existence of multiple values of k_c was not recognized; consequently the numerical method sometimes picks an inappropriate value of k_c , and sometimes fails to converge on any value.

Either method is suitable for use with non-south-facing surfaces. This topic is discussed further in the following chapter.

Chapter 2. Curve-Fitting the Hourly Utilizability Function

2.1 Introduction: Generation of a Data Base

The goal of the work described in this chapter is the development of a relatively simple alternative to Equation 1.5-6 for estimating hourly utilizability. The approach taken here is to directly correlate values of ϕ derived from many years of hourly horizontal insolation measurements, rather than to integrate a frequency distribution correlation. The methods used in the development of the correlation will be described in some detail.

The data on which the correlation is based are derived from 23 years of hourly horizontal radiation measurements in Madison, Wisconsin, 23 years in Albuquerque, New Mexico, and 15 years in Seattle, Washington (26). Since the integration of frequency distributions to obtain values of ϕ will tend to smooth out location-dependent fluctuations, it was felt that a sufficiently "generalized" result could be obtained from three locations. The locations were selected to cover a very broad range of average hourly clearness index values and a reasonable range of latitudes.

Values of ϕ were obtained by numerical integration using computer programs listed by Odegard (21). With a single exception to be discussed later, all tilted-surface calculations made use of the hourly diffuse fraction correlation recommended by Erbs (7):

$$\frac{I_d}{I} = \begin{cases} 1.0 - 0.09k, & k \leq 0.22 \\ 0.9511 - 0.1604k + 4.388k^2 - 16.638k^3 + 12.336k^4, & 0.22 < k \leq 0.80 \\ 0.165, & k > 0.80 \end{cases} \quad (2.1-1)$$

For each sunlit hour of each month, ϕ was calculated at fifty values of X_c in equal increments from $X_c = 0$ to $X_c = 2.45$, using values of I_T calculated from the horizontal data by Equations 1.3-13, 1.3-12, and 2.1-1. Long-term averages of \bar{I}_T and \bar{k} were obtained at the same time for use in developing the correlation. Pairs of (X_c, ϕ) values in which $\phi = 0$ were then eliminated from the data. Except where otherwise noted, attention was restricted to hours between 6 AM and 6 PM for which R_b is positive throughout the hour for the whole month. The correlation is based entirely on data for south-facing surfaces at several slopes: 0° , 60° , and 90° in Madison; 0° and 90° in Albuquerque; 30° and 90° in Seattle. Table 2.1-1 summarizes the hours considered in developing the correlation. The considerable expense of generating the data discouraged the use of more locations or slopes.

Data were also generated for a 43° surface in Madison at an azimuth angle of 45° and for a 90° surface in Madison at an azimuth angle of 90° (due west). The 45° azimuth data were generated using a correlation to the diffuse fraction curve of Liu and Jordan (13), rather than Equation 2.1-1. Odegard (21) has shown that ϕ is fairly insensitive to the choice of a diffuse correlation, since I_d/I is present in both the numerator and the denominator of ϕ . The 90°

Table 2.1-1

Hours considered in developing the correlation for ϕ

Month	Number of hours considered (azimuth=0°)							Times of day considered (non-zero azimuth) A.M.-P.M.	
	Madison Slope = :			Albuquerque Slope = :		Seattle Slope = :		Azimuth=45° Slope=43°	Azimuth=90° Slope=90°
	0°	60°	90°	0°	90°	30°	90°		
Jan	8	8	8	8	8	8	8	9-4	12-4
Feb	8	8	8	10	10	8	8	9-4	12-4
Mar	10	10	10	10	10	10	10	9-5	12-5
Apr	12	10	10	12	10	12	10	8-6	12-6
May	12	10	8	12	8	12	10	8-6	12-6
Jun	12	10	8	12	6	12	8	8-6	12-6
Jul	12	10	8	12	8	12	8	8-6	12-6
Aug	12	10	10	12	10	12	10	8-6	12-6
Sep	10	10	10	10	10	10	10	8-5	12-5
Oct	10	10	10	10	10	8	8	9-5	12-5
Nov	8	8	8	8	8	8	8	9-4	12-4
Dec	8	8	8	8	8	8	8	9-4	12-4

azimuth data were generated from 15 years of hourly measurements rather than 23 years. The hours considered for these non-south orientations are also listed in Table 2.1-1.

2.2 Derivation of Form for Correlation

From examination of graphs of ϕ vs. X_c such as those in Figure 1.4-3 it was reasoned that the curves could be adequately represented by a family of hyperbolas, as in Figure 2.2-1.

A hyperbola with its center at (h, k) and its transverse axis vertical is defined by:

$$\frac{(y - k)^2}{a^2} - \frac{(x - h)^2}{b^2} = 1 \quad (2.2-1)$$

where a is half the length of the transverse axis and b is half the length of the conjugate axis.

It is useful to define a parameter X_m as the lowest value of X_c at which $\phi = 0$:

$$X_m = X_c \Big|_{\phi=0} = \frac{I_{T, \max}}{\bar{I}_T} \quad (2.2-2)$$

As indicated in Figure 2.2-1, it is assumed that the vertex of the hyperbola coincides with X_m . The possibility of relaxing this restriction is discussed in Section 2.5. The assumption is equivalent to requiring that the slope of the curve is zero at $\phi = 0$, and specifies that $h = X_m$ and $k = -a$ in Equation 2.2-1.

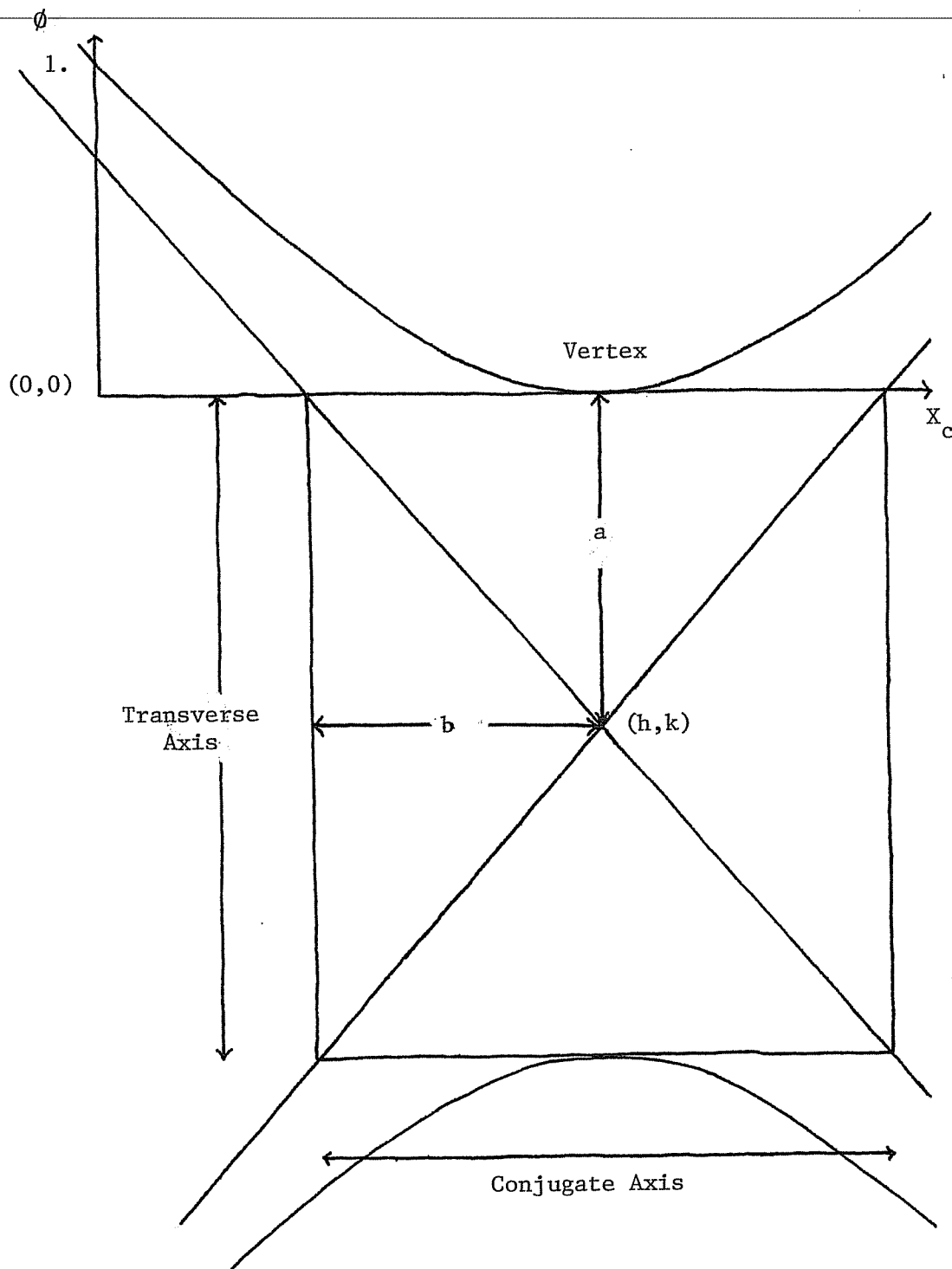


Figure 2.2-1: Form of Correlation for ϕ

Replacing y with ϕ and X with X_c , Equation 2.2-1 can be rearranged into the following forms:

$$\phi^2 + 2a\phi - \frac{a^2}{b^2} (X_c - X_m)^2 = 0 \quad (2.2-3)$$

and

$$\phi = -a \pm \sqrt{a^2 + \frac{a^2}{b^2} (X_c - X_m)^2} \quad (2.2-4)$$

The requirement that $\phi = 1$ when $X_c = 0$ can be applied to Equation 2.2-3, leading to:

$$\frac{1}{b^2} = \frac{1 + 2a}{a^2 X_m^2} \quad (2.2-5)$$

Substituting this expression into Equation 2.2-4:

$$\phi = -a \pm \sqrt{a^2 + (1 + 2a) \left(\frac{X_c - X_m}{X_m} \right)^2} \quad (2.2-6)$$

The slope of the curve at any point is given by

$$\frac{d\phi}{dX_c} = \frac{(1 + 2a) (X_c - X_m)}{X_m^2 \sqrt{a^2 + (1 + 2a) \left(\frac{X_c - X_m}{X_m} \right)^2}} \quad (2.2-7)$$

At $X_c = 0$, the slope of the curve should in theory be -1. However, it is quite possible that a better overall fit to the data can be obtained if the slope at $X_c = 0$ is permitted to vary. To allow for this possibility, a new parameter s is defined as the negative of the slope at $X_c = 0$:

$$s = - \left. \frac{d\phi}{dX_c} \right|_{X_c = 0} \quad (2.2-8)$$

It is expected that s will be in the general vicinity of 1. Combining Equations 2.2-8 and 2.2-7 with $X_c = 0$, and solving for a :

$$a = \frac{sX_m - 1}{2 - sX_m} \quad (2.2-9)$$

By definition, X_m cannot be less than one. The limiting curve for identical days is obtained from Equation 2.2-6 when $s = 1$ and $X_m = 1$:

$$\phi = 1 - X_c \quad (2.2-10)$$

Interpreting Equation 2.2-6 as a hyperbola, the parameter a represents a distance, taken as positive, as shown in Figure 2.2-1. From Equation 2.2-9, a is positive only for $1 < sX_m < 2$. The situation for $sX_m \geq 2$ requires further attention.

Consider first the case where $sX_m = 2$, for which a becomes infinite.

Substituting Equation 2.2-5 into Equation 2.2-3 and dividing through by a :

$$\frac{\phi^2}{a} + 2\phi - \left(\frac{1}{a} + 2\right) \left(\frac{X_m - X_c}{X_m}\right)^2 = 0 \quad (2.2-11)$$

It is apparent that

$$\lim_{a \rightarrow \infty} \phi = \left(1 - \frac{X_c}{X_m}\right)^2 \quad (2.2-12)$$

Thus Equation 2.2-6 describes a hyperbola for $1 < sX_m < 2$ and a parabola at $sX_m = 2$. For $sX_m > 2$ the equation can be shown to represent an ellipse, with the special case of a circle occurring at $sX_m = 1 + \sqrt{2}$.

To obtain a positive value of ϕ between 0 and 1, the square root term in Equation 2.2-6 must be added when $sX_m < 2$ and subtracted when $sX_m > 2$. One way to ensure that the appropriate result is obtained is to include absolute values in the expression. Thus, the proposed form for the correlation is given by:

$$\phi = \begin{cases} 0, & X_c \geq X_m \\ \left(1 - \frac{X_c}{X_m}\right)^2, & X_m = 2 \\ \left| |a| - \sqrt{a^2 + (1 + 2a) \left(\frac{X_m - X_c}{X_m}\right)^2} \right| & \text{otherwise} \end{cases} \quad (2.2-13)$$

where a is given by Equation 2.2-9.

2.3 Empirical Correlation Procedure

Assuming $s = 1$, Equation 2.2-13 has only one degree of freedom, X_m . A second degree of freedom can be added by allowing s to vary. The first question to be answered is whether the equation is capable of adequately representing the curves obtained from integration of long-term weather data.

For each location and slope, for each hour of each month, a non-linear regression program was used to find the values of X_m and s which minimize the root-mean-square (rms) error of ϕ , i.e., the

standard deviation of the differences between the actual values of ϕ and the corresponding estimated values from Equation 2.2-13. This procedure was repeated to find the optimum values of X_m alone when $s = 1$. Thus two sets of optimum values of X_m were obtained: one set corresponding to optimum values of s , and a second set when $s = 1$. These values are optimal in the sense that they minimize the difference (i.e., the rms error) between values of ϕ obtained from many years of weather data and values of ϕ obtained from Equation 2.2-13. In the following pages, both sets of optimum values of X_m are designated $X_{m,opt}$ and are distinguished by specifying whether s is variable or constant. The mean and range of optimum values of s will be discussed later in this section. Values of X_m derived from correlations to $X_{m,opt}$ are denoted $X_{m,est}$; $X_{m,act}$ will be used to indicate the minimum value of X_m at which the actual value of ϕ is less than 1×10^{-5} . "Actual" values of X_m and ϕ are calculated from many years of hourly horizontal data using Equations 1.3-12 and 2.1-1.

When $X_{m,opt}$ is used in Equation 2.2-13 to estimate ϕ , the residual error is a minimum. Table 2.3-1 lists values of the minimum rms error of ϕ for morning hours from 8 A.M. to noon for a surface tilted at 60° in Madison. Each number in the table represents the standard deviation of 25 to 50 observations, scaled such that ϕ varies from 0 to 100. Allowing s to vary does decrease the errors, although for most months and hours the improvement over the simpler one-parameter model is small. The magnitude of the errors is essen-

Table 2.3-1

Unavoidable error from the use of Eq. 2.2-13: Hourly Results

Madison, slope = 60°, azimuth = 0°, morning hours

Month	2-parameter model:				1-parameter model:			
	X_m and S selected for each hour by non-linear regression				S= 1; X_m selected for each hour by non-linear regression			
	Minimum RMS Error in ϕ (%)				Minimum RMS Error in ϕ (%)			
	<u>Hour</u>				<u>Hour</u>			
	<u>8-9</u>	<u>9-10</u>	<u>10-11</u>	<u>11-12</u>	<u>8-9</u>	<u>9-10</u>	<u>10-11</u>	<u>11-12</u>
Jan	1.12	1.21	1.06	1.04	1.72	1.82	1.61	1.68
Feb	1.40	1.47	1.30	1.14	2.40	2.25	1.84	1.54
Mar	1.12	1.16	1.11	1.08	1.60	1.64	1.64	1.62
Apr	1.07	1.15	1.27	1.27	1.28	1.37	1.62	1.50
May	0.73	0.83	0.84	0.68	0.95	1.09	1.09	0.89
Jun	0.63	0.75	0.73	0.54	0.75	0.92	0.85	0.61
Jul	0.63	0.66	0.52	0.47	0.81	0.73	0.57	0.57
Aug	0.69	0.61	0.52	0.56	0.93	0.79	0.59	0.71
Sep	0.98	1.07	1.02	0.84	1.38	1.58	1.47	1.27
Oct	0.66	0.92	1.11	1.09	0.91	1.49	1.80	1.86
Nov	0.30	1.29	1.40	1.41	0.64	1.46	1.68	1.87
Dec	0.25	1.30	1.34	1.24	0.41	1.51	1.63	1.58

tially independent of time of day, but tends to be larger for winter months than for summer months. Similar results are obtained for afternoon hours and for other tilts and locations.

Table 2.3-2 lists the combined rms error for all hours and months, using the one-parameter model, for each location and slope. Apparently the form of Equation 2.2-13 is quite adequate, even when s is set to 1, provided that an adequate correlation for X_m can be found.

The optimum values of X_m and s , or of X_m alone when $s = 1$, were examined using MINITAB (23), a linear statistics program. The procedure followed in correlating $X_{m,opt}$ is outlined briefly in Table 2.3-3. In general, a table of correlation coefficients between all pairs of parameters was generated. Only correlation coefficients to $X_{m,opt}$ are shown in Table 2.3-3. A single-parameter estimate of $X_{m,opt}$ was then found by linear regression, and a table of correlation coefficients was generated between all parameters and the error from the single-parameter model, $(X_{m,opt} - X_{m,est})$. Plots of the error versus any parameter of interest could be generated. This information was used either to suggest modifications to improve the single-parameter model, or to suggest a second parameter to add to the model. In either case the procedure was then repeated. Considerable trial-and-error was required, since the best one-parameter model does not necessarily lead to the best two-parameter model. Table 2.3-4 lists a number of models constructed in this manner for a subset of the data.

Table 2.3-2

Unavoidable error from the use of Eq. 2.2-13: Annual results
 1-parameter model: X_m selected for each hour by non-linear
 regression; $S = 1$. Combined results for all hour receiving any
 insolation whatsoever

<u>Location</u>	<u>Slope</u>	<u>Azimuth</u>	<u>Minimum r.m.s. error in ϕ (%)</u>
Albuquerque	0°	0°	1.09
Albuquerque	90°	0°	1.29
Madison	0°	0°	1.01
Madison	60°	0°	1.42
Madison	90°	0°	1.50
Seattle	30°	0°	1.39
Seattle	90°	0°	1.29
Madison	43°	45°	1.10
Madison	90°	90°	1.35

Table 2.3-3

Example of Correlation Procedure

Parameter:	R_b	V_{bd}	$\frac{1}{k}$	$\frac{1}{k^2}$	$\frac{R_b}{k}$	$\frac{V_{bd}}{k}$	$\frac{\tilde{R}}{k}$	$\frac{\tilde{R}}{k^2}$
Correlation coefficient : with $X_{m,opt}$.829	.835	.825	.825	.870	.851	.879	.883

Linear regression:

$$X_{m,est} = 1.183 + 0.278 \frac{R_b}{k}$$

Parameter:	\tilde{R}	\bar{k}	$\frac{1}{k}$	$\frac{\tilde{R}}{k^2}$	$\frac{R}{(\cos\delta)}$	$\frac{R_b - V_{bd}}{k}$
Correlation coefficient : with $(X_{m,opt} - \bar{X}_{m,est})$.493	-.419	-.362	.266	-.470	-.428
					-.425	-.208

Table 2.3-4

Linear estimation of X_m (optimum S)

Data from Madison 0°, Madison 60°, Albuquerque 0°, Albuquerque 90°

<u>Model</u>	<u>RMS Error of X_m</u>	<u>Correlation coefficient between $X_{m,opt}$ and $X_{m,est}$</u>
$X_m = 1.13 + 0.222 R_b / \bar{k}$.2058	.883
$X_m = 0.751 + 0.456 \tilde{R} / \bar{k}$.1844	.907
$X_m = 0.731 + 0.487 \tilde{R} \cos \delta / \bar{k}$.1809	.911
$X_m = 0.534 + 0.146 R_b / \bar{k} + 0.423 / \bar{k}$.1497	.940
$X_m = 1.07 + 0.490 \tilde{R} / \bar{k} - 0.665 \tilde{R} \cdot \bar{k}$.1351	.951
$X_m = 1.05 + 0.523 \tilde{R} \cos \delta / \bar{k} - 0.667 \tilde{R} \cdot \bar{k}$.1299	.955
$X_m = 1.50 + 0.869 \tilde{R} / \bar{k} - 1.05 \tilde{R} - 0.255 / \bar{k}$.1308	.954
$X_m = 1.13 + 0.554 \tilde{R} \cos \delta / \bar{k} - 0.757 \tilde{R} \cdot \bar{k}$ $- 0.0694 \cos \beta / \bar{k}$.1203	.962
$X_m = -0.252 + 0.917 \tilde{R} / \bar{k} - 1.13 \tilde{R} - 0.300 / \bar{k}$ $+ 1.89 \cos \delta$.1196	.962

The usefulness of this approach depends on the observation that although the rms error in estimating $X_{m,opt}$ is not linearly related to the rms error in estimating ϕ , it generally provides a reliable indication of the trend, i.e., models which estimate $X_{m,opt}$ more accurately generally lead to more accurate estimates of ϕ as well. This relationship is shown in Table 2.3-5.

The parameter s was found to have an average value of about 0.97 and a standard deviation of about 0.12. Attempts to correlate s met with little success, as Table 2.3-5 indicates. Adding a fourth term to an equation for X_m is more advantageous than adding a second term to an equation for s . Since setting s to 1 also makes very little difference, s was abandoned as a useful variable. This leaves Equation 2.2-13 with a single degree of freedom.

The procedure outlined above allowed a large number of possible correlations for X_m to be examined quickly and inexpensively. Tables 2.3-6 and 2.3-7 list a number of correlation attempts. Models containing the parameter V_{bd} (defined by Equation 1.4-6) look promising in Table 2.3-7, but were abandoned (perhaps prematurely) on the basis of the data presented in Table 2.3-8. The model selected for further investigation is the one given last in Tables 2.3-6 through 2.3-8:

$$X_m = C_1 + C_2 \frac{\tilde{R}}{\bar{k}^2} - C_3 (\cos\beta) / \bar{k}^2 - C_4 \bar{k} / (\cos\delta)^2 \quad (2.3-1)$$

Using data from four months of the year, with X_c varying in increments of 0.1 from $X_c = 0.05$ to $X_c = \text{minimum}(X_{m,act}, 2.45)$, the constants in Equation 2.3-1 were evaluated by non-linear re-

Table 2.3-5

Estimation of X_m and ϕ

Data from Madison 0° and 60°, Albuquerque 0° and 90°

ϕ calculated for 4 months only: January, April, July, October

Model	rms error of X_m	(combined data)				rms error of ϕ			
		Alb 0°	Alb 90°	Msn 0°	Msn 60°	Alb 0°	Alb 90°	Msn 0°	Msn 60°
$X_m = C_1 + C_2 \frac{\tilde{R}}{k} - C_3 \tilde{R} \cdot \tilde{k}; S = C_4$.1351	.01054	.01280	.01961	.02276	.02143			
$X_m = C_1 + C_2 \frac{R \cos \delta}{k} - C_3 \tilde{R} \tilde{k}; S = C_4$.1299	.01053	.01240	.01895	.02096	.02017			
$X_m = C_1 + C_2 \frac{R \cos \delta}{k} - C_3 \tilde{R} \tilde{k}; S = C_4 + C_5 R$.1299	.01054	.01010	.01897	.02023	.01983			
$X_m = C_1 + C_2 \frac{R \cos \delta}{k} - C_3 \tilde{R} \tilde{k} - C_4 \frac{\cos \beta}{k}; S = C_5$.1203	.01053	.01241	.01376	.02089	.01890			

Table 2.3-6

Linear estimation of X_m ($S = 1$) excluding Seattle dataData from Madison $0^\circ, 60^\circ, 90^\circ$; Albuquerque $0^\circ, 90^\circ$

Model	rms error of X_m	Correlation coefficient between $x_{m,opt}$ and $x_{m,est}$
$X_m = 0.739 + 0.506 \tilde{R}/\bar{k}$.2556	.884
$X_m = 0.766 \cos\delta + 0.508 \tilde{R}/\bar{k}$.2525	
$X_m = 1.07 + 0.163 \tilde{R}/\bar{k}^2$.2203	.915
$X_m = 1.06 + 0.174 \tilde{R}\cos\delta/\bar{k}^2$.2161	.918
$X_m = 1.04 + 0.186 \tilde{R}(\cos\delta)^2/\bar{k}^2$.2140	.920
$X_m = 1.11 + 0.558 \tilde{R}/\bar{k} - 0.847 \tilde{R}\cdot\bar{k}$.1994	.931
$X_m = 1.08 + 0.598 \tilde{R}\cos\delta/\bar{k} - 0.854 \tilde{R}\bar{k}$.1955	.934
$X_m = 1.20 + 0.163 \tilde{R}/\bar{k}^2 - 0.237 \cos\beta$.1933	.935
$X_m = 1.18 + 0.175 \tilde{R}\cos\delta/\bar{k}^2 - 0.222 \cos\beta/(\cos\delta)^2$.1869	.940
$X_m = 0.165 \tilde{R}/\bar{k}^2 - 0.235 \cos\beta + 1.24 \cos\delta$.1858	
$X_m = 1.17 + 0.187 \tilde{R}(\cos\delta)^2/\bar{k}^2 - 0.240 \cos\beta$.1852	.941
$X_m = 1.13 + 0.181 \tilde{R}/\bar{k}^2 - 0.659 (\cos\beta)/\bar{k}^2$.1811	.943
$X_m = -0.794 + 0.166 \tilde{R}/\bar{k}^2 - 0.231 \cos\beta + 2.05 \cos\delta$.1845	.941
$X_m = 1.19 + 0.559 \tilde{R}/\bar{k} - 0.772 \tilde{R}\cdot\bar{k} - 0.219(\cos\beta)/(\cos\delta)^2$.1689	.951
$X_m = 1.99 + 0.147 \tilde{R}/\bar{k}^2 - 0.0800(\cos\beta)/\bar{k}^2 - 1.14\bar{k}/(\cos\delta)^2$.1446	.964

Table 2.3-7

Linear estimation of X_m ($s = 1$)

Data from Madison 0°, 60°, 90°; Albuquerque 0°, 90°; Seattle 30°, 90°

Model	rms error of X_m	Correlation coefficient between $x_{m,opt}$ and $x_{m,est}$
$C_1 + C_2 V_{bd}$.566	.835
$C_1 + C_2/\bar{k}$.513	.841
$C_1 + C_2 V_{bd}/\bar{k}$.541	.850
$C_1 + C_2 R_b/k$.508	.869
$C_1 + C_2/\bar{k} + C_3 V_{bd}$.419	.913
$C_1 + C_2/\bar{k} + C_3 \left[V_{bd} + \rho \left(\frac{1 + \cos\beta}{2} \right) \right]$.368	.922
$C_1/k + C_2 \left[V_{bd} + \rho \left(\frac{1 - \cos\beta}{2} \right) \right]$.368	.922
$C_1 + C_2 \tilde{R}/\bar{k}$.453	.879
$C_1 + C_2 \tilde{R}/\bar{k}^2$.445	.883
$C_1 + C_2 \tilde{R}/\bar{k}^2 + C_3 \frac{\cos\beta}{\bar{k}^2}$.387	.913
$C_1 + C_2 \tilde{R}/\bar{k}^2 + C_3 \frac{\cos\beta}{\bar{k}^2} + C_4 \frac{k}{(\cos\delta)^2}$.343	.933

Table 2.3-8

Estimation of ϕ ϕ calculated for 4 months only: January, April, July, October

<u>Model</u>	RMS Error in ϕ (%)	
	<u>Albuquerque</u> 0° & 90°	<u>Madison</u> 0°, 60° & 90°
$X_m = \frac{C_1}{\bar{k}} + C_2 \left[V_{hd} + \rho \left(\frac{1 - \cos\beta}{2} \right) \right]$	1.92	3.45
$X_m = C_1 + C_2 \frac{\tilde{R}}{\bar{k}} + C_3 \tilde{R}\bar{k}$	1.34	2.88
$X_m = C_1 + C_2 \frac{\tilde{R}}{\bar{k}^2} + C_3 \frac{\cos\beta}{\bar{k}^2} + C_4 \frac{\bar{k}}{(\cos\delta)^2}$	1.18	2.12

gression to minimize the error from Equation 2.2-13. The evaluation was done for all locations combined, and repeated for each location independently. For the combined data the following results were obtained:

$$\begin{aligned}
 C_1 &= 1.856 \\
 C_2 &= 0.2024 \\
 C_3 &= 0.0980 \\
 C_4 &= 1.053
 \end{aligned}
 \tag{2.3-2}$$

Using these constants, the error was re-calculated for a few locations and slopes, and calculated for the first time for the data for non-south-facing surfaces. The results of these operations are summarized in Table 2.3-9. Large errors in Seattle occur primarily in winter months, particularly near sunrise and sunset, when radiation levels are unusually low. The results for azimuth angles other than zero are not entirely satisfying but are at least encouraging.

The constants C_1 and C_4 in Equation 2.3-1 are strongly correlated with each other ($r = 0.97$). Setting C_1 to zero and re-evaluating the constants for a 30° surface in Seattle increases the rms error to 4.56%. From the values of C_1 and C_4 obtained by fitting each location independently, the relationship between them is found to be approximately

$$C_4 = 1.2(C_1 - 1.0)$$

The value of C_1 is lowest for Albuquerque and highest for Seattle, suggesting a possible linear relationship to $1/\bar{k}$. Unfortunately, substituting these conditions into Equation 2.3-1 yields a negligible

decrease in the overall error, as shown by the first equation in Table 2.3-10.

The second equation in Table 2.3-10 is a modification of Equation 2.3-1 which could not be examined by linear regression using MINITAB. Again, no improvement was found.

Using MINITAB, the nature of the error in estimating X_m with Equations 2.3-1 and 2.3-2 (i.e., $X_{m,opt} - X_{m,est}$) was examined for each location and slope. The correlation coefficients and mean bias errors presented in Table 2.3-11 suggest that the constants obtained from the combined south-facing data represent compromise between the vertical surface in Seattle and all other data, and that the non-zero azimuth results might be better approximated if the 90° surface in Seattle were eliminated from the correlation.

On this basis the constants of Equation 2.3-1 were re-evaluated by non-linear regression for all south-facing data except the vertical surface in Seattle. Errors for the orientations excluded from this evaluation were then computed. The results are presented in Table 2.3-12. In effect, the accuracy of the predictions for Seattle 90° has been sacrificed to improve the accuracy of the predictions for non-south-facing surfaces. Further justification for the procedure will be provided in the following section.

Finally, the constants were evaluated for the six sets of data for south-facing surfaces, excluding Seattle 90°, for all twelve months. Again, all hours between 6 A.M. and 6 P.M. for which R_p is positive throughout the hour throughout the month were considered.

Table 2.3-10

Modification to Model for X_m

Data: All locations and slopes, zero azimuth

4 months: January, April, July, October

X_c in increments of 0.1

4777 observations total

RMS Error
of ϕ (%)

$$X_m = (c_1 + c_5/\bar{k}) + C_2 \frac{\tilde{R}}{k^2} - C_3 \frac{\cos\beta}{k} - C_4 (c_1 + c_5/\bar{k} - 1) \frac{k}{(\cos\delta)^2}$$

2.95

$$X_m = C_1 + C_2 \frac{\tilde{R}}{(\bar{k} - C_5)} - C_3 \frac{\cos\beta}{(\bar{k} - C_5)} - C_4 \frac{\bar{k}}{(\cos\delta)^2}$$

3.13

Equation 2.3-1

2.96

Table 2.3-11

Correlation coefficients with error, $(X_{m,opt} - X_{m,est})$

$$X_{m,est} = 1.856 + 0.2024 \frac{\tilde{R}}{\sqrt{k}} - 0.0980 \cos\beta \sqrt{\tilde{k}^2} - 1.053 \frac{\bar{k}}{(\cos\delta)^2}$$

<u>Azimuth</u>	<u>Location</u>	<u>Slope</u>	<u>$X_{m,opt}$</u>	<u>\tilde{R}/\sqrt{k}</u>	<u>$\cos\beta/\sqrt{k}$</u>	<u>$k/(\cos\delta)^2$</u>	<u>Mean Bias Error of X_m</u>	<u>rms Error</u>
0°	Albuquerque	0°	-.219	-.651	-.651	.687	-.005	± .109
0°	Albuquerque	90°	-.753	-.940	(--)	.628	-.126	± .204
0°	Madison	0°	-.045	-.631	-.631	.447	-.048	± .166
0°	Madison	60°	-.757	-.883	-.851	.695	-.200	± .244
0°	Madison	90°	-.471	-.675	(--)	.515	-.113	± .244
0°	Seattle	30°	.037	-.492	-.497	.185	.081	± .549
0°	Seattle	90°	.315	-.093	(--)	-.119	.227	± .695
45°	Madison	43°	-.309	-.768	-.470	.331	-.135	± .353
90°	Madison	90°	-.556	-.813	(--)	.497	-.285	± .415

Table 2.3-12

Final Correlation Data and Results

Data: Albuquerque 0°, 90°; Madison 0°, 60°, 90°; Seattle 30°

Azimuth = 0; 4 months: January, April, July, October

All hours between 6 AM and 6 PM for which $R_b > 0$ throughout
hour throughout month

Total, 4003 observations.

Results:
$$X_m = 1.871 + 0.1699 \frac{\bar{R}}{\bar{k}^2} - 0.0629 \frac{\cos \beta}{\bar{k}^2} - 1.045 \frac{\bar{k}}{(\cos \delta)^2}$$

RMS error of $\phi = 2.73\%$

<u>Azimuth</u>	<u>Location</u>	<u>Slope</u>	<u>RMS error of ϕ(%)</u>
0°	Seattle	90°	4.96
45°	Madison	43°	3.43
90°	Madison	90°	3.19

For computational reasons, values of X_c were taken in increments of 0.2 rather than 0.1. A total of 6329 observations were included in the regression. Repeating Equations 2.2-9 and 2.2-13, the final correlation is given by:

$$\phi = \begin{cases} 0, & X_c \geq X_m \\ \left(1 - \frac{X_c}{X_m}\right)^2, & X_m = 2 \\ \left| |a| - \sqrt{a^2 + (1 + 2a) \left(\frac{X_m - X_c}{X_m}\right)^2} \right|, & \text{otherwise} \end{cases}$$

where $a = \frac{X_m - 1}{2 - X_m}$ (2.3-4)

$$\text{and } X_m = 1.85 + 0.169 \tilde{R}/\bar{k}^2 - 0.0696 (\cos\beta)/\bar{k}^2 - 0.981 \bar{k}/(\cos\delta)^2$$

2.4 Correlation Results and Comparisons

The values of \bar{k} and \bar{I}_T used in developing Equation 2.3-4 are long-term averages calculated from the hourly weather data used to calculate ϕ . In practice, however, the correlation will be used with \bar{k} and \bar{I}_T estimated from the monthly-average daily clearness index, \bar{K} , by Equations 1.4-2 - 1.4-4 and 1.3-8 - 1.3-13. It is important to determine how the accuracy of the present correlation is affected by the use of these estimates. It is also instructive to compare the present correlation with the more complicated expression for ϕ presented by Huget (Equation 1.5-6).

Using published (6) values of \bar{K} , the parameters \bar{k} and \bar{I}_T were calculated using the equations listed above, and were used with Equation 2.3-4 to calculate ϕ . Figure 2.4-1 shows ϕ -curves obtained from long-term weather data and from the two correlations for a few sets of conditions. In practice, additional uncertainty enters through the need to estimate X_c . Estimates of X_c for use in Equation 2.3-4 were obtained from the "actual" values used previously:

$$X_{c,est} = X_{c,act} \frac{\bar{I}_{T,act}}{\bar{I}_{T,est}} = \frac{I_c}{\bar{I}_{T,est}} \quad (2.4-1)$$

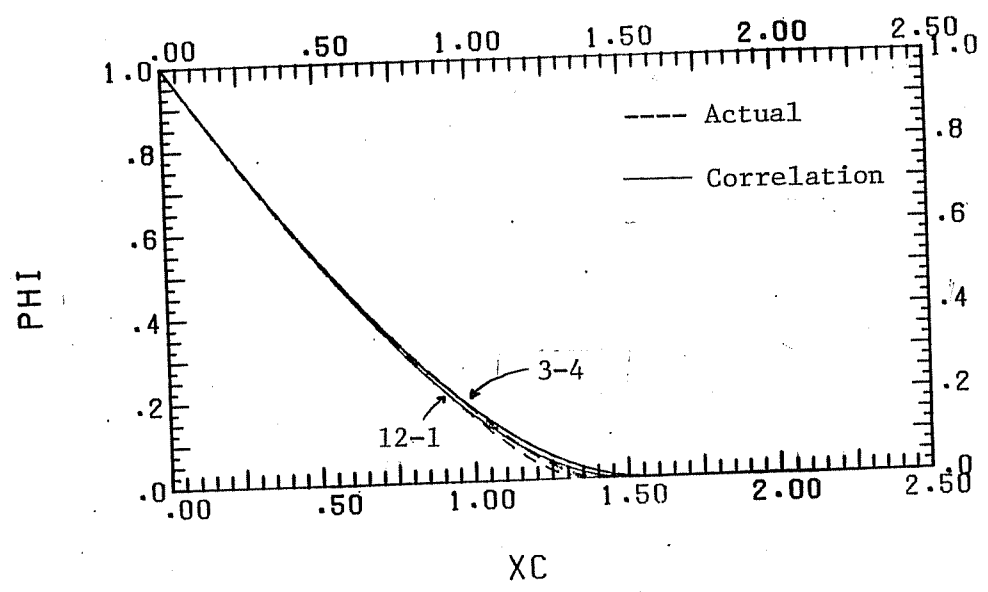
Estimates of \bar{I}_T and X_c are not required for the correlation of Huget, since calculation of \bar{I}_T is built into the equation and the critical level enters as I_c/\bar{I}_0 .

Table 2.4-1 lists the mean bias error and the standard deviation of the error (i.e., rms error) in estimating ϕ for each location and slope. A positive mean bias error indicates that on the average, over all months, hours, and critical levels considered, ϕ is underpredicted. Results are presented for the present correlation using actual long-term averages of \bar{k} and \bar{I}_T , and for both the present correlation and Equation 1.5-6 using appropriate estimated values.

For the present correlation, the use of estimated rather than actual radiation parameters significantly increases the uncertainty for steeply tilted surfaces. For horizontal or slightly tilted surfaces the effect on the uncertainty is small and may either increase

Madison 60° June

PRESENT CORRELATION, HOURS 12-1 AND 3-4



HUGET CORRELATION, HOURS 12-1 AND 3-4

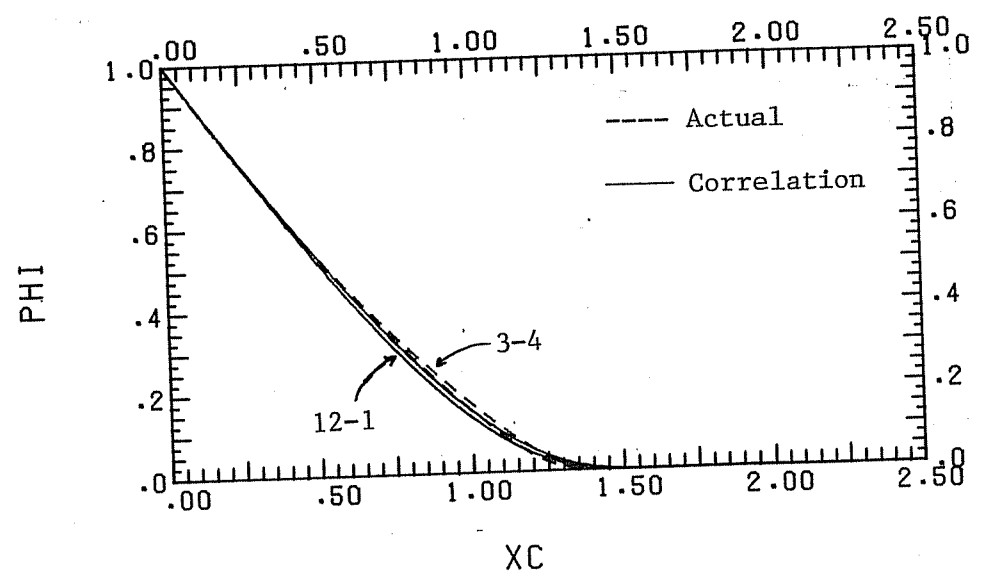
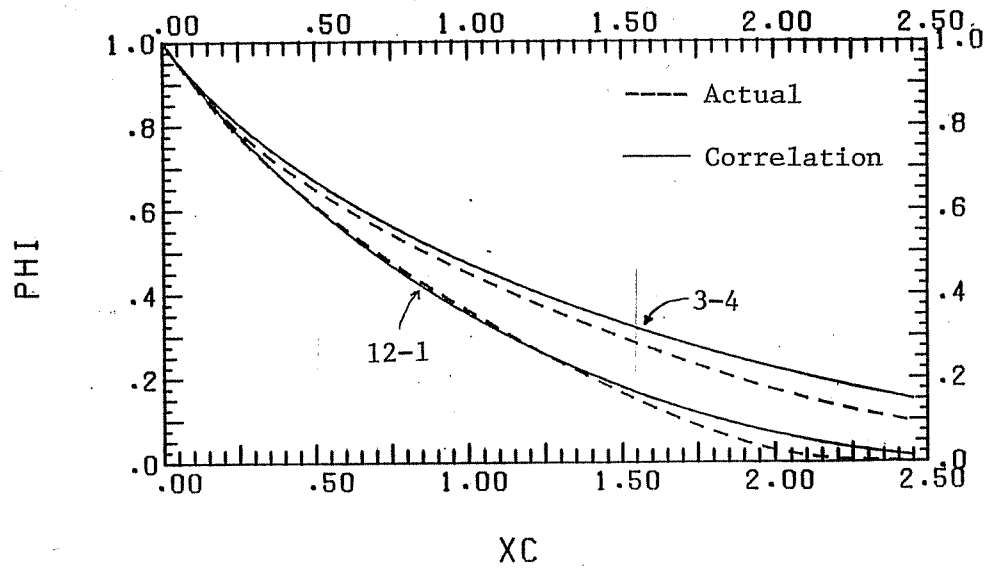


Figure 2.4-1: Comparison of Correlations with Long-Term Weather Results.

ϕ X_C

Madison 60⁰ December

PRESENT CORRELATION, HOURS 12-1 AND 3-4



HUGET CORRELATION, HOURS 12-1 AND 3-4

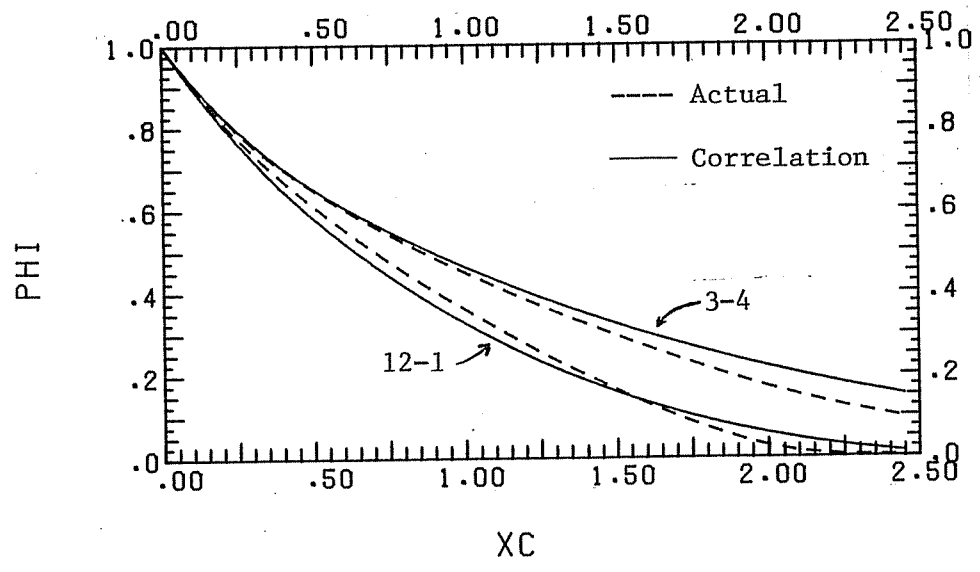
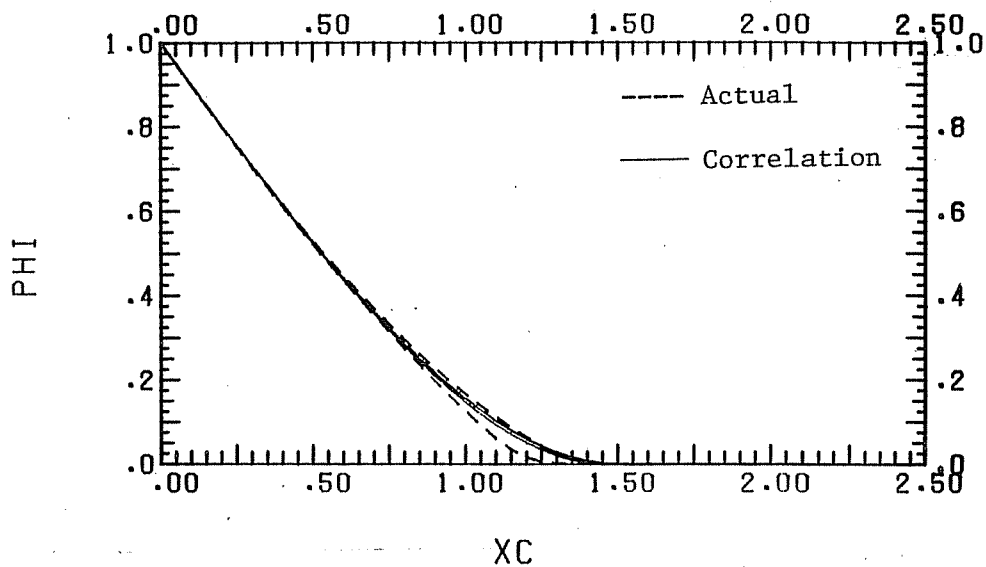


Figure 2.4-1 (continued)

Seattle 90° June

PRESENT CORRELATION, HOURS 12-1 AND 3-4



HUGET CORRELATION, HOURS 12-1 AND 3-4

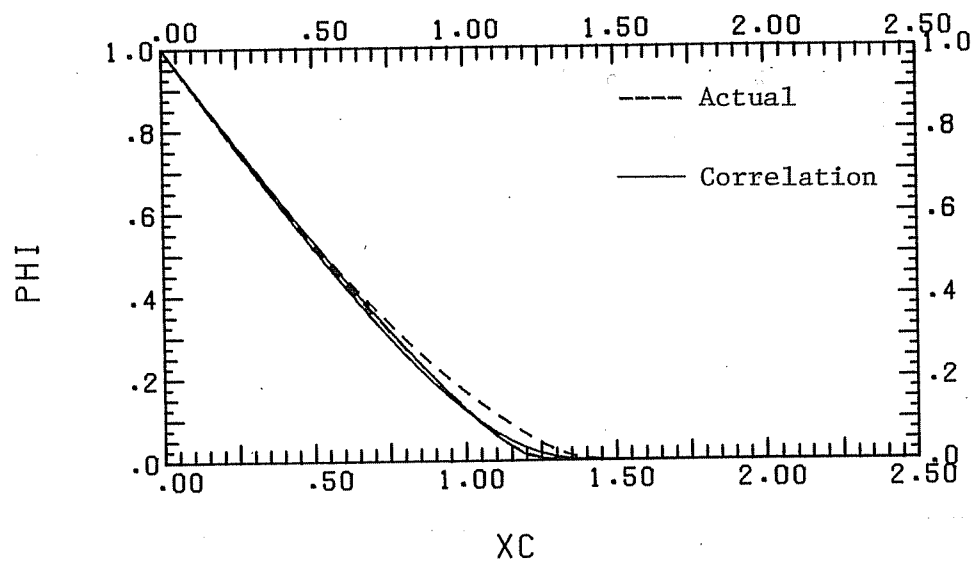
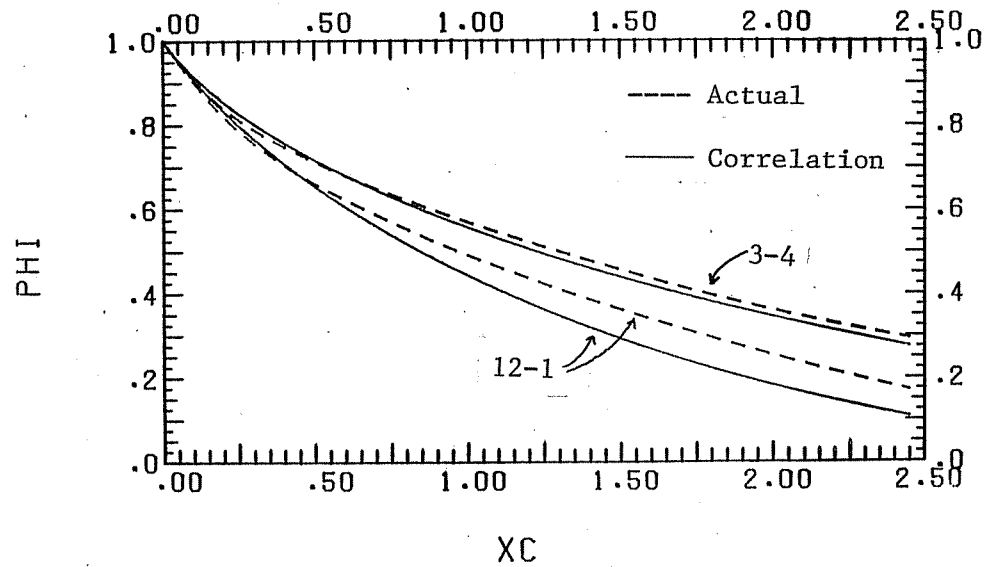


Figure 2.4-1 (continued)

Seattle 90° December

PRESENT CORRELATION, HOURS 12-1 AND 3-4



HUGET CORRELATION, HOURS 12-1 AND 3-4

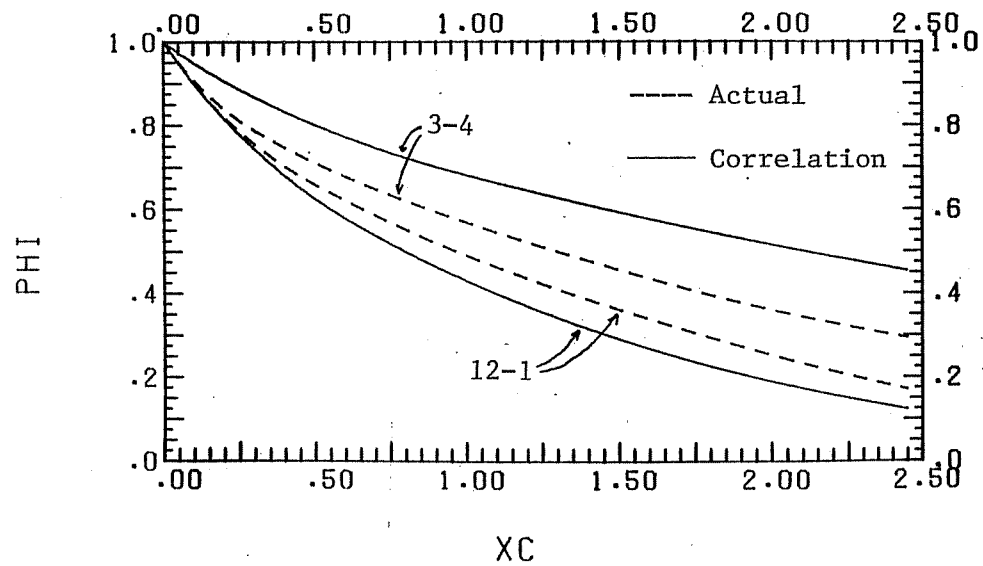


Figure 2.4-1 (continued)

Table 2.4-1

Comparison of correlation results and long-term weather results

Azimuth	Location	Slope	# of observations	Present Correlation (Eq. 2.3-4)			Hugot Correlation (Eq. 1.5-6)			
				Actual $\bar{k}, \bar{I}_T, \bar{X}_c$ Mean	Bias Error of $\phi(\%)$	rms Error	Estimated $\bar{k}, \bar{I}_T, \bar{X}_c$ Mean	Bias Error of $\phi(\%)$	rms Error	
0°	Albuquerque	0°	3847	-0.35	1.58	1.82	-0.42	1.82	1.02	2.46
0°	Albuquerque	90°	3390	-0.74	2.14	4.26	-0.81	4.26	1.50	4.75
0°	Madison	0°	4797	-0.46	2.01	1.74	-0.47	1.74	0.75	2.28
0°	Madison	60°	4579	-0.23	2.20	3.57	-0.45	3.57	1.04	4.94
0°	Madison	90°	4423	0.26	2.33	4.14	-0.12	4.14	0.84	5.55
0°	Seattle	30°	5158	1.16	3.74	3.54	1.16	3.54	2.25	5.06
0°	Seattle	90°	4610	2.70	4.93	5.62	2.81	5.62	3.10	6.43
45°	Madison	43°	4078	-0.76	3.38	4.52	-1.93	4.52	1.06	4.05
90°	Madison	90°	2477	-0.99	3.21	6.52	-2.32	6.52	-1.17	7.09

or decrease the rms error.

The first six lines of Table 2.4-1 represent the data used in evaluating the constants of the present correlation. For this data, Equation 2.3-4 is consistently slightly more accurate than Equation 1.5-6. The comparison is not entirely fair, however, since Equation 2.3-4 was specifically fitted to this data while Equation 1.5-6 was not. The present correlation (Eq. 2.3-4) is more accurate for two of the three remaining lines in the table.

Perhaps more significant is the correspondence between the uncertainties of the two methods. To a good approximation, the rms error of one method could be used to predict the rms error of the other method. The consistency of this relationship for the three locations considered suggests that the same may hold for other locations as well. The relative accuracy of the two methods for other locations has not been examined, but very similar accuracy can at least be expected.

The rms errors reported in Table 2.4-1 are somewhat misleading, since large errors are generally observed for hours near sunrise and sunset when the amount of energy involved is small. This is shown by Table 2.4-2, which gives rms errors of the present correlation for each morning hour of each month for a vertical south-facing surface in Albuquerque. Similar patterns are obtained for afternoon hours and for other slopes and locations.

An energy-weighted comparison is provided in Table 2.4-3. For this comparison, the same values of $\bar{I}_{T,est}$ were used throughout--

Table 2.4-2

rms errors (%) of present correlation for a vertical south-facing surface in Albuquerque

<u>Month</u>	<u>Time (A.M.)</u>				
	<u>7-8</u>	<u>8-9</u>	<u>9-10</u>	<u>10-11</u>	<u>11-12</u>
Jan	-	3.9	3.0	2.6	2.1
Feb	6.1	4.9	4.0	3.1	2.5
Mar	4.6	3.6	2.8	2.0	1.1
Apr	3.4	3.0	2.8	2.1	1.3
May	-	4.5	3.6	2.9	2.2
Jun	-	-	1.9	1.6	1.3
Jul	-	3.8	1.5	0.6	0.3
Aug	1.2	3.0	1.6	1.3	1.2
Sep	5.0	2.6	1.8	1.6	1.9
Oct	17.0	6.7	3.6	2.7	2.4
Nov	-	11.7	4.9	2.6	2.0
Dec	-	8.5	3.4	2.4	1.9

Table 2.4-3 Energy-Weighted Comparisons of Correlations for ϕ

Azimuth	Location	Slope	$(\bar{I}_{T,act,\phi} - \bar{I}_{T,est,\phi})$				$(\bar{I}_{T,act} - \bar{I}_{T,est})$							
			# of observations	Present Correlation	Mean	rms Error	Huget Correlation	Mean	rms Error	# of obs.	Mean Bias Error	rms Error		
0°	Albuquerque	0°	3847	$1 W/m^2$	$16 W/m^2$	0	25	8	$8 W/m^2$	21	124	$4 W/m^2$	23	W/m^2
0°	Albuquerque	90°	3390	0	25	0	25	10	10	29	106	7	30	
0°	Madison	0°	4797	0	7	0	7	4	4	11	122	1	8	
0°	Madison	60°	4579	1	18	1	18	8	8	23	112	4	22	
0°	Madison	90°	4423	2	18	2	18	5	5	21	106	2	22	
0°	Seattle	30°	5158	6	20	6	20	11	11	26	120	3	29	
0°	Seattle	90°	4610	9	20	9	20	11	11	23	106	3	23	
45°	Madison	43°	4078	-5	18	-5	18	7	7	20	103	1	16	
90°	Madison	90°	2477	-11	33	-11	33	-7	-7	34	61	-10	39	

the ones calculated as outlined above, not the ones given by the denominator of Equation 1.5-6. All energies are given in Watts per square meter. The uncertainties estimating \bar{I}_T alone are included in the table. These values are somewhat inflated by occasional small (± 0.01) discrepancies between the published value of \bar{K} used in this comparison and values obtained from the hourly data used to calculate ϕ_{act} .

The most striking feature of the data in Table 2.4-3 is the very strong relationship between the uncertainty of $\bar{I}_T\phi$ from either method and the uncertainty of \bar{I}_T alone. It should also be noted that for all locations and slopes examined, the present correlation is slightly more accurate than Equation 1.5-6 in estimating $\bar{I}_T\phi$, which represents either utilizable or unutilizable energy depending on the definition of I_c . These differences, however, are quite small, and may be reversed for other locations. The primary advantage of the present correlation is its simplicity.

2.5 Recommendations for Further Work

As shown in the previous section, the present correlation is slightly more accurate (i.e., closer to results obtained from long-term hourly horizontal radiation measurements) than the best method previously available, at least for the locations used in developing the present correlation. The strong similarity in the rms errors of the two methods suggest that this relationship may hold for other locations as well. Verification of the accuracy of the present correla-

tion for other locations would be desirable.

The possibility of giving Equation 2.2-13 a second degree of freedom by allowing the slope of the curve at $X_c = 0$ to vary was discussed in Section 2.3. If a second degree of freedom is deemed necessary, an alternative which might prove more fruitful is to allow the slope of the curve at $X_c = X_m$ to vary. This can be accomplished as shown in Figure 2.5-1. The equation for this curve is given by:

$$\phi = \left| \left| a - \sqrt{(1-a) \left[1 - a - X_{m2} + \frac{(X_c - X_{m2})^2}{X_{m2}} \right]} \right| \right|$$

$$a = \frac{(X_{m2} - X_m)^2 - X_{m2}^2 + X_{m2}}{(X_{m2} - X_m)^2 - X_{m2}^2 + 2X_{m2}} \quad (2.5-1)$$

where X_m and X_{m2} are defined as indicated in Figure 2.5-1.

Preliminary investigations using this equation indicate that caution is required in finding optimum values of X_{m2} . The sum of squares function apparently has local minima at $X_{m2} = X_m$ and $X_{m2} = X_m + \sim 0.5$. The latter is usually but not always the better of the two, and the value found by non-linear regression is not necessarily the better of the two. The minimum possible error from this equation is just slightly lower than the minimum possible error from the two-parameter model previously discussed. No attempt has been made to correlate X_{m2} .

Equation 2.2-13 could presumably be used just as well to correlate $\bar{\phi}$, the daily average fraction of incident energy above a daily

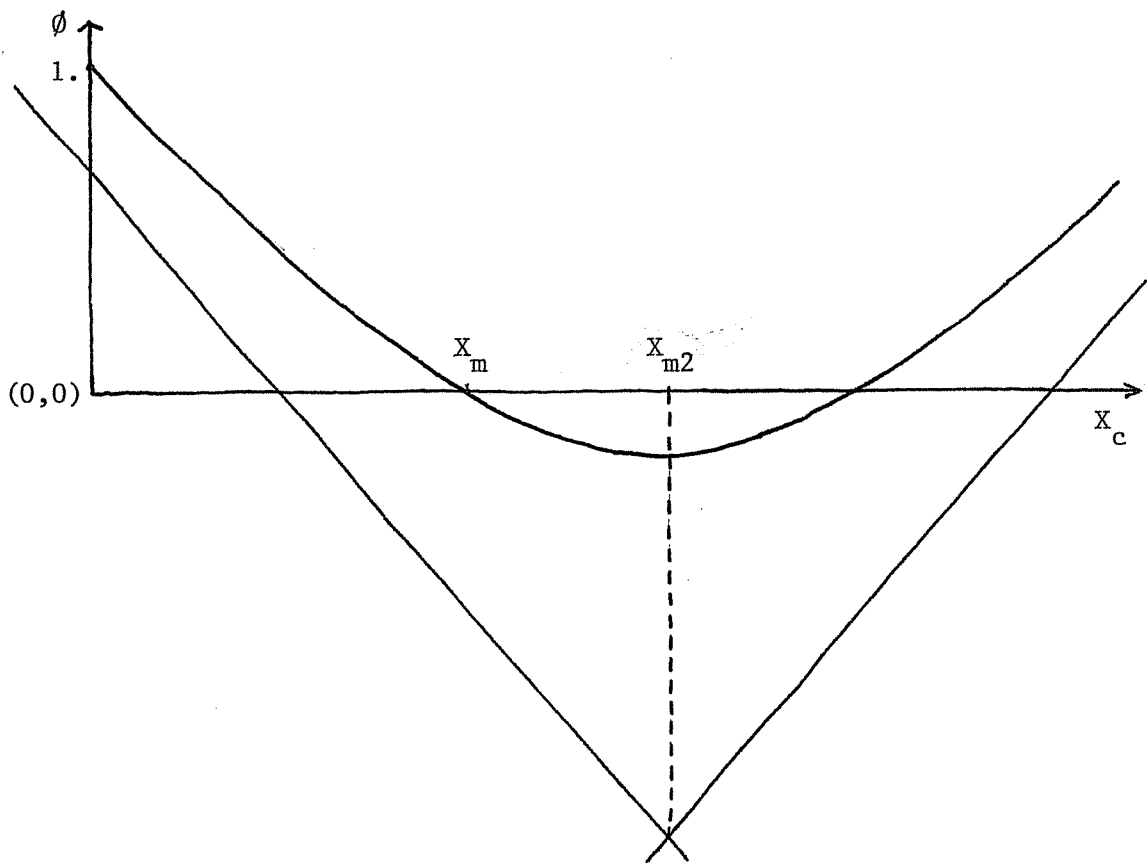


Figure 2.5-1: Alternative Form for Correlation of ϕ

average critical level. A different form might be required to correlate the daily equivalent of X_m , but the form and methods described in the present work should at least provide a useful point of departure. In the present correlation the effect of azimuth angle enters solely through the term \tilde{R} (i.e., \bar{I}_T/\bar{I}) and adequate results are obtained. Similarly, the effect of azimuth angle on $\bar{\phi}$ may be adequately represented by the daily equivalent, \bar{H}_T/\bar{H} .

Chapter 3. Photovoltaic Design Methods

3.1 Introduction

The present work began as an investigation into methods for predicting the long-term average performance of photovoltaic systems from system characteristics and monthly-average weather statistics. The type of system considered and the control strategy assumed in this study are discussed in Section 3.2. The development of correlations for estimating system performance is based on comparisons with hour-by-hour simulations. Hourly simulation programs are discussed in Section 3.3.

The problem of predicting photovoltaic system performance can be divided into three parts. First, the monthly-average efficiency of the photovoltaic array is required. Methods for estimating this average array efficiency have been developed by Evans (8, 9) and by Siegel (24). The equations proposed by Evans (8) are provided in Section 3.4. Once this electrical conversion efficiency is known, the total electrical energy generated by the array can be calculated.

Second, it is necessary to determine the fraction of the energy that can be used directly by the load. This depends strongly on the distribution of the load over the day, and can conveniently be approached by the method of hourly utilizability. This led to an investigation of methods for estimating hourly utilizability, the results of which are presented in Chapter 2. The use of the hourly utilizability function for predicting the performance of photovoltaic

systems without energy storage is also described in section 3.4.

This is a straightforward extension of a method proposed by Siegel (24) for estimating the performance of systems without storage exposed to a constant 24-hour load, using the daily utilizability function.

Energy generated in excess of the requirements of the load may be dissipated, sold to a utility, or stored in a battery for future use, depending on the system. In a system with a storage battery, energy must still be dissipated (or sold) when the battery is full; in general, not all of the energy available for storage can ultimately be used. In Section 3.5 an empirical correlation is proposed for estimating the effect of adding a storage battery to a photovoltaic system. This correlation, in conjunction with the equation for system performance without storage given in Section 3.4, can be used to estimate the overall performance of photovoltaic systems with storage, given any load profile.

The accuracy of the complete design method is examined in Section 3.6. A sample calculation is provided in Section 3.7. Recommendations for further work are given in Section 3.8.

3.2 Photovoltaic Systems

The type of system modeled in the present study is illustrated in Figure 3.2-1. The flat array of photovoltaic (PV) cells is passively cooled, and is required to face south since the methods for estimating monthly-average array efficiency discussed in Section 3.4 were de-

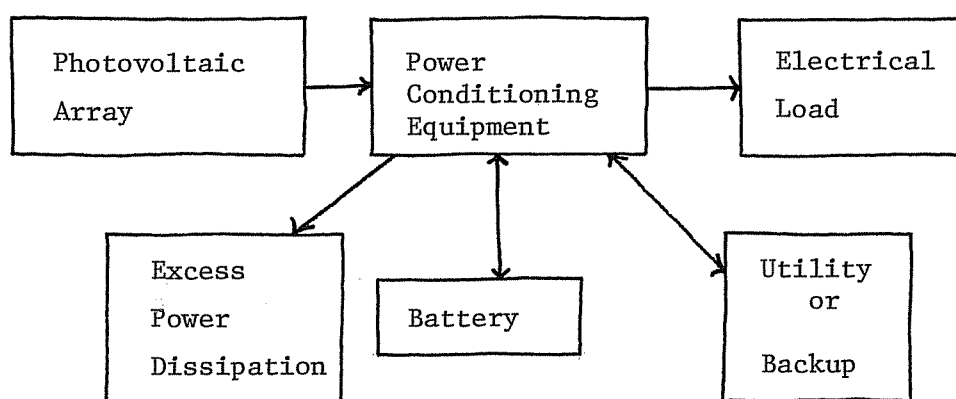


Figure 3.2-1: Schematic of Photovoltaic System Configuration

veloped for south-facing surfaces.

The power conditioning equipment must include a maximum power tracker, an electronic device which continuously adjusts the voltage across the array to maximize the power output of the array. For a maximum power tracking array, the instantaneous electrical conversion efficiency, η_e , can be treated as a linear function of PV cell temperature:

$$\eta_e = \eta_r [1 - \beta(T_c - T_r)] \quad (3.2-1)$$

where T_c is the instantaneous cell temperature, η_r is a reference efficiency at a specified reference temperature T_r (often 28 C), and β is a temperature coefficient dependent on the cell composition, roughly equal to 0.005 C^{-1} for silicon cells. Values of η_r , T_r , and β should be obtained from manufacturer's data.

The power conditioning equipment also includes voltage regulators, control logic, and an inverter for converting d.c. power from the array or storage battery to a.c. power. In the present work the efficiencies of the maximum power tracker, η_{mp} , and of the remainder of the power conditioning equipment, η_{pc} , are treated separately and are both assumed constant. The total instantaneous electrical energy generated by the array is given by:

$$E = A_c G_T \tau \eta_e \eta_{mp} \quad (3.2-2)$$

where A_c is the total PV cell area, G_T is the instantaneous incident insolation per unit area, τ is the transmittance of any protective

glazing not included in the determination of the reference efficiency, and η_e and η_{mp} are defined above.

The storage battery in Figure 3.2-1 represents a collection of lead-acid cells connected in series and in parallel. The battery is considered to be charged only by the array, never by the auxiliary power source. Priority is given to meeting the load; the auxiliary power source is used only when the battery is empty, and the battery is charged only when the entire load is met by the array and excess power is available.

The major inefficiency in using a storage battery is due to the higher voltages encountered when charging than when discharging, and depends on the typical charge and discharge rates at which the battery is operated. Based on extensive computer simulations using detailed battery models, Evans et al. (8) recommend using a constant average battery storage efficiency, η_b , of about 0.87 for lead-acid batteries.

The shape of the load profile can have a significant effect on system performance. The load is taken as a known input for each hour of the day, and is assumed to be repetitive from day to day. Evans et al. have examined the effect of random fluctuations about an average base load, and have found that monthly-average system performance is remarkably insensitive to such fluctuations. Thus the assumption of a smooth and repetitive diurnal load profile appears justified.

3.3 Computer Simulation Models

Detailed computer programs currently exist (11, 16) for predicting PV system performance from hourly meteorological data. All of the computer simulations reported in this chapter were performed using TRNSYS (16), a general simulation program for solar energy systems. The photovoltaic system components now available in TRNSYS-- a thermal/photovoltaic collector, a regulator-inverter, a storage battery, and a combined electrical subsystem--were provided by Evans et al. (10). The combined thermal/photovoltaic collector model was used in its simplest mode, with thermal collection turned off and with the collector thermal loss coefficient, U_L , and cover transmittance, τ , assumed constant.

The battery model, in its simplest mode of operation, multiplies incoming power by a constant battery efficiency without calculating currents and voltages. For purposes of the present study, a modest decrease in the expense of simulations was achieved by writing a combined regulator-inverter-battery subroutine comparable to the simplest modes of the battery and regulator-inverter models supplied by Evans. A listing of this subroutine is provided in Appendix B. The regulator in this subroutine differs from the regulator model supplied by Evans in that energy quantities within a single timestep can be partitioned between storage and dump or between storage and auxiliary if the battery is nearly full or nearly empty at the beginning of the timestep. Evans's regulator treats energy to or from the battery as an indivisible lump sum over a single timestep, in

order to minimize the need for iterative calculations when a more complex battery model is used. The effect of this difference between regulator models is greatest when the battery capacity is small relative to both electrical generation and electrical demand and when the timestep is large. A comparison between the results of the two simulation models is shown in Table 3.3-1. In this table, and throughout this chapter, \bar{L} represents the average daily load, \bar{D} represents the average daily energy dissipated (or not collected, or sold to a utility) when the storage battery is full, and f represents the fraction of the load met by the photovoltaic system. B_c is the battery storage capacity, and \bar{E} is the average daily electricity generated:

$$\bar{E} = \frac{1}{N} \sum_{\text{hours}} A_c I_t \tau \eta_e \eta_{mp} \quad (3.3-1)$$

where N is the number of days in the month.

Results are shown for two timestep sizes, $t = 0.05$ and $t = 0.5$. The two models yield very similar results with the shorter timestep. The present model is nearly unaffected by increasing the length of the timestep. A half-hour timestep was used in all simulations described in this chapter. In order to avoid the expense of simulating multiple years of operation, the Typical Meteorological Year (TMY) data base (27) was used for all simulations.

Table 3.3-1

Comparison of simulated models

	$\Delta t = 0.05$		$\Delta t = 0.5$	
	$\overline{D/L}$	\underline{f}	$\overline{D/L}$	\underline{f}
Present model	0.129	0.488	0.130	0.488
Evans model	0.127	0.489	0.123	0.493

System: Madison, January TMY data

$$\frac{B_c}{L} = 0.28$$

$$\frac{B_c}{E} = 0.39$$

3.4 Previous Design Methods for Photovoltaic Systems

On an instantaneous or hourly basis, the photovoltaic electrical conversion efficiency, η_e , can be treated as a linear function of PV cell temperature as given by Equation 3.2-1, provided that the associated control equipment includes maximum power tracking circuitry. From this equation and an energy balance on the array, Siegel (24) and Evans et al. (8) have derived approximate equations for the monthly-average array efficiency, $\bar{\eta}_e$. Both equations are limited to south-facing arrays, and both agree well with simulation results obtained using Equation 3.2-1 on an hourly basis. The equation given by Evans et al. has been used in the present work because it is computationally simpler and because it can be used iteratively to improve the accuracy of the prediction:

$$\bar{\eta}_e = \eta_r \left[1 - \beta \left(\frac{C_f \tau (\alpha - \eta_r) X}{U_L} + T_a - T_r + 3 \text{ }^\circ\text{C} \right) \right] \quad (3.4-1)$$

where

$$X = \begin{cases} 0.789 + 2.996 \bar{K} \text{ MJ/m}^2\text{hr} \\ 0.219 + 0.832 \bar{K} \text{ kW/m}^2 \end{cases} \quad (3.4-2)$$

and

$$C_f = 1. - 1.17 \times 10^{-4} (S_m - S)^2 \quad (3.4-3)$$

Here S is the collector slope, and S_m is the optimum slope for the month, given in Table 3.4-1. T_a is the monthly mean ambient temperature, α is the solar absorptance of the PV cells, and U_L is the

Table 3.4-1

 Optimum Slope (S_m) of South-facing Arrays for use in Equation 3.4-3

<u>Month</u>	<u>S_m (degrees)*</u>
Jan	L + 29
Feb	L + 18
Mar	L + 3
Apr	L - 10
May	L - 22
Jun	L - 25
Jul	L - 24
Aug	L - 10
Sep	L - 2
Oct	L + 10
Nov	L + 23
Dec	L + 30

*L is Latitude (Degrees).

thermal loss coefficient of the array. The reference efficiency in the term $(\alpha - \eta_r)$ serves as a first approximation of $\bar{\eta}_e$, and a slight improvement in accuracy can be achieved by substituting $(\alpha - \bar{\eta}_e)$ for $(\alpha - \eta_r)$ and repeating the calculation. In general, however, the thermal loss efficient, U_L , and the solar absorbance, α , will not be known with sufficient precision to justify iteration. Evans et al. provide recommendations for estimating the ratio U_L/α from manufacturer's data.

Once the monthly-average array efficiency is known, the average daily d.c. power generation can be calculated:

$$\bar{E} = A_c \bar{H}_T \bar{\tau} \bar{\eta}_e \eta_{mp} \quad (3.4-4)$$

Evans et al. (9) have prepared a set of graphs for predicting the solar load fraction met by a photovoltaic system with energy storage for 41 load profiles. Table 3.4-2 provides a comparison between this graphical method and TRNSYS simulation results. While the accuracy of the graphical method appears to be quite satisfactory, an analytical method suitable for computer implementation is desirable.

Assuming a constant 24-hour load, Siegel (24) has applied the monthly-average daily utilizability approach to estimate system performance. A critical insolation level, H_c , is defined as the radiation level at which the rate of electrical energy production is just equal to the daily demand:

$$H_c = \frac{\bar{L}}{A_c \bar{\tau} \bar{\eta}_e \eta_{mp}} = \frac{\bar{L} \bar{H}_T}{\bar{E}} \quad (3.4-5)$$

Table 3.4-2

Comparison between design method of Evans (9) and TRNSYS simulation

<u>Month</u>	<u>Solar Load Fraction</u>			
	$\frac{B_c}{L} = 0$		$\frac{B_c}{L} = 0.7$	
	<u>Evans</u>	<u>TRNSYS</u>	<u>Evans</u>	<u>TRNSYS</u>
Jan	.26	.26	.29	.29
Feb	.36	.41	.46	.46
Mar	.50	.54	.71	.75
Apr	.62	.56	.87	.84
May	.66	.67	.91	.93
Jun	.69	.67	.96	.93
Jul	.71	.68	.96	.97
Aug	.69	.58	.94	.93
Sep	.55	.55	.82	.83
Oct	.42	.49	.60	.62
Nov.	.28	.28	.32	.32
Dec	.19	.22	.23	.23
Year	.49	.49	.67	.68

System: Seattle, slope = latitude, "Unimodal Load #6" from
Evans et al. (9) (see Table 3.5-2)

The value of the monthly-average daily utilizability function, $\bar{\phi}$, calculated (28) from this critical level is the fraction of the electrical power which must be dissipated in a system without storage or utility feedback capabilities. The monthly-average rate at which energy is dissipated from such a system is given by

$$\bar{D}_o = A_c \bar{H}_T \bar{\eta}_e \bar{\eta}_{mp} \bar{\phi} = \bar{E} \bar{\phi} \quad (3.4-6)$$

and the solar load fraction without storage, f_o , is given by

$$f_o = A_c \bar{H}_T \bar{\eta}_e \bar{\eta}_{mp} \eta_{pc} (1 - \bar{\phi})/L = \bar{E}(1-\bar{\phi})/L \quad (3.4-7)$$

In a system with battery storage, energy is dissipated only when the battery is full. Siegel has proposed a correlation for estimating the actual rate of energy dissipation in a system with storage, \bar{D}_a , as a function of the dissipation rate without storage, \bar{D}_o , and the ratio of the battery capacity to the average load, B_c/\bar{L} .* The monthly solar load fraction with storage is then given by

$$f = f_o + \eta_b \eta_{pc} (\bar{D}_o - \bar{D}_a)/L \quad (3.4-8)$$

This method for predicting system performance is limited to systems exposed to a constant 24-hour load profile. A comparison between this

*The battery storage capacity has units of energy (e.g., Watt-hours). Since the average load has units of power, the ratio B_c/\bar{L} has units of time, and must be expressed in days. Alternatively, the storage capacity can be considered a daily quantity, e.g., Watt-hours per day, in which case B_c/\bar{L} is a dimensionless ratio.

method, the graphical method of Evans, and TRNSYS simulation results is provided in Table 3.4-3. The accuracy of the two design methods is quite similar--both yield rms errors between 2% and 3%.

For systems without storage, hourly utilizability can be applied in a straightforward manner to extend the method of Siegel to allow prediction of system performance for any load profile. For the i^{th} hour of the day, a critical level can be defined in terms of L_i , the average load for that hour:

$$I_{c,i} = \frac{L_i}{A_c \bar{\tau} \bar{\eta}_e \eta_{mp} \eta_{pc}} \quad (3.4-9)$$

The fraction of insolation received at a rate exceeding this level, ϕ_i , can be calculated by methods described in Chapter 2. The monthly solar load fraction without storage is found by summing hourly results over a typical day of the month:

$$f_o = \left[\sum_i A_c \bar{I}_{T,i} \bar{\tau}_i \bar{\eta}_e \eta_{mp} \eta_{pc} (1 - \phi_i) \right] / \left(\sum_i L_i \right) \quad (3.4-10)$$

The monthly-average daily energy which must be dissipated is given by

$$\bar{D}_o = \sum_i A_c \bar{I}_{T,i} \bar{\tau}_i \bar{\eta}_e \eta_{mp} \phi_i \quad (3.4-11)$$

This approach to estimating photovoltaic system performance provided the motivation for the examination of hourly utilizability methods presented in Chapter 2. The remaining problem, estimation of the effect of adding a storage battery to a photovoltaic system, is

Table 3.4-3

Comparison between design methods (9, 24) and TRNSYS simulation

Month	Solar Load Fraction					
	$\frac{B_c}{L} = 0$			$B_c/\bar{L} = 0.25$		
	Evans	Siegel	TRNSYS	Evans	Siegel	TRNSYS
Jan	.16	.16	.16	.17	.20	.17
Feb	.23	.21	.22	.26	.28	.26
Mar	.35	.31	.33	.42	.44	.41
Apr	.37	.36	.40	.48	.49	.46
May	.45	.40	.43	.55	.53	.54
Jun	.46	.41	.46	.57	.54	.56
Jul	.47	.43	.47	.62	.57	.61
Aug	.38	.40	.46	.54	.54	.57
Sep	.37	.35	.36	.42	.48	.47
Oct	.31	.26	.27	.36	.37	.34
Nov	.18	.17	.18	.19	.23	.19
Dec	.14	.11	.12	.14	.14	.14
Year	.32	.30	.32	.39	.40	.40

System: Seattle, Slope = 60°, constant load

the topic of the next section.

3.5 Estimation of the Effect of Electrical Storage

The performance of a photovoltaic system without energy storage, given any load profile, can be estimated using Equations 3.4-1, 3.4-9, 2.3-4, and 3.4-10. \bar{D}_O , defined by Equation 3.4-11, represents energy which cannot be sent directly from the photovoltaic array to the load, but must be dissipated, sold, or stored. Siegel (24) has proposed a correlation for estimating \bar{D}_A , the energy dissipated from a system with storage; this correlation is applicable only for a constant 24-hour load profile. In this section a correlation is developed for estimating Δf_s , defined as the increase in the solar load fraction met by the system due to the addition of storage:

$$\Delta f_s = f - f_o \quad (3.5-1)$$

where f is the solar load fraction met by the system with storage, and f_o is the solar load fraction met by an equivalent system with no storage. The primary objective is to predict Δf_s as accurately as possible regardless of the shape of the diurnal load profile.

If all energy dissipated without storage could be stored, (i.e., $\bar{D}_A = 0$), the resulting value of Δf_s would be \bar{D}_O/\bar{L} multiplied by the battery storage efficiency and the efficiency of the power conditioning equipment. This combination of parameters will be used frequently, and for the sake of brevity will be referred to as x :

$$x = \eta_b \eta_{pc} \bar{D}_o / \bar{L} \quad (3.5-2)$$

It is useful to begin by considering the physical constraints which limit the possible values of Δf_s . If x is much less than B_c / \bar{L} , the ratio of the storage capacity to the average load, then the battery is never filled and \bar{D}_A is zero. Regardless of the storage capacity, this limiting case occurs as x approaches zero:

$$\lim_{x \rightarrow 0} \Delta f_s = x \quad (3.5-3)$$

Therefore a graph of Δf_s vs. x should have a slope of one at $x = 0$.

Next consider the case where x is very large. A quantity Δf_{\max} can be defined as the limiting value of Δf_s as the energy available for storage becomes very large relative to the load:

$$f_{\max} = \lim_{x \rightarrow \infty} \Delta f_s \quad (3.5-4)$$

Clearly Δf_s cannot exceed $1 - f_o$, since the load fraction met by the system cannot exceed unity:

$$\lim_{x \rightarrow \infty} \Delta f_s \leq 1 - f_o \quad (3.5-5)$$

For sufficiently large x , all of the daytime portion of the load will be met directly from the array. The battery will then be discharged only at night, and Δf_s may be limited by the effective daily storage capacity of the battery relative to the load:

$$\lim_{x \rightarrow \infty} \Delta f_s \leq \eta_{pc} B_c / \bar{L} \quad (3.5-6)$$

Combining Equations 3.5-4 through 3.5-6, the limiting value of

Δf_s as x becomes very large is

$$\Delta f_{\max} = \min(1 - f_o, \eta_{pc} B_c \sqrt{L}) \quad (3.5-7)$$

An equation for Δf_s which satisfies the constraints described above for very large and very small values of x is:

$$\Delta f_s = \frac{1}{2A} \left[x + \Delta f_{\max} - \sqrt{(x + \Delta f_{\max})^2 - 4Ax \Delta f_{\max}} \right] \quad (3.5-8)$$

Taking Δf_s as the ordinate and x as the abscissa, this equation describes a hyperbola which passes through the origin with a slope of one. One asymptote of the hyperbola is a horizontal line at $\Delta f_s = \Delta f_{\max}$. The parameter A , which is the only degree of freedom in this equation, has no apparent physical significance; in terms of a graph of the equation it is the inverse of the slope of the second asymptote. In practical terms, A can be used to vary the rate at which Δf_s approaches Δf_{\max} as x increases. In Figure 3.5-1, Equation 3.5-8 is graphed for several values of A , with $\Delta f_{\max} = 0.5$. When $A = 1$, the equation yields two intersecting straight line segments: for this special case, the equation is equivalent to

$$\Delta f_s \Big|_{A=1} = \min(x, \Delta f_{\max}) \quad (3.5-9)$$

This is precisely the result expected for infinite storage capacity, provided that energy carryover from month to month can be neglected. Thus Equation 3.5-8 is suitable for all battery sizes as well as for all values of x . The remaining problem is to develop a correlation

FORM OF ELECTRICAL STORAGE CORRELATION

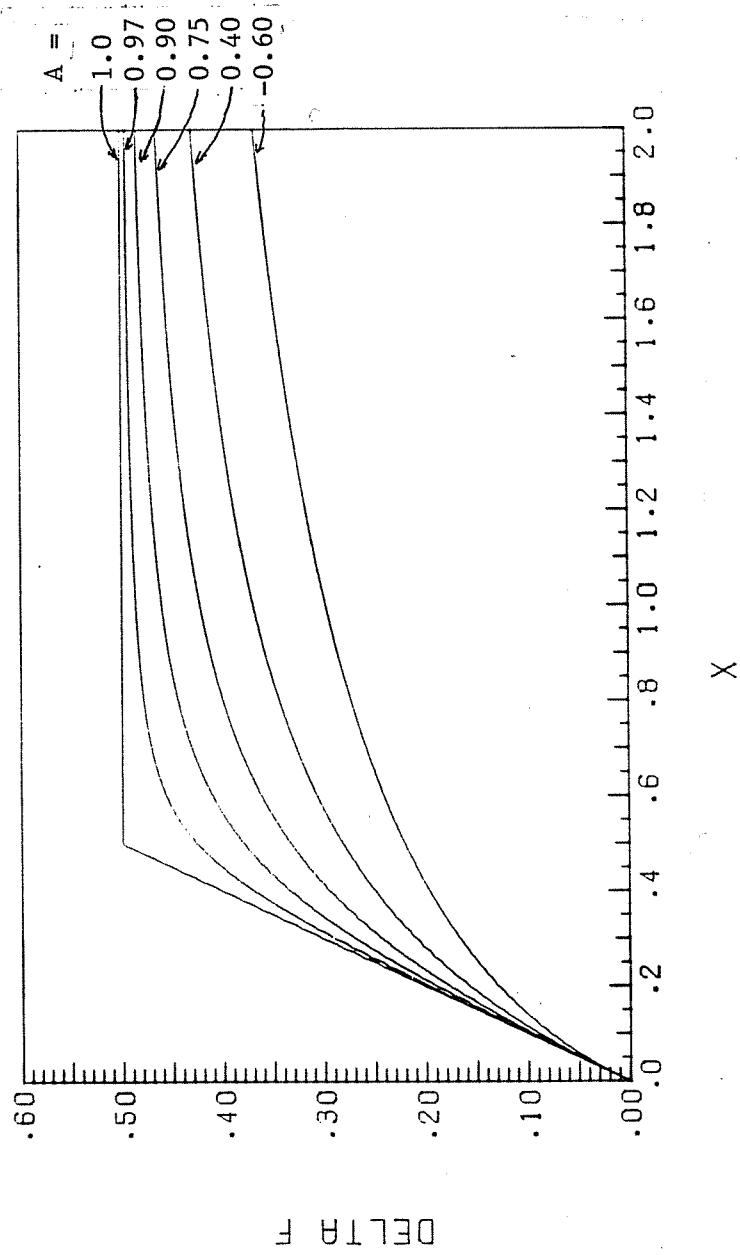


Figure 3.5-1: Form of Correlation for Δf_s

for A to minimize the difference between Equation 3.5-8 and hourly simulation results.

The simulations used in developing the correlation can be divided into three sets. In the first and most extensive set, an array in Madison with a slope equal to the latitude (43°) was modeled; all system parameters were held constant except for the array area, the storage capacity, and the shape of the load profile. Fifteen different load profiles were used in conjunction with three battery capacities and a variety of array areas, for a total of 56 simulation years. The conditions used for these simulations are summarized in Table 3.5-1. The fifteen load profiles are depicted in Figure 3.5-2. Only the daytime portion of the load is shown, together with the percentage of the load occurring during the day. Since the battery storage efficiency is assumed constant, the distribution of the night-time portion of the load is irrelevant. These load profiles are not necessarily realistic, but are intended to cover the spectrum from very well-matched to entirely mis-matched loads.

The second set of simulations consists of nine years: three battery capacities in Albuquerque, three in Madison, and three in Seattle, with the slope equal to the latitude and all other parameters fixed. The parameter values used in these simulations are given in Table 3.5-2.

The third set of simulations consists of eight years, using two battery capacities, two battery efficiencies, two power condi-

Table 3.5-1

Parameter values for first set of TRNSYS simulations: 56 years
(672 months)

Data base: Madison, WI TMY

Latitude = 43°	$\beta = 0.0045 \text{ C}^{-1}$
Slope = 43°	$\eta_r = 0.0902$
Azimuth = 0°	$T_r = 47 \text{ C}$
$\rho = 0.2$	$\eta_{mp} = 0.96$
$\tau = 0.9$	$\eta_b = 0.85$
$\alpha = 0.8$	$\eta_{pc} = 0.87$
$U_L = 24 \text{ W/m}^2 \text{ C}$	$\bar{L} = 25 \text{ Watts}$

$B_c/\bar{L} = 0.25, 0.50, 1.00$

Array area: $0.5 \text{ m}^2 \leq \text{Area} \leq 3.5 \text{ m}^2$

15 load distributions: see Figure 3.5-2

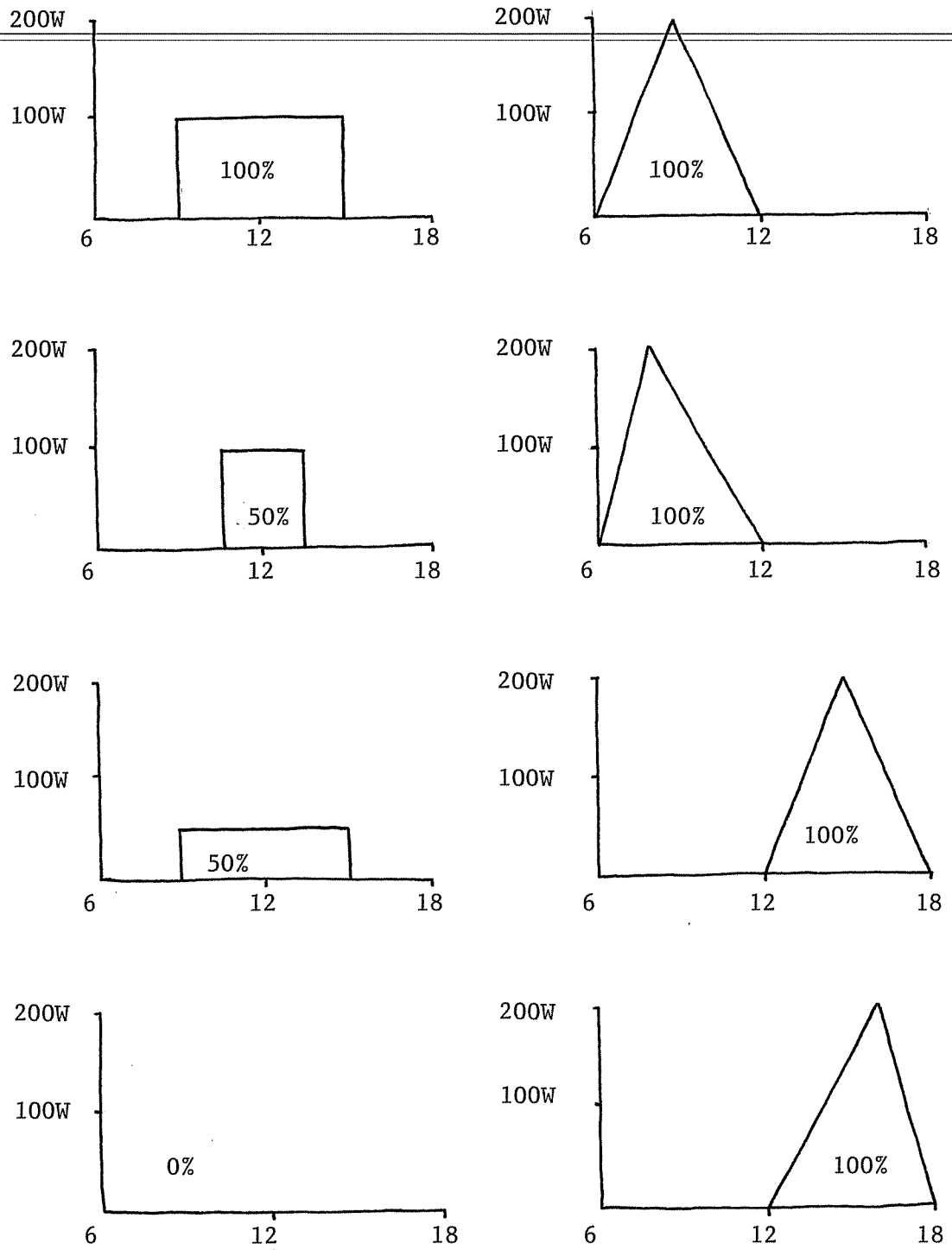


Figure 3.5-2: Load Distributions Used in First Set of Hourly Simulations

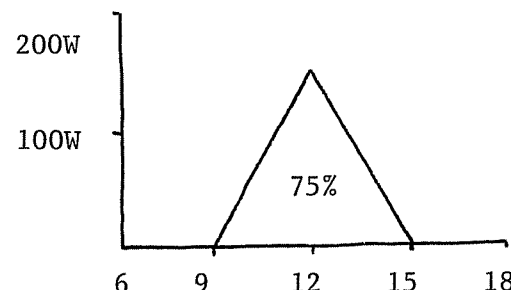
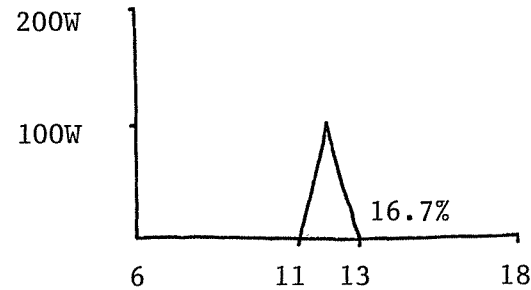
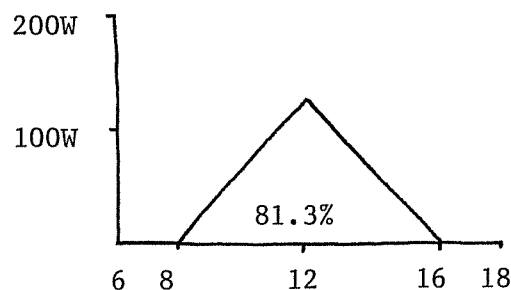
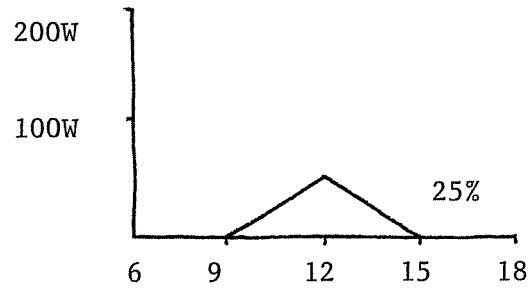
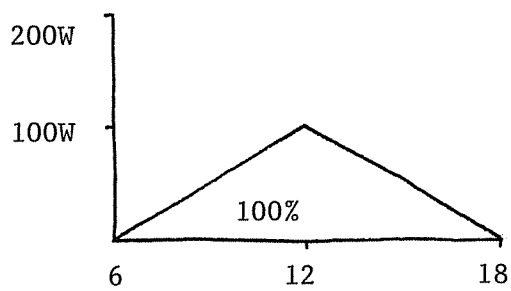
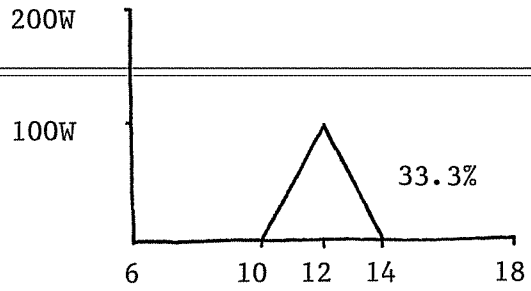
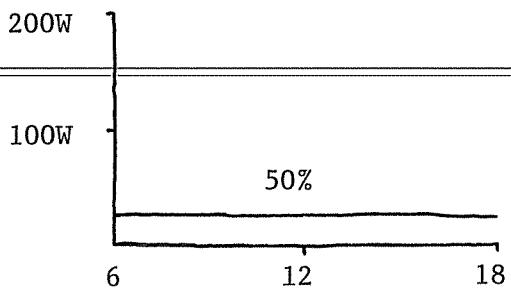


Figure 3.5-2 (continued)

Table 3.5-2

Parameter values for second set of TRNSYS simulations: 9 years
(108 months)

3 locations: Albuquerque, NM	Latitude = 35.05°
Madison, WI	Latitude = 43.13°
Seattle, WA	Latitude = 47.45°

3 battery sizes at each location: $\frac{\eta_{pc} B_c}{\bar{L}} = 0.25, 0.75, 2.0$

For all simulations:

Slope = Latitude

$$U_L = 24 \text{ W/m}^2 \text{ C}$$

Azimuth = 0°

$$\beta = 0.0045 \text{ C}^{-1}$$

Area = 2.0 m²

$$\eta_r = 0.0902$$

$\bar{L} = 25$ Watts

$$T_r = 47 \text{ C}$$

$\tau = 0.9$

$$\eta_{mp} = 0.96$$

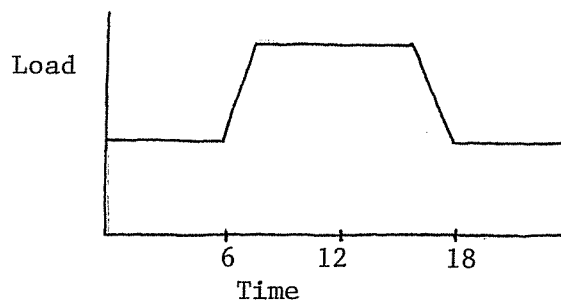
$\alpha = 0.8$

$$\eta_b = 0.9$$

$\rho = 0.2$

$$\eta_{pc} = 0.8$$

Load distribution:
"Unimodal Load #6" from
Evans et al. (9)



tioning equipment efficiencies, and two array slopes (horizontal and vertical). The arrangement of these simulations, given in Table 3.5-3, is suitable for a half-fraction factorial analysis of variance; this will be discussed in Section 3.6.

In developing a correlation for the parameter A in Equation 3.5-8, the values of all other parameters were taken from simulation results, rather than using estimates from Equations 3.4-1, 3.4-10, and 3.4-11. Taking simulation results for the values of x (defined by Equation 3.5-2), Δf_{\max} (Equation 3.5-7), and Δf_s , Equation 3.5-8 can be solved explicitly for the "correct" value of A for each month. Unfortunately, unlike the situation described in Chapter 2 for correlating X_m , the accuracy of attempted correlations for estimating A is not strongly related to the resulting error in Δf_s . As examination of Figure 3.5-1 indicates, small changes in the value of A have a relatively large effect when x is nearly equal to Δf_{\max} and A is near one. The sensitivity of Equation 3.5-8 to changes in A decreases as A decreases, and the value of A becomes nearly irrelevant when x is very small. Consequently the use of linear regression to minimize the error in estimating A is not a reliable tool for minimizing the error of Δf_s . All hypothetical models for A were therefore evaluated in terms of their effect on the root-mean-square (rms) error of Δf_s , using a non-linear regression program.

Initial correlation attempts used only the first set of simulations described above, consisting of 672 monthly observations (56 years). If A is assumed constant for all months and conditions, the

Table 3.5-3

Parameter values for third set of TRNSYS simulations: 8 years
(96 months)

<u>Year #</u>	<u>η_{pc}</u>	<u>η_b</u>	<u>Slope</u>	<u>B_c/\bar{L}</u>
1	0.6	0.6	0°	0.25
2	1.0	0.6	0°	2.0
3	0.6	1.0	0°	2.0
4	1.0	1.0	0°	0.25
5	0.6	0.6	90°	2.0
6	1.0	0.6	90°	0.25
7	0.6	1.0	90°	0.25
8	1.0	1.0	90°	2.0

For all simulations:

$$\text{Area} = 2.0 \text{ m}^2$$

$$\eta_r = 0.0902$$

$$\text{Load} = 25 \text{ Watts (constant)}$$

$$T_r = 47 \text{ C}$$

$$\text{Azimuth} = 0^\circ$$

$$\eta_{mp} = 0.96$$

$$\tau = 0.9$$

$$\alpha = 0.8$$

$$\rho = 0.2$$

$$U_L = 24 \text{ W/m}^2 \text{ C}$$

$$\beta = 0.0045 \text{ C}^{-1}$$

best value of A for this set of data is 0.90, and the resulting rms error of Δf_s is ± 0.037 . Table 3.5-4 lists a number of attempted correlations for A and the corresponding rms errors of Δf_s . The last equation in this table was selected for further study.

The second set of simulations covers a broad range of values of the monthly-average daily clearness index, \bar{K} . Examination of this set of data suggested that \bar{K} should be included in a correlation for A. Table 3.5-5 lists five models for A and the resulting rms error of Δf_s , based on the combined data from all three sets of simulations--a total of 876 observations (73 years). The first model in this table is of the same form as the last model in Table 3.5-4. The remaining four models introduce \bar{K} in various forms. The last equation in this table is the final result of the present study:

$$A = 1.315 - 0.1059 \frac{f_o \bar{L}}{\eta_{pc} B_c} - \frac{0.1847}{\bar{K}} \quad (3.5-10)$$

The use of this equation in Equation 3.5-8 results in an rms error of 3.0% in estimating Δf_s , based on 876 simulated months, when values of x and f_o are taken from the simulations. Correlation coefficients between the error in Δf_s and various parameters are given in Table 3.5-6 for each of the three sets of simulations. A positive correlation coefficient indicates a tendency for Δf_s to be increasingly underpredicted (or decreasingly overpredicted) as the parameter in question increases. The proportion of the error in Δf_s that can be explained by a linear relationship to the parameter in question is given by the square of the correlation coefficient. Thus, for

Table 3.5-4

Attempted correlations for the parameter A in Eq. 3.5-8

Data: 672 monthly simulations (56 years) summarized in Table 3.5-1

<u>Model</u>	<u>rms error of Δf_s</u>
$A = 0.9005$	0.0368
$A = 0.968 - 0.193 f_o - 0.0231 \frac{\bar{D}_o}{\eta_{pc} B_c}$	0.0346
$A = 1. - \frac{\bar{L}}{\eta_{pc} B_c} (0.0402 - 0.118 f_o)$	0.0344
$A = 1. - 0.124 \frac{\bar{E}}{\eta_{pc} B_c} + 0.119 \frac{\eta_b \bar{D}_o}{B_c}$	0.0343
$A = 0.979 - 0.150 f_o - 0.0248 \frac{\bar{E}}{\eta_{pc} B_c}$	0.0343
$A = 0.948 - \frac{\bar{L}}{\eta_{pc} B_c} (0.00469 - 0.119 f_o)$	0.0337
$A = 0.940 - f_o \left(0.0363 - 0.141 \frac{\bar{L}}{\eta_{pc} B_c} \right)$	0.0337
$A = 0.942 - 0.122 \frac{f_o \bar{L}}{\eta_{pc} B_c}$	0.0337

Table 3.5-5

Attempted correlations for the parameter A in Eq. 3.5-8

Data: 876 monthly simulations (73 years) summarized in Tables 3.5-1 through 3.5-3

<u>Model</u>	<u>rms error of Δf_s</u>
$A = 0.952 - 0.110 \frac{f_o \bar{L}}{\eta_{pc} B_c}$	0.03368
$A = 0.862 - 0.0869 \frac{f_o \bar{L}}{\eta_{pc} B_c} + 0.1806 \frac{\eta_{pc} B_c \bar{K}}{\bar{L}}$	0.03269
$A = 1.021 - 0.0658 \frac{f_o \bar{L}}{\eta_{pc} B_c} - 0.0316 \frac{\bar{L}}{\eta_{pc} B_c \bar{K}}$	0.03180
$A = 0.586 - 0.1123 \frac{f_o \bar{L}}{\eta_{pc} B_c} + 0.7194 \bar{K}$	0.03061
$A = 1.315 - 0.1059 \frac{f_o \bar{L}}{\eta_{pc} B_c} - \frac{0.1847}{\bar{K}}$	0.03015

Table 3.5-6

Correlation coefficients between $(\Delta f_{s,TRNSYS} - \Delta f_{s,DESIGN})$ and various parameters

Parameter	Data Set		
	#1	#2	#3
$\Delta f_{s,TRNSYS}$.105	.339	.735
$\eta_b \eta_{pc} \overline{D_o} / \overline{L}$	-.196	.033	.277
$\eta_{mp} \overline{E} / \overline{L}$	-.257	.101	.321
Δf_{max}	.011	.099	.317
f_o	-.190	.227	.460
$\eta_{pc} B_c / \overline{L}$	-.023	.351	.547
\overline{K}	.027	.014	.278

example, in the first set of data only 6.6% of the error in Δf_s can be accounted for by a linear relationship to $\eta_{mp} \overline{E/L}$; in the second and third sets of data, the error is weakly correlated to $\eta_{mp} \overline{E/L}$ in the opposite sense. The accuracy of the predicted values of Δf_s is essentially independent of all of the parameters in Table 3.5-6. The relatively large correlation coefficients in the third set of data are most likely a consequence of the particular load profile used in generating the data, since both the first and third sets use precisely the same weather data.

In practice, values of f_o and x for use in Equations 3.5-10 and 3.5-8 must be estimated rather than taken from simulation results. In the next section the accuracy of the design method as a whole is examined.

3.6 Analysis of Design Method Results

On a monthly-average basis, the fraction of any specified load that will be met by a photovoltaic system without storage, f_o , can be estimated by Equation 3.4-10, using the hourly utilizability function correlation developed in Chapter 2. The energy available for storage is estimated by Equation 3.4-11, and the increase in the load fraction met by a photovoltaic system due to the presence of storage batteries, Δf_s , is estimated by Equations 3.5-10 and 3.5-8. The load fraction met by a photovoltaic system with storage is then simply

$$f = f_o + \Delta f_s \quad (3.6-1)$$

A computer program which performs all of the necessary calculations is listed in Appendix C. In this section, the accuracy of the design method program relative to hourly simulations using TRNSYS (16) is examined. Results are presented primarily in terms of the mean bias error, which is the average difference between simulation and design method results, positive when the design method underpredicts performance, and the root-mean-square (rms) error, which is the standard deviation of the differences between simulation and design method results.

Errors in the monthly solar load fractions, f_o , Δf_s , and f , tend to average out over a year. Consequently the rms errors of estimated annual solar load fractions, F_o , ΔF_s , and F , are considerably smaller than the rms errors of the monthly values. Rms errors are presented below on both monthly and annual bases.

Results from the first set of simulations, based on a single location and a wide variety of load profiles, are given in Table 3.6-1. The mean bias errors are less than +1% in all cases, indicating that the design method has very little tendency to systematically underpredict or overpredict performance. The rms error of 3.9% in the monthly load fraction is due primarily to errors in estimating the effect of storage; prediction of the load fraction without storage is remarkably accurate. The same is true on an annual basis.

Table 3.6-1

 Accuracy of Design Method relative to first set of hourly simulations

<u>672 Monthly Load fractions</u>	<u>Mean bias error (%)</u>	<u>rms error (%)</u>
f_o	0.3	1.7
Δf_s	-0.8	3.7
f	-0.5	3.9
<u>56 Annual Load fractions</u>		
F_o	0.3	0.7
ΔF_s	-0.8	2.5
F	-0.5	2.4

The second set of simulations examines three locations and three battery capacities, using a single load profile. Results are summarized in Table 3.6-2 for the combined data, for each location, and for each battery capacity. Mean bias errors are the same whether calculated monthly or annually, and are given only with the monthly results. On a monthly basis, the uncertainty in the predictions is greatest for Seattle and for the large storage capacity. The annual rms errors based on only three years should be considered rough approximations; in general they are comparable to or less than the annual rms errors from the first set of data. In contrast to the monthly results, the uncertainty in the annual load fraction is smallest for Seattle.

Figures 3.6-1 and 3.6-2 are scatter plots of simulated vs. estimated monthly load fractions. In Figure 3.6-1 the data are identified by location, and in Figure 3.6-2 the same data are identified by storage capacity. The design method tends to underpredict large load fractions and to overpredict small load fractions, regardless of the location or the storage capacity. Examination of the correlation coefficients given in Table 3.5-6 suggests that this trend is primarily a consequence of the single load profile used, not a general property of the design method. The large rms error of the Seattle data is apparently due to the fact that the values of f cover the broadest range in Seattle. No other location-dependent trend is apparent.

Table 3.6-2

Accuracy of design method relative to second set of hourly simulations

Mean bias error \pm rms error of:

<u>Data</u>	\underline{f}_o	$\underline{\Delta f}_s$	\underline{f}
Combined	.013 \pm .022	-.008 \pm .038	.004 \pm .046
Albuquerque	.013 \pm .016	-.010 \pm .021	.003 \pm .020
Madison	.008 \pm .023	.004 \pm .038	.012 \pm .050
Seattle	.016 \pm .026	-.020 \pm .050	-.003 \pm .059
$\eta_{pc} B_c / \bar{L} = 0.25$.013 \pm .022	-.009 \pm .027	.003 \pm .038
0.75	.013 \pm .022	-.015 \pm .033	-.003 \pm .040
2.0	.013 \pm .022	-.0003 \pm .050	.012 \pm .058

Mean bias error of:

<u>Data</u>	$\underline{\Delta F}_s$	\underline{F}
Combined	.020	.017
Albuquerque	.018	.016
Madison	.021	.024
Seattle	.021	.009
$\eta_{pc} B_c / \bar{L} = 0.25$.018	.015
0.75	.017	.005
2.0	.025	.026

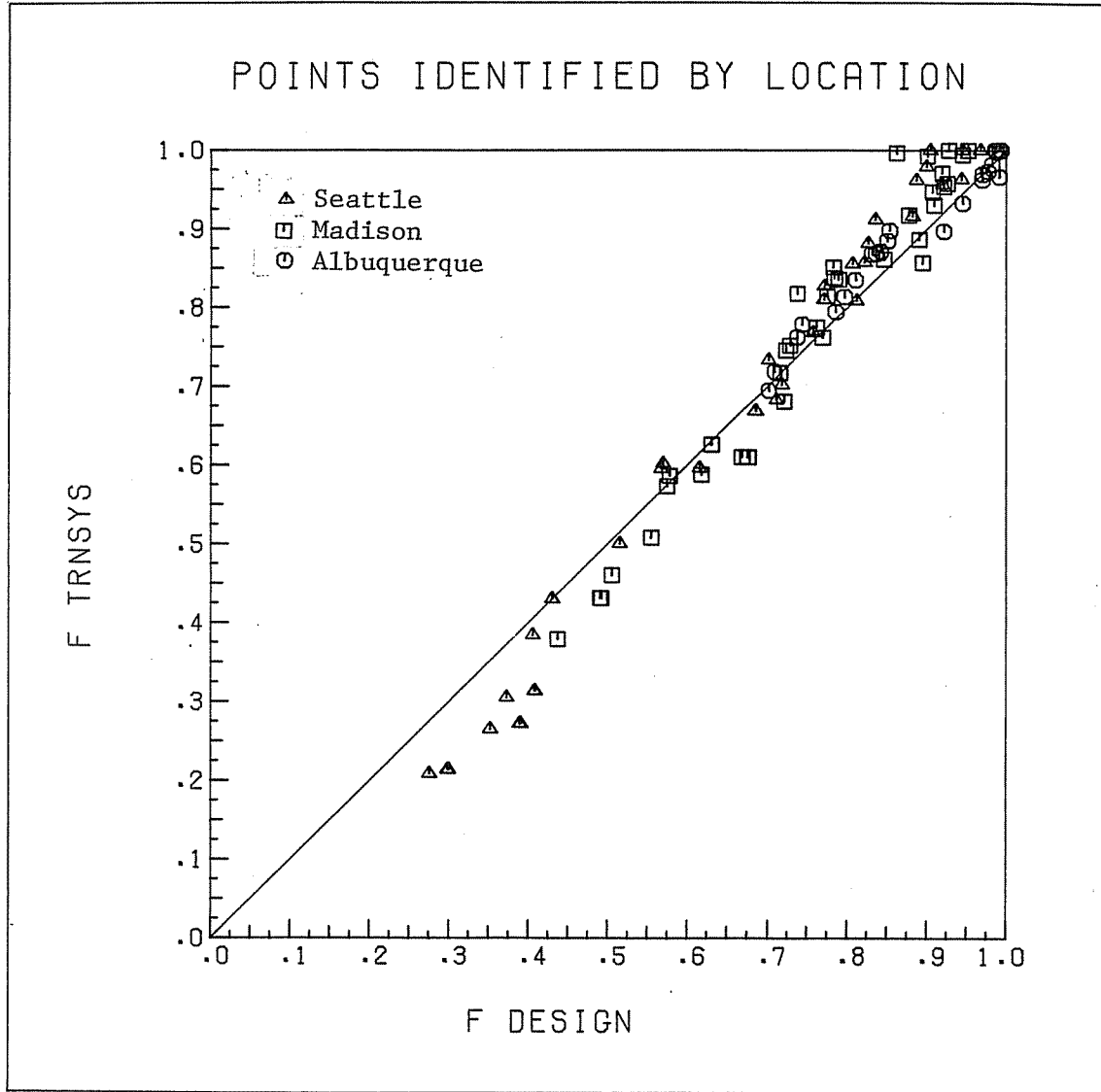


Figure 3.6-1: Simulated vs. Estimated Monthly Load Fractions Identified by Location

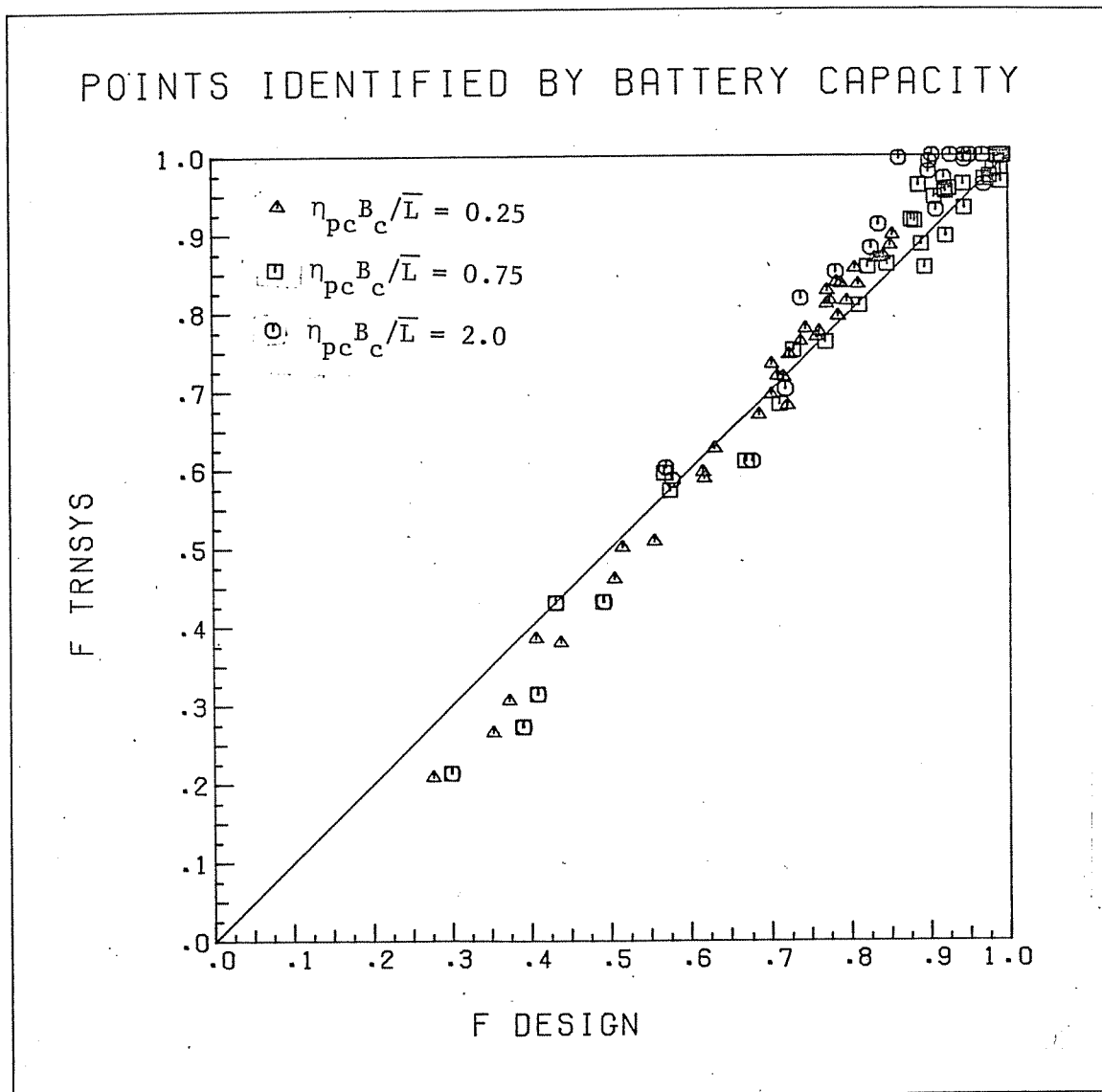


Figure 3.6-2: Simulated vs. Estimated Monthly Load Fractions Identified by Storage Capacity

The purpose of the third set of data is to examine the influence of the power conditioning equipment efficiency, the battery efficiency, the slope of the array, and the storage capacity to average load ratio on the accuracy of the design method. The procedure used is a half-fraction factorial analysis, details of which can be found in reference (2). Briefly, each of the four parameters is used at a high level and a low level as shown in Table 3.5-3. The effect of a parameter on the error is given by the average error at the high level of the parameter minus the average error at the low level. A large effect indicates that changing the parameter changes the accuracy of the design method; ideally all effects should be small. Second-order effects are confounded with each other in a half-fraction analysis. For example, the effect of changing both the power conditioning efficiency and the storage capacity ratio cannot be distinguished from the effect of changing both the battery efficiency and the slope.

Seven effects can be calculated: the effect of each parameter separately, and three pairs of second-order effects. (The four first-order effects are actually confounded with third-order effects, which are assumed negligible.) These effects are listed in Table 3.6-3 in order of decreasing magnitude. All effects are positive, indicating that for each parameter the design method underpredicts performance more (or overpredicts less) at the high level of the parameter than at the low level.

Table 3.6-3

Results of factorial analysis of variance

<u>Parameter</u>	<u>Effect of parameter on ($f_{\text{SIMULATION}} - f_{\text{DESIGN}}$)</u>
B_c/L	.0272
η_{pc}	.0163
$\eta_b \cdot B_c/L, \eta_{pc} \cdot S$.0150
$\eta_{pc} \cdot B_c/L, \eta_b \cdot S$.0142
S	.0117
$S \cdot B_c/L, \eta_b \cdot \eta_{pc}$.0029
η_b	.0025

For the constant 24-hour load profile used in this study, changing the storage capacity to load ratio from 0.25 to 2.0 changes the error of the design method by 2.7%. Whether or not a similar effect of the storage ratio on design method accuracy would be found for other load distributions remains unclear. The correlation coefficients given in Table 3.5-6 indicate that for the first set of data, the error in estimating Δf_s is independent of the storage ratio, but no ratios greater than 1.0 were used. For the second and third sets of data, the error in Δf_s correlates relatively well with the storage ratio, but only a single load profile was used in each case.

The fact that the six remaining effects in Table 3.6-3 are all of the same sign indicates that they are not entirely random. However, since all are relatively small, the effects of the power conditioning efficiency, the slope of the array, the battery efficiency, and the various second-order interactions on the accuracy of the design method can be considered unimportant.

In conclusion, the design method agrees with hourly simulation results with a standard deviation of less than 4% on a monthly basis, and about 2.4% on an annual basis. The accuracy of design method predictions is nearly independent of all parameters examined, with the possible exception of storage to load ratios greater than 1.0. Reasonable results are obtained with storage ratios of 2.0, the largest storage capacity considered. The form of the correlation is such that reasonable results are expected for even larger storage ratios, provided that significant seasonal storage does not

occur.

3.7 Sample Calculation

In this section the use of the design method is demonstrated by the analysis of a hypothetical photovoltaic system in Boston, Massachusetts. The characteristics of the system are given in Table 3.7-1. Based on limited information, the load profile used is appropriate for an average residential application (i.e., several houses) (8).

From reference (6), the average rate of horizontal insolation in Boston in January is 62.45 W/m^2 , the mean ambient temperature is -1 C , and the average day of the month is the 17th. From Equation 1.3-4 the declination is

$$\delta = 23.45 \sin \left[\frac{360}{365} (284 + 17) \right] = -20.9^\circ \quad (3.7-1)$$

and from Equation 1.3-5 the sunset hour angle is

$$\omega_s = \cos^{-1} (-\tan 42.37 \tan -20.9) = 69.6^\circ \quad (3.7-2)$$

Average daily extraterrestrial radiation is given by Equation 1.3-3 with $n = 17$:

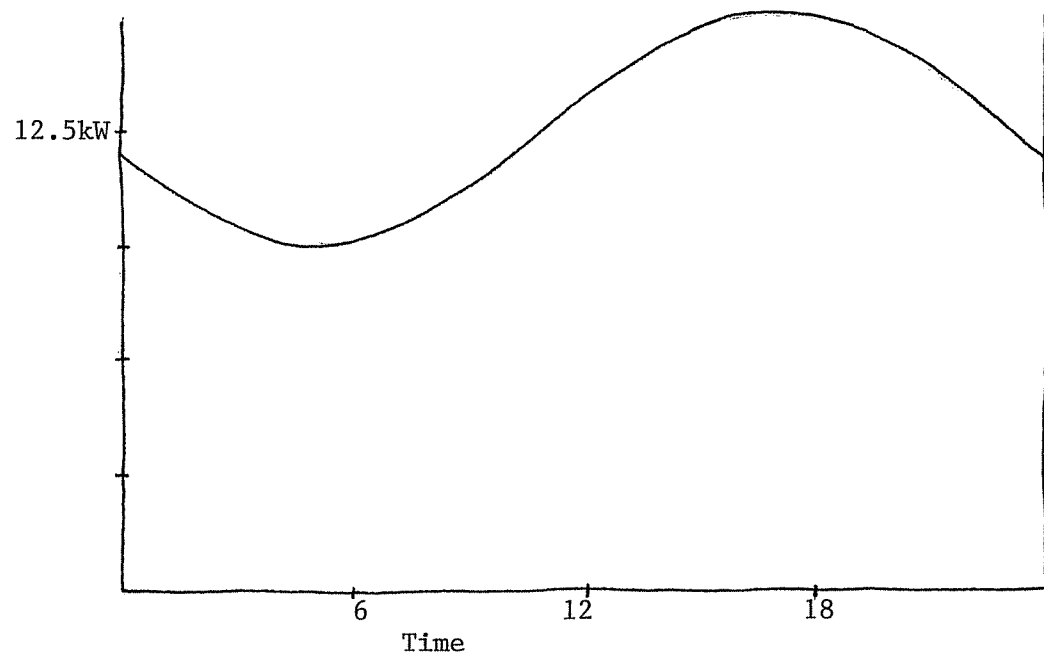
$$\begin{aligned} \bar{H}_o = & \frac{(1353 \text{ W/m}^2)}{\pi} \left[1 + 0.033 \cos \left(17 \cdot \frac{360}{365} \right) \right] \\ & \left(\cos 42.37 \cos -20.9 \sin 69.6 \right. \\ & \left. + \frac{69.6\pi}{180} \sin 42.37 \sin -20.9 \right) = 157.7 \text{ W/m}^2 \end{aligned} \quad (3.7-3)$$

Table 3.7-1

Photovoltaic system characteristics for sample calculation

Boston, MA	Latitude = 42.37°
Area = 600 m ²	$\eta_r = 0.10$
Slope = 50°	$T_r = 28 \text{ C}$
$U_L = 40 \text{ W/m}^2 \text{ C}$	$\beta = 0.0039 \text{ C}^{-1}$
$\tau = 1.0$	$\eta_{mp} = 0.98$
$\alpha = 0.88$	$\eta_{pc} = 0.90$
$\rho = 0.2$	$\eta_b = 0.87$
$B_c = 140 \text{ KW-hr}$	$\bar{L} = 12.5 \text{ kW}$

Load profile: sinusoidal, peak at 17:00, amplitude/average = 0.25



and from Equation 1.3-2, the daily clearness index is

$$\bar{K} = 62.45/157.7 = 0.396 \quad (3.7-4)$$

The daily average diffuse fraction is calculated from Equation 1.4-4:

$$\bar{H}_d/\bar{H} = 1.317 - 3.023(.396) + 3.372(.396)^2 - 1.76(.396)^3 = 0.539 \quad (3.7-5)$$

The next step is to determine the monthly-average electrical conversion efficiency, $\bar{\eta}_e$. From Table 3.4-1, the optimum slope for January is

$$S_m = 42.37 + 29 = 71.37^\circ \quad (3.7-6)$$

and from Equation 3.4-3 the correction factor for non-optimum slope is

$$C_f = 1 - 1.17 \times 10^{-4} (71.37 - 50)^2 = 0.947 \quad (3.7-7)$$

Since U_L is given in W/m^2C , Equation 3.4-2 is converted to W/m^2 :

$$X = 0.219 + 0.832 \cdot 0.396 = .5485 \text{ kW/m}^2 = 548.5 \text{ W/m}^2 \quad (3.7-8)$$

Equation 3.4-1 gives the average array efficiency as

$$\bar{\eta}_e = 0.10 \left[1 - .0039 \left(\frac{0.947 \cdot 1 \cdot (0.88 - 0.10) \cdot 548.5}{40} + (-1) - 28 + 3 \right) \right] = 0.106 \quad (3.7-9)$$

Next the day is divided into hours, and system performance is estimated for each hour. In January the first hour after sunrise is from 8:00 ($\omega = 60^\circ$) to 9:00 ($\omega = 45^\circ$). At the midpoint of the hour, the hour angle is 52.5° . The average hourly clearness index is estimated from Equation 1.4-2:

$$\begin{aligned} a &= 0.409 + 0.5016 \sin(69.6 - 60) = 0.493 \\ b &= 0.6609 - 0.4767 \sin(69.6 - 60) = 0.581 \\ \bar{k} &= 0.396 (.493 + .581 \cos 52.5) = 0.335 \end{aligned} \quad (3.7-10)$$

The hourly average diffuse fraction is estimated from Equations 1.4-3 and 3.7-5:

$$\bar{I}_d/\bar{I} = 0.539/(\bar{k} + .581 \cos 52.5) = 0.637 \quad (3.7-11)$$

The ratio of tilted-surface to horizontal beam radiation from Equations 1.3-9 and 1.3-10 is

$$\begin{aligned} R_b &= \frac{\cos\theta}{\cos\theta_z} = [\sin(-20.9)\sin 42.37\cos 50 - \sin(-20.9)\cos 42.37\sin 50 \\ &\quad + \cos(-20.9)\cos 42.37\cos 50\cos 52.5 \\ &\quad + \cos(-20.9)\sin 42.37\sin 50\cos 52.5] \\ &\quad \cdot [\sin(-20.9)\sin 42.37 + \cos(-20.9)\cos 42.37\cos 52.5]^{-1} \\ &= 0.611/0.180 \\ &= 3.40 \end{aligned} \quad (3.7-12)$$

Using Equation 1.3-12 with the average hourly diffuse fraction, the average ratio of tilted-surface to horizontal total radiation is

$$\begin{aligned} \tilde{R} &= (1 - .637) \cdot 3.40 + .637 \cdot \frac{1+\cos 50}{2} + 0.2 \cdot \frac{1-\cos 50}{2} \\ &= 1.79 \end{aligned} \quad (3.7-13)$$

The hourly extraterrestrial radiation from Equation 1.3-8 is

$$I_o = 1353 \cdot 0.180 \left[1 + 0.033 \cos \left(17 \cdot \frac{360}{365} \right) \right] = 250.9 \text{ W/m}^2 \quad (3.7-14)$$

From Equation 1.3-13, the average hourly radiation incident on the array is

$$\bar{I}_T = 250.9 \cdot 0.335 \cdot 1.79 = 150.8 \text{ W/m}^2 \quad (3.7-15)$$

The average load for the hour from 8 to 9 is found to be 10614 Watts. From Equation 3.4-9, the critical insolation level for the hour is

$$I_c = \frac{10614}{600 \cdot 1 \cdot 0.106 \cdot 0.98 \cdot 0.90} = 189.21 \text{ W/m}^2 \quad (3.7-16)$$

The critical insolation ratio is

$$X_c = I_c / \bar{I}_T = 189.21 / 150.8 = 1.25 \quad (3.7-17)$$

The hourly utilizability function given by Equation 2.3-4 is then evaluated:

$$\begin{aligned} X_m &= 1.85 + 0.169 \cdot 1.79 / (0.335)^2 - 0.0696 \cos 50 / (0.335)^2 \\ &\quad - 0.981 \cdot 0.335 / (\cos(-20.9))^2 = 3.77 \end{aligned}$$

$$a = \frac{3.77 - 1}{2 - 3.77} = -1.565$$

$$\phi = \left| -1.565 \pm \sqrt{(-1.565)^2 + (1 + 2(-1.565)) \left(\frac{3.77-1.25}{3.77} \right)^2} \right|$$

$$\phi = 0.341 \quad (3.7-18)$$

The average electrical energy generated for this hour is given by

$$\begin{aligned} E &= A_c \bar{I}_T \bar{\tau} \bar{\eta}_e \eta_{mp} = 600 \cdot 150.8 \cdot 1.0 \cdot 106 \cdot 0.98 \\ &= 9399 \text{ W-hr} \end{aligned} \quad (3.7-19)$$

The energy dissipated without storage is the product of E and ϕ :

$$D_o = 9399 \cdot 0.341 = 3205 \text{ W-hr} \quad (3.7-20)$$

The energy received directly by the load is

$$E_L = \eta_{pc} E(1-\phi) = 0.9 \cdot 9399(1-0.341) = 5575 \text{ W-hr} \quad (3.7-21)$$

The calculations represented by Equations 3.7-10 through 3.7-21 are repeated for each hour between sunrise and sunset. Results of these calculations for January are shown in Table 3.7-2. The numbers in this table for the hour from 8 to 9 differ slightly from the numbers shown above because more decimal places were carried in the former.

Summing the hourly results and averaging over a 24-hour day,

$$\bar{E}_L = \frac{1}{24} \Sigma E_L = 2910 \text{ W} \quad (3.7-22)$$

and

$$\bar{D}_o = \frac{1}{24} \Sigma D_o = 2749 \text{ W} \quad (3.7-23)$$

Table 3.7-2

Results from sample calculation for January

<u>Time</u>	<u>Load(W)</u>	<u>\bar{k}</u>	<u>\bar{I}_T (W/m²)</u>	<u>X_c</u>	<u>ϕ</u>	<u>E_L (W-hr)</u>	<u>D_o (W-hr)</u>
8-9	10614.0	.336	150.0	1.268	.356	5561	3124
9-10	11314.5	.378	259.2	0.782	.465	7746	7468
10-11	12095.5	.408	348.9	0.621	.528	9195	11423
11-12	12904.5	.424	399.5	0.579	.545	10147	13499
12-13	13686.0	.424	399.5	0.614	.524	10623	12971
13-14	14386.5	.408	348.9	0.739	.463	10464	10014
14-15	14958.0	.378	259.2	1.034	.354	9339	5698
15-16	15362.5	.336	150.0	1.835	.191	6774	1776

The solar load fraction without storage is

$$f_o = \frac{\overline{E}_L}{L} = \frac{2910}{12500} = 0.233 \quad (3.7-24)$$

The next step is to determine the effect of the storage battery. From Table 3.7-1,

$$\frac{B_c}{L} = \frac{140 \text{ kW-hr/day}}{(12.5 \text{ kW})(24 \text{ hr/day})} = 0.4667 \quad (3.7-25)$$

From Equation 3.5-2,

$$x = 0.87 \cdot 0.90 \cdot 2749/12500 = 0.1722 \quad (3.7-26)$$

and from Equation 3.5-7,

$$\Delta f_{\max} = \min[(1 - .223), 0.9 \cdot 0.4667] = 0.420 \quad (3.7-27)$$

Equation 3.5-10 yields

$$A = 1.315 - \frac{0.1059 \cdot 0.223}{0.9 \cdot 0.4667} - \frac{0.1847}{0.396} = 0.79 \quad (3.7-28)$$

The increase in the solar load fraction due to storage, from Equation 3.5-8, is

$$\begin{aligned} \Delta f_s &= \frac{1}{2(.79)} \left[.1722 + .420 - \sqrt{(.1722 + .420)^2 - 4(.79)(.1722)(.420)} \right] \\ &= 0.154 \end{aligned} \quad (3.7-29)$$

The fraction of the load met by the system in January is then

$$f = 0.233 + 0.154 = 0.387 \quad (3.7-30)$$

The entire procedure is repeated for each month. In Table 3.7-3 the results of the design method calculations for each month are compared with results from an hourly simulation of the system using TRNSYS. The results without storage are in remarkably close agreement. The agreement of the overall results with storage is less spectacular, but certainly adequate for design purposes.

3.8 Recommendations for Further Work

The design method described in the previous sections is limited to south-facing arrays only for the purpose of calculating the monthly-average array efficiency. The assumption that the array faces south enters the design method through Equation 3.4-3. In effect, this equation accounts for the influence of the slope of the array on its average operating temperature. An array which does not face south will operate at a slightly lower temperature and therefore a slightly higher average efficiency than a similar south-facing array. Since array efficiency decreases as the temperature increases, a well-designed array will have a large thermal loss coefficient, and the effect of the azimuth angle on photovoltaic cell temperature will be small. Furthermore, the array efficiency is a fairly weak function of temperature--for silicon cells, a temperature coefficient of 0.0045 per degree celsius is typical. It seems likely, therefore, that the effect of the azimuth angle in Equation 3.4-1 can be ignored with minimal loss of accuracy.

Table 3.7-3

Results from design method and from hourly simulation using TRNSYS (16)

<u>Month</u>	<u>f_o</u>		<u>f</u>	
	<u>Design</u>	<u>Simulation</u>	<u>Design</u>	<u>Simulation</u>
Jan	.233	.233	.386	.402
Feb	.295	.285	.494	.513
Mar	.332	.330	.565	.578
Apr	.379	.362	.619	.610
May	.408	.405	.656	.677
Jun	.425	.454	.681	.754
Jul	.417	.422	.668	.704
Aug	.392	.410	.633	.682
Sep	.376	.374	.636	.675
Oct	.326	.309	.563	.542
Nov	.230	.242	.371	.401
Dec	.215	.214	.344	.347
Year	.336	.337	.552	.574

For example, under reasonably typical conditions ($\beta = 0.0045$

$C^{-1} \eta_r = 0.10, T_r = 28C, T_a = 20C, U_L = 20 \text{ W/m}^2C, \bar{K} = 0.5, \alpha = 0.9$), changing the slope of a south-facing array from $S = S_m$ to $S = S_m + 40^\circ$ changes the average efficiency from 9.08% to 9.18%. Increasing U_L decreases the effect of the slope. Since U_L is unlikely to be much less than 20 W/m^2C , and arbitrarily assuming the effect of changing the azimuth angle is unlikely to be much greater than the effect of a 40° change in the slope of a south-facing array, the use of Equations 3.4-1 through 3.4-3 for non-south-facing arrays is expected to overpredict array efficiency by less than 0.1%. A more detailed examination of the effect of the azimuth angle on the accuracy of Equation 3.4-1, and the resulting effect on the accuracy of the design method as a whole, would be desirable.

For the purpose of estimating the effect of energy storage, the shape of the load profile is characterized by f_o , the solar load fraction without storage, and by $\eta_b \eta_{pc} \bar{D}_o / \bar{L}$, the potentially useful load fraction available for storage. The data presented in Section 3.6 suggest that the correlation might benefit from the inclusion of additional information about the shape of the load profile in Equation 3.5-10. In addition, or perhaps alternatively, there is evidence that inclusion of a parameter (other than \bar{K}) which varies seasonally, such as the declination or the sunset hour angle, might be useful. These parameters were not examined in the development of Equation 3.5-10.

APPENDIX: COMPUTER PROGRAM LISTINGS

	<u>Page</u>
Appendix A: Hourly Phi Calculations; Method of Huget (12)	123
Appendix B: Regulator-Inverter-Battery Model for TRNSYS	126
Appendix C: Design Method for Photovoltaic Systems	130

APPENDIX A

```

C THIS PROGRAM CALCULATES HOURLY VALUES OF XC AND PHI
C USING THE METHOD OF HUGET (12), INPUTS ARE AS FOLLOWS:
C IC: CRITICAL RADIATION LEVEL
C IHOR: AVERAGE HOURLY HORIZONTAL RADIATION
C HRKTAV: AVERAGE HOURLY CLEARNESS INDEX
C RB: RATIO OF TILTED-SURFACE TO HORIZONTAL BEAM RADIATION
C SLOPE: IN DEGREES
C
SUBROUTINE HRPHI(IC,IHOR,HRKTAV,RR,SLOPE,XC,PHI)
DIMENSION AKT(6),P(3),Q(3),E1(6),E2(6),E3(6),ROOT(5)
REAL IC,IHOR
DATA PI/3.14159/XKMAX/0.864/AKT/0.,0.35,0.75,0.864,0.,0./
DATA P/1.0,1.557,0.177/Q/0.249,1.84,0./
RDCONV=PI/180.
DO 5 I=1,5
5 ROOT(I)=1.
NROOTS=0
VRD=RR-(1.+COS(SLOPE*RDCONV))/2.
D=0.2*(1.-COS(SLOPE*RDCONV))/2.
G=IC*HRKTAV/IHOR
GAMMA=0.
IF(HRKTAV.LE.0.288)GO TO 10
GAMMA=F(HRKTAV)
EO=1./GAMMA
C FIND CRITICAL CLEARNESS INDEX: XKCR
10 B=RB+D-VRD
XKCR=G/B
IF(ABS(VRD).LT.1.E-6)GO TO 80
DET=B*B+0.996*VRD*G
IF(DET.LT.0.)GO TO 20
ROOT(1)=((-B)-SQRT(DET))/(.498*VRD)
ROOT(2)=((-B)+SQRT(DET))/(.498*VRD)
20 B=RB+D-1.557*VRD
DET=B*B+7.36*VRD*G
IF(DET.LT.0.)GO TO 40
ROOT(3)=((-B)-SQRT(DET))/(3.68*VRD)
ROOT(4)=((-B)+SQRT(DET))/(3.68*VRD)
40 B=RB+D-0.177*VRD
IF(ABS(B).LT.1.E-8)GO TO 80
ROOT(5)=G/B
XKCR=1.
XKCR2=0.
DO 60 I=1,3
IF(ROOT(2*I-1).LT.AKT(I).OR.ROOT(2*I-1).GT.AKT(I+1))GO TO 50
NROOTS=NROOTS+1
IF(NROOTS.GE.3)GO TO 60
XKCR=AMIN1(ROOT(2*I-1),XKCR)

```

```

XKCR2=AMAX1(XKCR2,ROOT(2*I-1))
50 IF(L.GE.3)GO TO 60
IF(ROOT(2*I).LT.AKT(I).OR.ROOT(2*I).GT.AKT(I+1))GO TO 60
NROOTS=NROOTS+1
XKCR=AMIN1(ROOT(2*I),XKCR)
XKCR2=AMAX1(XKCR2,ROOT(2*I))
60 CONTINUE
80 IF(XKCR.GT.1.)XKCR=1.
AKT(5)=XKCR
AKT(6)=XKCR2
C
C XKCR HAS BEEN FOUND. PROCEED WITH PHI CALCULATION.
C
ACRINT=0.
AINT=0.
IF(GAMMA.GT.0.)GO TO 85
DO 82 I=1,6
E1(I)=0.5*AKT(I)*AKT(I)
E2(I)=E1(I)*AKT(I)*2./3.
82 E3(I)=E2(I)*AKT(I)*3./4.
CRTERM=G*(XKMAX/2.-XKCR+XKCR*XKCR/(2.*XKMAX))
GO TO 95
85 DO 90 I=1,6
E1(I)=E0*(AKT(I)-E0)
E2(I)=E0*(AKT(I)*AKT(I)-2.*E1(I))
90 E3(I)=E0*(AKT(I)**3-3.*E2(I))
CRTERM=G*((E0-E1(4)/XKMAX)*EXP(GAMMA*XKMAX)-(E0-E1(5)/XKMAX)*EXP
1 (GAMMA*XKCR))
95 DO 110 I=1,3
C1=RB+D-VBD*P(I)
C2=VBD*Q(I)
AHI=(C1*(E1(I+1)-E2(I+1)/XKMAX)+C2*(E2(I+1)-E3(I+1)/XKMAX))*EXP
1 (GAMMA*AKT(I+1))
ALO=(C1*(E1(I)-E2(I)/XKMAX)+C2*(E2(I)-E3(I)/XKMAX))*EXP(GAMMA
1 *AKT(I))
AINT=AINT+AHI-ALO
IF(XKCR.GE.AKT(I+1))GO TO 110
IF(XKCR.LE.AKT(I))GO TO 100
ALO=(C1*(E1(5)-E2(5)/XKMAX)+C2*(E2(5)-E3(5)/XKMAX))*EXP(GAMMA
1 *AKT(5))
100 IF(XKCR2.LE.XKCR.OR.XKCR2.GE.AKT(I+1))GO TO 105
IF(XKCR2.LE.AKT(I))GO TO 110
AHI=(C1*(E1(6)-E2(6)/XKMAX)+C2*(E2(6)-E3(6)/XKMAX))*EXP(GAMMA
1 *AKT(6))
CRTERM=G*((E0-E1(6)/XKMAX)*EXP(GAMMA*XKCR2)-(E0-E1(5)/XKMAX)*EXP
1 (GAMMA*XKCR))
105 ACRINT=ACRINT+AHI-ALO
110 CONTINUE
IF(NROOTS.LT.3) GO TO 120
EA=E0*(ROOT(5)-E0)

```

```

EB=E0*(ROOT(5)*ROOT(5)-2.*EA)
EC=E0*(ROOT(5)**3-3.*EB)
CRCAP=G*((E0-E1(4)/XKMAX)*EXP(GAMMA*XKMAX)-(E0-EA/XKMAX)*EXP
1 (GAMMA*ROOT(5)))
AHI=(C1*(E1(4)-E2(4)/XKMAX)+C2*(E2(4)-E3(4)/XKMAX))*EXP(GAMMA
1 *AKT(4))
ALO=(C1*(EA-EB/XKMAX)+C2*(EB-EC/XKMAX))*EXP(GAMMA
1 *ROOT(5))
ACRINT=ACRINT+AHI-ALO
CRTERM=CRTERM+CRCAP
120 CONTINUE
C=2./XKMAX
IF(GAMMA.GT.0.)C=GAMMA*GAMMA*XKMAX/(EXP(GAMMA*XKMAX)-GAMMA*
1 XKMAX-1.)
XC=G/(C*AIINT)
PHI=(ACRINT-CRTERM)/AIINT
IF(PHI.LT.0.)PHI=0.
IF(G.LE.0.)PHI=1.
RETURN

C
C
FUNCTION F(XKTAV)
DIMENSION ARRAY(52)
DATA ARRAY/.0481,.2848,0.5158,0.7419,0.9637,1.1819,1.3971,1.6097,
1 1.8204,2.0296,2.2378,2.4454,2.6529,2.8607,3.0693,3.2790,3.4905,
2 3.7042,3.9205,4.1400,4.3632,4.5909,4.8236,5.0621,5.3071,5.5596,
3 5.8206,6.0911,6.3724,6.6660,6.9735,7.2968,7.6382,8.0002,8.3860,
4 8.7992,9.2442,9.7262,10.2516,10.8284,11.4661,12.1769,12.9760,
5 13.8827,14.9223,16.1276,17.5433,19.2306,21.2764,23.8093,27.0268,
6 31.2497/
IF(XKTAV.GT.0.8)XKTAV=0.8
I=INT(100.*(XKTAV-0.28))
REMDR=100.*XKTAV-INT(100.*XKTAV)
IF(I.GE.1)GO TO 10
F=AMAX1((XKTAV-0.288)/0.002,0.)*ARRAY(1)
RETURN
10 F=ARRAY(I)+REMDR*(ARRAY(I+1)-ARRAY(I))
RETURN
END

```

APPENDIX B

```

C THIS PROGRAM MODELS A COMBINED PEAK-POWER TRACKER, REGULATOR,
C INVERTER, AND BATTERY. THE BATTERY IS MODELED BY MULTIPLYING
C POWER IN BY A CHARGING EFFICIENCY; THUS FILLING THE BATTERY
C REQUIRES MORE ENERGY THAN EMPTYING IT. THE MODEL DEALS WITH
C POWER ONLY, NOT CURRENT AND VOLTAGE.
C
C PARAMETERS:
C 1) EFMPT: MAX POWER TRACKER EFFICIENCY
C 2) EFINV: INVERTER EFFICIENCY
C 3) EFBAT: BATTERY CHARGING EFFICIENCY
C 4) FMAX: MAXIMUM FRACTIONAL STATE OF CHARGE OF BATTERY
C 5) FMIN: MINIMUM DITTO
C 6) BCAP: TOTAL BATTERY CAPACITY IN WATT-HOURS
C 7) F: INITIAL FRACTIONAL STATE OF CHARGE OF BATTERY
C
C INPUTS:
C 1) PA: POWER FROM ARRAY (KJ)
C 2) PL: POWER DEMANDED BY LOAD
C
C OUTPUTS:
C 1) PA*EFMPT: USABLE POWER FROM ARRAY (BEFORE INVERSION ETC.)
C 2) F: FRACTIONAL STATE OF CHARGE OF BATTERY
C 3) BIN: POWER RECEIVED BY BATTERY (AFTER CHARGING LOSSES)
C 4) BOUT: POWER DRAWN FROM BATTERY
C 5) BW: POWER WASTED IN CHARGING BATTERY
C 6) PL: POWER RECEIVED BY LOAD FROM PV SYSTEM
C 7) FUTIL: POWER SENT TO LOAD FROM UTILITY
C 8) DUMP: POWER THROWN OUT OR SOLD TO UTILITY DUE TO FULL BATTERY
C 9) DNS: POWER DUMPED IN EQUIVALENT SYSTEM WITH NO STORAGE
C 10) PLNS: POWER RECEIVED BY LOAD FROM PV SYSTEM IN EQUIVALENT
C SYSTEM WITH NO STORAGE.
C
C SUBROUTINE TYPE35(TIME,XIN,OUT,P, DPBT,PAR,INFO)
C DIMENSION XIN(2),OUT(20),PAR(7),INFO(10)
C COMMON/SIM/TIME0,TIMEF,DELT
C INTEGER CASE
C IF(INFO(7).GE.0)GOTO 10
C INFO(6)=20
C CALL TYPECK(1,INFO,2,7,0)
C
C SET PARAMETERS
C EFMPT=PAR(1)
C EFINV=PAR(2)
C EFBAT=PAR(3)
C FMAX=PAR(4)
C FMIN=PAR(5)
C BCAP=PAR(6)

```

F0=PAR(7)

```

C
10  CONTINUE
    IF(INFO(7).EQ.-1)OUT(16)=F0
    IF(INFO(7).EQ.0)OUT(16)=OUT(2)
    FI=OUT(16)
    F=OUT(2)
    PA=XIN(1)*EFMPT
    IF(PA.LT.0.)PA=0.
    PL=XIN(2)
    PXS=(PA-PL/EFINV)*DELT
    IF(PXS.LE.0.)GO TO 20
    BXS=(FMAX-F)*RCAP/EFBAT
    IF(BXS.GE.PXS)CASE=1
    IF(BXS.LT.PXS)CASE=2
    IF(BXS.LE.0.)CASE=3
    GO TO (100,200,300),CASE
20  B=(F-FMIN)*BCAP
    IF(B.GE.-PXS)CASE=4
    IF(B.LT.-PXS)CASE=5
    IF(B.LE.0.)CASE=6
    GO TO (400,500,600),CASE-3
C
C CASE 1: EXCESS ENERGY; BATTERY CAN HOLD ALL
100 BIN=PXS*EFBAT
    F=F+BIN/BCAP
    BOUT=0.
    BW=(1.-EFBAT)*PXS
    PUTIL=0.
    DUMP=0.
    DNS=PXS
    PLNS=PL
    GO TO 900
C
C CASE 2: EXCESS ENERGY; BATTERY CAN HOLD SOME BUT NOT ALL
200 F=FMAX
    BIN=BXS*EFBAT
    BOUT=0.
    BW=(1.-EFBAT)*BXS
    PUTIL=0.
    DUMP=PXS-BXS
    DNS=PXS
    PLNS=PL
    GO TO 900
C
C CASE 3: EXCESS ENERGY; BATTERY FULL
300 F=FMAX
    BIN=0.
    BOUT=0.
    BW=0.

```

```
PUTIL=0.
DUMP=PXS
DNS=PXS
PLNS=PL
GO TO 900

C
C CASE 4: ARRAY ENERGY INSUFFICIENT; BATTERY CAN SUPPLY ALL OF DEFICIT
400 BIN=0.
    BOUT=-PXS
    F=FI-BOUT/BCAP
    BW=0.
    PUTIL=0.
    DUMP=0.
    DNS=0.
    PLNS=PA*EFINV
    GO TO 900

C
C CASE 5: ARRAY INSUFFICIENT; BATTERY CAN SUPPLY SOME OF DEFICIT
500 F=FMIN
    BIN=0.
    BOUT=B
    BW=0.
    PUTIL=PL-(PA+B/DELT)*EFINV
    PL=PL-PUTIL
    DUMP=0.
    DNS=0.
    PLNS=PA*EFINV
    GO TO 900

C
C CASE 6: ARRAY INSUFFICIENT; BATTERY EMPTY
600 F=FMIN
    BIN=0.
    BOUT=0.
    BW=0.
    PUTIL=PL-PA*EFINV
    PL=PL-PUTIL
    DUMP=0.
    DNS=0.
    PLNS=PA*EFINV

C
900 OUT(1)=PA
    OUT(2)=F0
    IF (TIME.GT.TIME0)OUT(2)=F
    OUT(3)=BIN/DELT
    OUT(4)=BOUT/DELT
    OUT(5)=BW/DELT
    OUT(6)=PL
    OUT(7)=PUTIL
    OUT(8)=DUMP/DELT
    OUT(9)=DNS/DELT
```

OUT(10)=PLNS

RETURN

END

:

APPENDIX C

```

C THIS PROGRAM CALCULATES PHOTOVOLTAIC SYSTEM PERFORMANCE.
C MONTHLY-AVERAGE WEATHER STATISTICS AND SYSTEM PARAMETERS
C ARE ENTERED AS FOLLOWS:
C
C HBAR: MONTHLY-AVERAGE DAILY HORIZONTAL RADIATION (W/M2) --12 VALUES
C TAMB: MONTHLY-AVERAGE AMBIENT TEMPERATURE (CELSIUS) --12 VALUES
C ALAT: LATITUDE IN DEGREES
C SLOPE: IN DEGREES
C RHO: GROUND REFLECTANCE
C TAU: TRANSMITTANCE OF PROTECTIVE GLAZING (GENERALLY TAU=1.)
C ALPHA: SOLAR ABSORPTANCE OF PHOTOVOLTAIC CELLS
C ETAREF: REFERENCE EFFICIENCY OF ARRAY (GENERALLY INCLUDES
C TRANSMITTANCE OF PROTECTIVE GLAZING)
C TREF: TEMPERATURE CORRESPONDING TO ETAREF
C BETA: TEMPERATURE COEFFICIENT OF CELLS
C ETAMP: EFFICIENCY OF MAXIMUM POWER TRACKING CIRCUITRY
C ETAPC: EFFICIENCY OF POWER CONDITIONING EQUIPMENT (EXCLUDING
C MAX POWER TRACKER)
C UL: THERMAL LOSS COEFFICIENT OF ARRAY (WATTS/M2C)
C ETAB: BATTERY STORAGE EFFICIENCY
C BC: EFFECTIVE BATTERY CAPACITY; NOMINAL BATTERY CAPACITY IN
C WAIT-HOURS TIMES FRACTION OF BATTERY USED
C LPROF: ZERO IF A SINGLE LOAD PROFILE IS TO BE USED FOR ALL MONTHS
C ONE IF A LOAD PROFILE IS TO BE ENTERED FOR EACH MONTH.
C AREA: TOTAL AREA OF PHOTOVOLTAIC CELLS (M2)
C N, (TIME(I),XLOAD(I),I=1,N) ; N MUST BE AT LEAST 2 AND NOT MORE
C THAN 25. TIME(1)=0., TIME(N)=24.
C XLOAD IS IN WATTS.
C THIS SET OF PARAMETERS IS ENTERED 12 TIMES IF LPROF=1
C
C DIMENSION HBAR(12),TAMB(12),TIME(25),XLOAD(25),DAY(12),SN(12)
C REAL IT,IHOR,I0,IC
C DATA DAY/17.,47.,75.,105.,135.,162.,198.,228.,258.,288.,318.,344./
C DATA SN/29.,18.,3.,-10.,-22.,-25.,-24.,-10.,-2.,10.,23.,30./
C DATA PI/3.14159265/SC/1353./
C RDCONV=PI/180.
C READ(*,*)HBAR
C READ(*,*)TAMB
C READ(*,*)ALAT,SLOPE,RHO,TAU,ALPHA
C READ(*,*)ETAREF,TREF,BETA,ETAMP,ETAPC
C READ(*,*)UL,ETAB
C READ(*,*)LPROF
C READ(*,*)BC,AREA
C READ(*,*)N,(TIME(I),XLOAD(I),I=1,N)
C PRINT OUT PARAMETERS, AND HEADINGS FOR RESULTS.
C WRITE(*,4)AREA,ALAT,SLOPE,UL

```

```

WRITE(%,5)TAU,ALPHA,ETAMP,ETAPC
WRITE(%,6)RHO,ETAREF,TREF,BETA
WRITE(%,8)BC,ETAB
WRITE(%,2)HBAR,TAMB
WRITE(%,7)
2  FORMAT(/' HBAR: ',12F9.0/' TEMP: ',12F9.1/)
4  FORMAT(' AREA = ',F7.2,T19,' LAT = ',F7.2,T37,' SLOPE = ',
+ F7.2,T55,' UL = ',F7.2)
5  FORMAT(' TAU = ',F7.2,T19,' ALPHA = ',F7.2,T37,' ETAMP = ',
+ F7.2,T55,' ETAPC = ',F7.2)
6  FORMAT(' RHO = ',F6.1,T19,'ETAREF = ',F7.2,T37,' TREF = ',
+ F6.1,T55,' BETA = ',F9.4)
8  FORMAT(' BCAP = ',F8.3,T19,'ETABAT = ',F7.2)
7  FORMAT(T30,'SOLAR LOAD FRACTION'/T16,'AVERAGE'/3X,'ARRAY',T17,
+ 'LOAD',T29,'WITHOUT',T42,'WITH'/1X,'EFFICIENCY',5X,'(KW)',T29,
+ 'STORAGE',T42,'STORAGE'/)
C
DO 100 MN=1,12
IF(LPROF,NE.1 .OR. MN.EQ.1)GO TO 20
READ(%,*)N,(TIME(I),XLOAD(I),I=1,N)
20 CONTINUE
DECL=23.45*SIN((284.+DAY(MN))/365.*2.*PI)
SINDEC=SIN(DECL*RDCONV)
COSDEC=COS(DECL*RDCONV)
TANDEC=SINDEC/COSDEC
SINLAT=SIN(ALAT*RDCONV)
COSLAT=COS(ALAT*RDCONV)
TANLAT=SINLAT/COSLAT
COSSLP=COS(SLOPE*RDCONV)
COSWS=-TANDEC*TANLAT
WS=ACOS(COSWS)
SINWS=SIN(WS)
WSP=ACOS(-TANDEC*TAN((ALAT-SLOPE)*RDCONV))
WSP=AMIN1(WS,WSP)
D=COSLAT*COSDEC*SINWS+WS*SINLAT*SINDEC
HO=0*SC/PI*(1.+0.033*COS(2.*PI*DAY(MN)/365.))
C HO IS IN WATTS/M2
XKT=HBAR(MN)/HO
C CALCULATE MONTHLY-AVERAGE ELECTRICAL CONVERSION EFFICIENCY, ETAPV
CF=1.-0.000117*(SM(MN)+ALAT-SLOPE)*(SM(MN)+ALAT-SLOPE)
X=219.+832.*XKT
C X HAS UNITS OF WATTS/M2 TO MATCH UNITS OF UL.
A=TAU*(ALPHA-ETAREF)*CF*X/UL
ETAPV=ETAREF*(1.-BETA*(A+TAMB(MN)-TREF+3.))
A=TAU*(ALPHA-ETAPV)*CF*X/UL
ETAPV=ETAREF*(1.-BETA*(A+TAMB(MN)-TREF+3.))
C INITIALIZE MONTHLY VALUES TO ZERO.
E=0.
DO=0.

```

```

      PLO=0.
      DEMAND=0.
      HT=0.
C   CYCLE THRU LOAD PROFILE, DIVIDE TIME INTERVALS INTO INCREMENTS OF
C   ONE HOUR OR LESS, INTERPOLATING LOAD.
      DO 300 I=2,N
      DELT=TIME(I)-TIME(I-1)
      DL=XLOAD(I)-XLOAD(I-1)
      ISTEP=INT(DELT+.999)
      STEP=ISTEP
      DO 300 J=1,ISTEP
      X=J
      T1=TIME(I-1)+DELT*(X-1)/STEP
      T2=TIME(I-1)+DELT*X/STEP
      XL1=XLOAD(I-1)+DL*(X-1)/STEP
      XL2=XLOAD(I-1)+DL*X/STEP
      AVLOAD=(XL2+XL1)/2.
      DT=T2-T1
      DEMAND=DEMAND+AVLOAD*DT
C   AVLOAD IS IN WATTS
C   DEMAND IS IN WATT-HOURS/DAY
      W1=(T1-12.)*PI/12.
      W2=(T2-12.)*PI/12.
      W=(W1+W2)/2.
      IF(W1.LT.-WS.OR.W2.GT.WS)GO TO 300
C   CALCULATE HOURLY RADIATION PARAMETERS
      ANGLE=(ALAT-SLOPE)*RDCONV
      COSTH=COS(ANGLE)*COSDEC*COS(W)+SIN(ANGLE)*SINDEC
      COSTHZ=COSLAT*COSDEC*COS(W)+SINLAT*SINDEC
      RB=COSTH/COSTHZ
      RD=(1.+COSSLP)/2.
      D=RHO*(1.-COSSLP)/2.
      IO=12./PI*SC*(1.+0.033*COS(2.*PI*DAY(MN)/365.))*(COSLAT*COSDEC*
1   (SIN(W2)-SIN(W1))+(W2-W1)*SINLAT*SINDEC)
C   IO IS EXTRATERRESTRIAL RADIATION IN WATT-HOURS/M2 (DECLARED REAL)
C   HOURLY CLEARNESS INDEX FROM COLLARES-PEREIRA & RABL CORRELATION
      A=0.409+0.5016*SIN(WS-60.*RDCONV)
      B=0.6609-0.4767*SIN(WS-60.*RDCONV)
      HRKT=XKT*(A+B*COS(W))
C   ERBS CORRELATION FOR DAILY AVERAGE DIFFUSE FRACTION CONVERTED TO
C   HOURLY AVERAGE FRACTION USING RELATIONSHIPS OF LIU&JORDAN AND
C   COLLARES-PEREIRA&RABL.
      FKT=((-1.76*XKT+3.372)*XKT-3.023)*XKT+1.317
      FKT=FKT/(A+B*COS(W))
      R=(1.-FKT)*RB+FKT*RD+D
      IHOR=HRKT*IO
      IT=IHOR*R
      IF(IT.LE.0..OR.IHOR.LE.0.)GO TO 300
C   IC IS IN WATT-HRS/M2

```

```

      IC=AVLOAD*IT/(AREA*ETAPV*TAU*ETAMP*ETAPC)
C  CALCULATE PHI
      XC=IC/IT
      XM=1.85+.169*R/(HRKT*HRKT)-.0696*COSSLP/(HRKT*HRKT)-.981*HRK1/
      . (COSDEC*COSDEC)
      PHI=0.
      IF(XC.GE.XM)GO TO 40
      IF(XM.NE.2)GO TO 30
      PHI=(1.-XC/XM)*(1.-XC/XM)
      GO TO 40
30  A=(XM-1.)/(2.-XM)
      DISCR=A*A+(1.+2.*A)*(XM-XC)*(XM-XC)/(XM*XM)
C** THE NEXT 5 LINES APPEAR TO BE UNNECESSARY AND COULD BE DELETED.
      IF(DISCR.GE.0.)GO TO 35
      WRITE(%,17)XC,XM,A,DISCR,W,MN
19  FORMAT(' PHI PROBLEM: XC,XM,A,DISCR,W,MN: ',5F10.4,2I4)
      DISCR=0.
35  CONTINUE
      PHI=ABS(ABS(A)-SQRT(DISCR))
40  CONTINUE
C  CALCULATE HOURLY AVERAGE ELECTRICAL RESULTS WITHOUT STORAGE
      EHR=AREA*IT*TAU*ETAPV*ETAMP
      DHR=EHR*PHI
      PL=EHR*(1.-PHI)*ETAPC
C  SUMMED VALUES: E,DO,PLO,HT
C  SUFFIX 0 INDICATES NO STORAGE
      E=E+EHR
      DO=DO+DHR
      PLO=PLO+PL
      HT=HT+IT
300 CONTINUE
      FO=PLO/DEMAND
      EL=E/DEMAND
C  CALCULATE EFFECT OF STORAGE
      DFS=0.
      IF(BC.LE.0.)GO TO 60
      A=1.315-0.1059*FO*DEMAND/(ETAPC*BC)-0.1847/XKT
      A=AMIN1(A,1.)
      X=ETAB*ETAPC*DO/DEMAND
      DFM=AMIN1(1.-FO,ETAPC*BC/DEMAND)
      DISCR=(X+DFM)*(X+DFM)-4.*A*X*DFM
C** THE NEXT 5 LINES APPEAR TO BE UNNECESSARY AND COULD BE DELETED.
      IF(DISCR.GT.0.)GO TO 80
      WRITE(%,17)A,X,DFM,DISCR,MN
17  FORMAT(' WARNING: DFS ERROR. A,X,DFM,DISCR,MN: ',4F10.4,2I4)
      DISCR=0.
80  CONTINUE
      DFS=(X+DFM-SQRT(DISCR))/(2.*A)
60  CONTINUE

```

```
F=F0+DFS
AVLOAD=DEMAND/24000
WRITE(*,9)ETAPV,AVLOAD,F0,F
9  FORMAT(4X,F4.3,T15,F7.3,T30,F4.3,T43,F4.3)
   SUMPLO=SUNPLO+PLO
   SUMPLS=SUMPLS+DFS*DEMAND
   SUMLD=SUNLO+DEMAND
100 CONTINUE
    AVLOAD=SUMLD/(24000.*12.)
    F0=SUMPLO/SUMLD
    F=(SUMPLO+SUMPLS)/SUMLD
    WRITE(*,11)AVLOAD,F0,F
11  FORMAT(/14X,F7.3,T30,F4.3,T43,F4.3)
    STOP
    END
;
```

REFERENCES

1. Bendt, P., Rabl, A., and Collares-Pereira, M. "The Frequency Distribution of Daily Insolation Values." Solar Energy 27 (1981): 1-5.
2. Box, G.E.P., Hunter, W.G., and Hunter, J.S. Statistics for Experimenters. New York: John Wiley and Sons, 1978.
3. Cole, R. "Long-Term Average Performance Predictions for Compound Parabolic Concentrator Solar Collectors." Proceedings of the American Section of the International Solar Energy Society, Orlando, FL: 1977.
4. Collares-Pereira, M., and Rabl, A. "The Average Distribution of Solar Radiation--Correlations Between Diffuse and Hemispherical and Between Daily and Hourly Insolation Values." Solar Energy 22 (1979): 155-164.
5. Collares-Pereira, M., and Rabl, A. "Derivation of a Method for Predicting Long Term Average Energy Delivery of Solar Collectors." Solar Energy 23 (1979): 223-234.
6. Duffie, J.A., and Beckman, W.A. Solar Engineering of Thermal Processes. New York: Wiley-Interscience, 1980.
7. Erbs, D.G. Methods for Estimating the Diffuse Fraction of Hourly, Daily, and Monthly-Average Global Solar Radiation. Masters Thesis in Mechanical Engineering. University of Wisconsin, Madison. Madison, WI: 1980.
8. Evans, D.L., Facinelli, W.A., and Koehler, L.P. Simulation and Simplified Design Studies of Photovoltaic Systems. Report SAND 80-7013, Sandia Laboratories. Albuquerque, NM: 1980.
9. Evans, D.L., Facinelli, W.A., and Koehler, L.P. Simplified Design Guide for Estimating Photovoltaic Flat Array and System Performance. Report SAND 80-7185, Sandia Laboratories. Albuquerque, NM: 1980.
10. Evans, D.L., Facinelli, W.A., and Otterbein, R.T. Combined Photovoltaic/Thermal System Studies. Report SAND 78-7031, Arizona State University. Tempe, AZ: 1978.
11. Hoover, E.R. SOLCET II: An Improved Photovoltaic System Analysis Program. Report SAND 79-1785, Sandia Laboratories. Albuquerque, NM: 1979.

12. Huget, R.G. A Method for Estimating the Daily Utilizability of Flat Plate Solar Collectors. Masters Thesis in Mechanical Engineering. University of Waterloo. Waterloo, Ontario: 1981.
13. Klein, S.A. A Design Procedure for Solar Heating Systems. Ph.D. Thesis in Chemical Engineering. University of Wisconsin-Madison. Madison, WI: 1976.
14. Klein, S.A. "Calculation of Flat-Plate Collector Utilizability." Solar Energy 21 (1978): 393-402.
15. Klein, S.A., and Beckman, W.A. "A General Design Method for Closed-Loop Solar Energy Systems." Solar Energy 22 (1979): 269-282.
16. Klein, S.A., et al. TRNSYS--A Transient Simulation Program. Report 38-11, Solar Energy Laboratory, University of Wisconsin-Madison. Madison, WI: 1981.
17. Klein, S.A., and Theilacker, J.C. "An Algorithm for Calculating Monthly-Average Radiation on Inclined Surfaces." Journal of Solar Energy Engineering 103 (1981): 29-33.
18. Liu, B.Y.H., and Jordan, R.C. "The Interrelationship and Characteristic Distribution of Direct, Diffuse and Total Solar Radiation." Solar Energy 4 (1960): 1-19.
19. Liu, B.Y.H., and Jordan, R.C. "A Rational Procedure for Predicting the Long Term Average Performance of Flat Plate Solar Energy Collectors." Solar Energy 7 (1963): 53-74.
20. Monsen, W.A. Design Methods for Building-Integrated Solar Heating Components. Masters Thesis in Mechanical Engineering. University of Wisconsin-Madison. Madison, WI: 1980.
21. Odegard, D.S. Insolation Utilizability and the Prediction of Industrial Process Heating System Performance. Masters Thesis in Mechanical Engineering. University of Wisconsin-Madison. Madison, WI: 1980.
22. Orgill, J.F., and Hollands, K.G.T. "Correlation Equation for Hourly Diffuse Radiation on a Horizontal Surface." Solar Energy 19 (1977): 357-359.
23. Ryan, T.A., Joiner, B.L., and Ryan, B.F. MINITAB Student Handbook. North Scituate, MA: Duxbury Press, 1976.

24. Siegel, M.D. Simplified Design Methods for Photovoltaic Systems. Masters Thesis in Engineering. University of Wisconsin-Madison. Madison, WI: 1980.

25. Siegel, M.D., Klein, S.A., and Beckman, W.A. "A Simplified Method for Estimating the Monthly-Average Performance of Photovoltaic Systems." Solar Energy 26 (1981): 413-418.
26. SOLMET. "Hourly Solar Radiation Surface Meteorological Observations." TD-9724 (1979).
27. SOLMET Typical Meteorological Year, Tape Deck 9734. National Oceanic and Atmospheric Administration, Environmental Data Service, National Climatic Center. Asheville, NC.
28. Theilacker, J.C. An Investigation of Monthly-Average Utilization for Flat Plate Solar Collectors. Masters Thesis in Mechanical Engineering. University of Wisconsin-Madison. Madison, WI: 1980.
29. Whillier, A. Solar Energy Collection and Its Utilization for House Heating. Ph.D. Thesis in Mechanical Engineering. M.I.T. Cambridge, Massachusetts: 1953.